

**ENGINEERING MULTIVALENT NANOBODIES AGAINST
AMYLOID PROTEINS AND OTHER ANTIGENS**

A Dissertation
Presented to
The Academic Faculty

by

Nikki McArthur

In Partial Fulfillment
of the Requirements for the Degree
Doctor of Philosophy in Bioengineering in the
School of Chemical & Biomolecular Engineering

Georgia Institute of Technology
December 2024

COPYRIGHT © 2024 BY NIKKI MCARTHUR

ENGINEERING MULTIVALENT NANOBODIES AGAINST AMYLOID PROTEINS AND OTHER ANTIGENS

Approved by:

Dr. Ravi Kane, Advisor
School of Chemical and Biomolecular
Engineering
Georgia Institute of Technology

Dr. Corey Wilson
School of Chemical and Biomolecular
Engineering
Georgia Institute of Technology

Dr. John Blazeck
School of Chemical and Biomolecular
Engineering
Georgia Institute of Technology

Dr. Levi Wood
School of Mechanical Engineering
Georgia Institute of Technology

Dr. Julie Champion
School of Chemical and Biomolecular
Engineering
Georgia Institute of Technology

Date Approved: July 24, 2024

ACKNOWLEDGEMENTS

The work that I have completed during my five years at Georgia Tech has been a collaborative effort, and I am extremely grateful to all of the people who have supported me along the way, whether they were directly involved in my research or not.

I would like to thank my advisor Dr. Ravi Kane for his mentorship and guidance throughout the past five years. I am grateful for all of the ideas you gave me when I was stuck and couldn't figure out which direction to go. Thank you for listening to and supporting my research ideas when I did know how to approach the problem that we were tackling. I would like to thank my committee members Dr. John Blazeck, Dr. Julie Champion, Dr. Corey Wilson, and Dr. Levi Wood for their helpful suggestions and thoughtful questions. Our discussions have made me a more thorough and informed researcher. I appreciate the help of my collaborators Dr. Anton Bryksin, Naima Djeddar, Dr. Rakez Kayed, Dr. Nemil Bhatt, Madison Kidd, Dr. Peter Tessier, Dr. Jennifer Zupancic, Dr. Alec Desai, Dr. Levi Wood, Felix Rivera Moctezuma, Abigail Holberton, Dr. Anant Paravastu, Dr. Terrone Rosenberry, and Dr. Jens Watzlawik. I am thankful for the support of Laura Paige and everything she does to ensure the Bioengineering Program runs smoothly.

Thank you to the undergraduate students that I have worked with, Claire Kang, Akber Shaikh, Oge Onyeachonam, and Jay Squire, for all of the hard work that you put into our research and the fun that you brought to the lab. It has been amazing to watch you become more independent researchers. Thank you to all of the past and current Kane Lab members that I have worked with, Dr. Ana Castro, Dr. Mark Stathos, Dr. Steven Frey, Dr.

Troy Batugal, Dr. Geetanjali Pendyala, Kathryn Loeffler, Augustine Duffy, Jennifer Lee, Raj Patel, Daniel Kim, Alex Wee, and Ayomide Oluwajoba. I appreciate all of your help and suggestions for my research. You guys have made our lab a great place to work. Augustine, I am grateful for your help with the XBB nanobodies project and for your time talking with me about SARS-CoV-2 variants, phylogenetic trees, and antigenic maps. Jenny, I'm so glad that I got to work with you on the XBB nanobodies project. It was really fun teaching you what I know about yeast display and sorting, and it has been a pleasure to collaborate with you on this project. Thanks to Raj for your help with transfections and your suggestions for my adherent SH-SY5Y cells. Also, thank you for organizing most of the social events in our lab and for, with Kathryn, turning the office into a garden oasis. I am especially grateful to Geet for all of your companionship and advice for the past five years. Thank you for your suggestions on research, writing, presentations, and more. Finally, thank you to Kathryn for being a wonderful lab mate and friend. I appreciate your daily advice on my experiments, writing, collaborations, and presentations. Thank you for your support during all of the highs and lows of the past five years. I am so glad that we got to go through our PhD milestones together; I could not imagine doing this without you.

To all of the friends that I have made in Atlanta, especially Devan, Lisa, and David, thank you for welcoming me into your climbing circles and into your lives. Spending time with you is always the highlight of my week. I would not have been able to get through the past few years without your friendship and support. Thank you to Gabriela for always being there for me for so long. Thank you for listening to me talk about everything and anything. You give the best advice and always know what to say to make me feel better when I'm down. I am extremely grateful for your friendship.

I want to thank all of my family, my aunts, uncles, and cousins for their love and encouragement for the past five years and beyond. Thank you for being excited about my interests, my achievements, and my future. I am grateful to my family in Alpharetta, Aunt Ann, Uncle Rick, and their pup Fender, for their support while I've been in Atlanta. Thank you for all of the dinners, brewery visits, and celebrations. It has been so nice knowing you are always there for me.

Thank you to my sister Evonne, brother-in-law Ankith, and their pup Hero. Thank you for always calling me on the weekends, for listening to me talk about lab, climbing, and plants. You give the most thoughtful advice and suggestions. Thank you for supporting me when things get tough and celebrating my achievements, even the little ones. Thank you to Evonne for being the best role model and for your advice on school, research, and life. There is no one who I would trust more than you with these things.

Finally, thank you to my parents Dave and Stephanie. Thank you for supporting me and loving me in every way. I am grateful for your constant enthusiasm and interest in my research and my hobbies. Thank you for being excited about all of my achievements inside and outside of the lab. All that you do for me means so much to me. Thank you for teaching me to be curious, to be dedicated, and to pursue my passions.

TABLE OF CONTENTS

ACKNOWLEDGEMENTS	iii
LIST OF TABLES	ix
LIST OF FIGURES	x
SUMMARY	xii
CHAPTER 1. Introduction	1
1.1 Antibodies, Antibody Fragments, and Antibody Development	1
1.2 Neurodegenerative Diseases and Amyloid Proteins	5
1.3 COVID-19 and the SARS-CoV-2 Virus	9
CHAPTER 2. Development of a Pan-Tau Multivalent Nanobody	13
2.1 Introduction	13
2.2 Materials and Methods	15
2.2.1 Tau monomer and oligomer expression and purification	15
2.2.2 Tau biotinylation	18
2.2.3 Tau, amyloid- β , and α -synuclein fibril formation	18
2.2.4 SDS-PAGE	19
2.2.5 Tau immunoblot characterization	19
2.2.6 Dynamic light scattering	21
2.2.7 Yeast cell culture	21
2.2.8 Magnetic-activated cell sorting	21
2.2.9 Fluorescence-activated cell sorting and individual nanobody selection	22
2.2.10 Flow cytometry	24
2.2.11 Expression and purification of bivalent and tetravalent MT3.1-Fc	24
2.2.12 Expression and purification of MT3.1, bivalent MT3.1(3) and MT3.1(10)	25
2.2.13 MT3.1 immunoblot characterization	26
2.2.14 MT3.1 binding epitope analysis	27
2.2.15 MT3.1 ELISA binding analysis	28
2.2.16 Western blotting of transgenic mouse samples	29
2.3 Results and Discussion	31
2.3.1 Identification of tau-directed nanobodies	31
2.3.2 Characterization of nanobody MT3.1	35
2.3.3 Design and characterization of multivalent pan-tau nanobodies	38
2.3.4 MT3.1 detection of tau aggregates from mouse tissues	39
2.4 Conclusions and Future Work	41
CHAPTER 3. Modification and Characterization of Tau Fibril-Selective Antibodies	43
3.1 Introduction	43
3.2 Materials and Methods	46
3.2.1 Expression and purification of bivalent and tetravalent P8.A1.A21	46

3.2.2	Competition ELISA	47
3.2.3	Antibody epitope analysis	47
3.2.4	Expression and purification of bispecific antibody shuttles	48
3.2.5	SDS-PAGE	49
3.2.6	ELISA	49
3.3	Results and Discussion	50
3.3.1	Characterization of tau conformational nanobody WA2.22 specific for pathological aggregates	50
3.3.2	Characterization of tau fibril conformational antibody ATA1.459.3	52
3.3.3	MACS-based development and characterization of tau fibril-specific nanobody P8.A1.A21	54
3.3.4	Modification of fibril-specific nanobodies to improve their delivery across the BBB	57
3.4	Conclusions and Future Work	59
CHAPTER 4. Generation of Nanobodies With Conformational Specificity for Amyloid Oligomers		61
4.1	Introduction	61
4.2	Materials and Methods	64
4.2.1	Expression and purification of tau monomer and oligomers	64
4.2.2	Tau biotinylation	65
4.2.3	Tau fibril formation	66
4.2.4	Dynamic light scattering	66
4.2.5	SDS-PAGE	66
4.2.6	Tau immunoblot characterization	67
4.2.7	Yeast cell culture	68
4.2.8	Magnetic-activated cell sorting	68
4.2.9	Fluorescence-activated cell sorting	70
4.2.10	Individual nanobody selection	70
4.2.11	Flow cytometry	71
4.2.12	Expression and purification of bivalent OT2.4-Fc, OT2.6-Fc, and MT3.1-Fc	71
4.2.13	OT2.4 and OT2.6 western blot characterization	72
4.2.14	OT2.4 and OT2.6 dot blot characterization	72
4.2.15	Binding epitope analysis	72
4.2.16	Western blotting of human tissue lysates	73
4.2.17	Sorting against amyloid- β oligomer	75
4.3	Results and Discussion	75
4.3.1	Identification of tau oligomer-specific nanobodies	75
4.3.2	Characterization of nanobodies confirms specificity to tau oligomers	79
4.3.3	Epitope mapping reveals that nanobodies interact with tau oligomers via multiple non-overlapping epitopes	81
4.3.4	OT2.4 and OT2.6 recognize tau oligomers from human Alzheimer's disease and healthy older adult brain tissues	82
4.3.5	Sorting of a nanobody library against amyloid- β oligomers	84
4.4	Conclusions and Future Work	85

CHAPTER 5. Development of Potent Nanobodies That Protect Against the SARS-CoV-2 XBB Variant	87
5.1 Introduction	87
5.2 Materials and Methods	90
5.2.1 XBB RBD and S expression and purification	90
5.2.2 XBB RBD and S biotinylation	91
5.2.3 SDS-PAGE	91
5.2.4 Yeast cell culture	92
5.2.5 Magnetic-activated cell sorting	92
5.2.6 Fluorescence-activated cell sorting	93
5.2.7 Individual nanobody selection	94
5.2.8 Flow cytometry	94
5.2.9 Expression and purification of bivalent Fc fusion XNb nanobodies	95
5.2.10 XNb ELISA binding analysis	95
5.2.11 Competition ELISAs	96
5.2.12 Neutralization assays	97
5.2.13 Challenge experiments	97
5.3 Results and Discussion	97
5.3.1 Identification of nanobodies targeting the XBB spike protein	97
5.3.2 Nanobodies bind with high affinity to the XBB spike protein	100
5.3.3 Nanobodies neutralize XBB and protect against an XBB challenge	102
5.4 Conclusions and Future Work	104
CHAPTER 6. Conclusion and Future Directions	106
APPENDIX. Supplementary Tables	112
REFERENCES	116

LIST OF TABLES

Table 1	Sequences of CDR1, CDR2, and CDR3 of the ten selected nanobodies	78
Table 2	Sequences of CDR1, CDR2, and CDR3 of the ten selected nanobodies	99
Table 3	Selected nanobody sequences from screens against tau monomer	112
Table 4	Tau fibril-binding nanobody and scFv sequences	112
Table 5	TfR-binding single-domain antibody sequences	113
Table 6	Selected nanobody sequences from screens against tau oligomer	113
Table 7	Sample data	114
Table 8	Selected nanobody sequences from screens against XBB RBD	115

LIST OF FIGURES

Figure 1	Antibodies and antibody fragments	2
Figure 2	Tau primary structure	6
Figure 3	Size characterization of tau monomer, oligomers, and fibrils	32
Figure 4	Immunoblot characterization of tau monomer, oligomers, and fibrils	32
Figure 5	Selection of tau-directed nanobodies	34
Figure 6	MT3.1 binds to recombinant tau monomer, oligomers, and fibrils	35
Figure 7	Identification of MT3.1 binding epitope	37
Figure 8	Characterization of multivalent MT3.1	39
Figure 9	Western blotting of transgenic mice tissues	40
Figure 10	Identification of WA2.22 binding epitope	51
Figure 11	Peptide scanning analysis of ATA1.459.3 epitope	53
Figure 12	Conformational specificity of P8.A1.A21	55
Figure 13	Identification of P8.A1.A21 binding epitope	56
Figure 14	Design of bispecific antibody shuttles	57
Figure 15	Bispecific antibody shuttle characterization	58
Figure 16	Tau immunoblot characterization	76
Figure 17	Selection of tau oligomer-specific nanobodies	77
Figure 18	Single clone analysis of selected nanobodies	78
Figure 19	Bivalent Fc fusion proteins	80
Figure 20	Western blotting with OT2.4 and OT2.6	80
Figure 21	Analysis of OT2.4 and OT2.6 specificity towards tau oligomers	81
Figure 22	Binding epitope analysis of OT2.4 and OT2.6	82
Figure 23	Binding of OT2.4 and OT2.6 to tau oligomers from human brain samples	84

Figure 24	Selection of amyloid- β oligomer-targeting nanobodies	85
Figure 25	Enrichment of nanobody binding to XBB RBD	98
Figure 26	Single clone analysis of selected nanobodies	100
Figure 27	<i>In vitro</i> analysis of XBB S-binding nanobodies	101
Figure 28	XNb 4.13 and XNb 4.14 protect against XBB challenges	104
Figure 29	Tau oligomer-induced cytotoxicity in SH-SY5Y neuroblastoma cells	109

SUMMARY

Tauopathies, such as Alzheimer's disease, are neurodegenerative diseases that involve the misfolding and deposition of aggregates of the amyloid protein tau. These diseases are among the most widespread neurodegenerative diseases, yet there are few safe and effective disease-modifying treatments for them. Conformational antibodies and antibody fragments that target the various aggregate forms of tau are promising candidates for treatments to slow the progression of these tauopathies and are useful as reagents to understand the aggregation of tau and its role in disease progression. In this dissertation, we have explored the *in vitro* development and characterization of multivalent nanobodies, or single-domain antibody fragments, targeting complex and heterogeneous tau aggregates.

We began with the development of a simple approach using a synthetic yeast surface display nanobody library and *in vitro* cell sorting to identify a pan-tau nanobody with specificity for tau protein relative to other amyloid proteins. We have shown that multivalent versions of our lead tau-binding nanobody have increased avidity towards tau aggregates and recognize pathogenic tau found in the brains of tau transgenic mice. We have also characterized tau fibril-specific nanobodies and modified them for improved delivery past the blood-brain barrier. Next, we modified our sorting strategy to generate conformational nanobodies that target oligomeric tau, a form of aggregated tau which is suspected to be the most toxic form present in Alzheimer's disease. We demonstrated that our nanobodies are specific for tau oligomers relative to tau monomer and fibrils and bind to tau oligomers in brain samples from Alzheimer's disease patients. We have extended this work to screen for nanobodies that target oligomers of another amyloid protein

involved in Alzheimer's disease, amyloid- β . Finally, we applied our *in vitro* antibody discovery strategies to target an antigen involved in infectious disease—the spike protein of the SARS-CoV-2 virus. We created multivalent nanobodies that bind with high affinity to the XBB spike protein and provide protection against an XBB challenge in mice.

Overall, this work demonstrates significant progress in the development and characterization of nanobodies specific for complex multimeric antigens. The multivalent nanobodies that we have generated can be used to study amyloid proteins and their involvement in neurodegenerative disease progression and can be further engineered into potent therapies for neurodegenerative or infectious diseases.

CHAPTER 1. INTRODUCTION

1.1 Antibodies, Antibody Fragments, and Antibody Development

Monoclonal antibodies (mAbs, Figure 1a) are large biomolecules that can bind with high affinity and specificity to a wide variety of target antigens including soluble and surface bound proteins, lipids, nucleic acids, carbohydrates, and small molecules.^{1,2} Different amino acid compositions of the variable domains, specifically the three complementarity-determining regions (CDRs) of each variable domain, within antibodies give them their ability to bind to such a large and diverse set of antigens. Due to their great binding strength and specificity, mAbs are extremely effective and important tools for research, diagnostics, and therapeutics. Since the 1980s, it has become possible to generate large amounts of pure humanized mAbs, and this has led to the rapid development of mAbs or mAb-derived therapies to treat cancer, autoimmune diseases, infectious diseases, neurological diseases, and other diseases.³⁻⁵ mAbs are used in many medical diagnostic tests with one of the most well-known being over the counter pregnancy tests. Analytical techniques such as immunoblotting, immunohistochemistry, immunofluorescence, and immunoprecipitation rely on mAbs for specific binding to a desired antigen and have aided biological and medical research and engineering for over 50 years. Modified antibodies such as bispecifics and antibody-drug conjugates have been developed to improve drug delivery or alter biological function.⁶

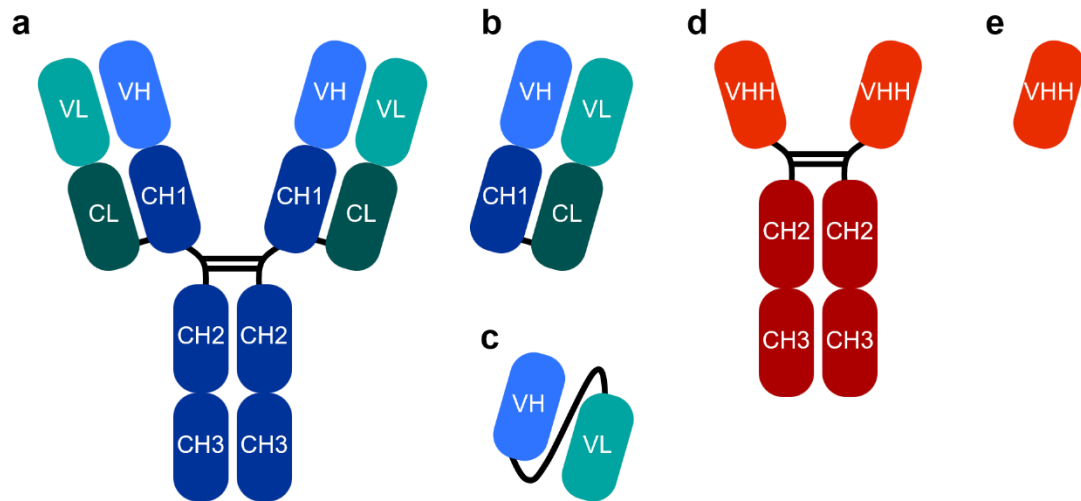


Figure 1. Antibodies and antibody fragments. a) A conventional IgG, b) Fab, c) scFv, d) camelid heavy chain antibody, and e) nanobody. The variable domain of the light chain (VL) and heavy chain (VH or VHH) and constant domain of the light chain (CL) and heavy chain (CH1, CH2, and CH3) are labeled).

Antibody fragments of different sizes have been created that are also used as highly specific binding molecules in research, therapy, and diagnostics (Figure 1b, c, e).⁶ Fabs are antibody fragments that contain the antigen-binding regions of an antibody and consist of one variable and one constant domain from both the heavy and light chains (Figure 1b). The heavy and light chains of a Fab are connected by naturally occurring disulfide bonds. Single-chain variable fragments (scFvs) are engineered fusion proteins containing only the variable domains of the heavy and light chains of an antibody (Figure 1c). They are connected by a nonnatural polypeptide linker. Many therapeutic Fabs and scFvs have been approved by the FDA to treat macular degeneration, autoimmune disease, and blood coagulation disorders.⁷

Single-domain antibodies are antibody fragments consisting of only a single variable domain from the binding region of a heavy chain antibody. Heavy chain antibodies (Figure 1d) consist of only two copies of a heavy chain and exist in camelids and

cartilaginous fish, and single-domain antibodies derived from these heavy chain antibodies are called nanobodies (VHHs, Figure 1e) and variable new antigen receptors (VNARs), respectively.⁸ The small molecular weight of a nanobody, 15 kDa, and extended CDR3 loop give them the ability to bind to hidden or concave epitopes inaccessible to conventional IgGs.⁹ Unlike IgGs, nanobodies can be expressed in bacteria and yeast cells.⁹ They have high thermal stability and can be lyophilized or aerosolized.^{9,10} As they are small, single chain molecules, nanobodies can be treated as modular units and are easily covalently linked into multivalent constructs. The single chain nature of nanobodies, like scFvs, also allows for their development *in vitro* using techniques such as phage display and yeast surface display. In 2019, the FDA approved the United States' first nanobody-based therapeutic, caplacizumab, for treatment against acquired thrombotic thrombocytopenic purpura, a blood clotting disease.¹¹ Caplacizumab is a bivalent nanobody that targets von Willebrand factor, a protein involved in blood coagulation.¹¹

mAbs have traditionally been developed through the immunization of an animal with a chosen antigen and the collection of B cells from the spleen of the animal. The B cells are fused with myeloma cells and the resulting hybridoma cells are cultured in selective media.¹² Unique antibodies produced by individual hybridoma clones with desired properties including specificity and stability are selected. Alternative *in vitro* antibody discovery methods have been developed that have advantages over the traditional hybridoma approach.¹²⁻¹⁵ With *in vitro* antibody discovery, mAbs can be developed more quickly than using the hybridoma approach and the discovery can be done completely *in vitro* without the need for animal immunizations. *In vitro* antibody discovery can be used

to identify antibodies to toxic antigens or non-immunogenic antigens that cannot be used to immunize an animal.

In vitro antibody discovery involves the development of a synthetic antibody library and the screening of this library against a target antigen. Antibody fragments like scFvs or nanobodies are randomly or systematically mutated, often in the CDRs, to create a library of antibodies with the potential to bind to millions of different antigens. Once a synthetic antibody fragment library is created, it can be screened against different antigens to make new antibodies with different properties.

To facilitate the screening of a synthetic antibody library, a display system such as phage display², bacterial display¹⁶, yeast surface display^{17,18}, mRNA display¹⁹, or ribosome display²⁰ is used. This display system links the phenotype, or binding ability, of the selected antibodies with their genotype and allows for the expansion of the library between rounds of screening. In yeast surface display, antibody fragments are expressed in the yeast cell and then displayed on the cell surface through the genetic fusion of the antibody fragment to the cell wall. Each yeast cell displays many copies of a unique antibody fragment from the library on its surface. Using yeast surface display to engineer antibodies is advantageous over phage and bacterial display because yeast are eukaryotes and have protein folding and secretory machinery and can perform post-translational modifications similar to mammalian cells. This allows for better expression of antibody fragments compared to bacteria.^{18,21} Yeast surface display can be used to select for antibodies with high specificity, affinity, expression levels, and stability.¹⁷

To screen a yeast surface displayed library against a desired target antigen, yeast displaying the library are incubated with the antigen. Sorting methods like magnetic-activated cell sorting (MACS) and fluorescence-activated cell sorting (FACS) are then used to separate the yeast expressing antibodies that bind to the target antigen from those that do not bind. The resulting population of yeast expressing binding antibodies are expanded, and this process is repeated with increasingly stringent conditions to identify the highest affinity antibodies.

In this work, we have used *in vitro* antibody discovery and a synthetic nanobody library to develop multivalent nanobodies that target amyloidogenic proteins involved in neurodegenerative diseases including tau and amyloid- β proteins. We have extended this work to create multivalent nanobody binders to another multivalent target, the spike protein receptor-binding domain (RBD) of SARS-CoV-2, the virus that causes COVID-19.

1.2 Neurodegenerative Diseases and Amyloid Proteins

Neurodegenerative diseases are some of the least understood, most difficult to treat, and most widespread disorders affecting society.²² They disproportionately affect older adults, and their impact will continue to grow as the size and life expectancy of the human population continues to increase. Alzheimer's disease (AD) is the most common neurodegenerative disease, and the Alzheimer's Association estimates that in 2024, 6.9 million people in the United States age 65 and older have Alzheimer's disease.²³ AD is characterized by the misfolding and aggregation of tau and amyloid- β proteins into neurofibrillary tangles (NFTs) and amyloid plaques, respectively, within and around neurons in the brain. Tau misfolding and aggregation is linked to many other

neurodegenerative diseases, termed tauopathies, including progressive supranuclear palsy, Pick's disease, and corticobasal degeneration.²⁴

Tau is an intrinsically disordered protein and exists in a flexible, unfolded state without well-defined secondary and tertiary structure.²⁵ There are six different isoforms of human tau generated from alternative splicing of the *MAPT* gene that range from 352 to 441 amino acids long.²⁶ Full length tau (Figure 2), also called 2N4R, contains two copies of an insert sequence in the N-terminal end and four imperfect repeats in the microtubule-binding domain. Shorter isoforms contain zero, one, or two copies of the N-terminal insert and three or four copies of the repeat region.



Figure 2. Tau primary structure. Full length tau primary structure with the N-terminal insert sequences (purple), repeat regions (red), projection domain, microtubule-binding domain, repeat domain, proline-rich region, and fibril core labeled.

Tau belongs to the family of microtubule-associated proteins and natively exists as an unfolded monomer bound to microtubules.²⁷ Tau stabilizes and promotes the assembly of microtubules and facilitates axonal transport along microtubules. In AD, tau undergoes hyperphosphorylation and other post-translational modifications such as acetylation, glycosylation, and truncation.²⁸ These post-translational modifications affect the ability of tau to bind to microtubules, and soluble, hyperphosphorylated tau misfolds and aggregates intracellularly. Detachment of tau from microtubules promotes microtubule instability and disassembly and can lead to loss of cell structure and impaired intracellular trafficking.²⁹

Intracellular tau accumulation is followed by loss of synapses, neuronal dysfunction and death, and brain atrophy.

Hyperphosphorylated and misfolded tau assembles into aggregates of different sizes and structures. Tau oligomers are small, soluble tau aggregates that can spread from cell to cell in the brain. Fibrillar tau structures called paired helical filaments (PHFs) and straight filaments (SFs) also form from misfolded tau.^{26,30} PHFs and SFs make up insoluble NFTs which are a main pathological hallmark of AD. Tau oligomers and fibrils can induce misfolding and aggregation of tau monomer, and this seeding leads to the propagation and spreading of tau pathology.³¹

Tau pathology is closely related to the progression and symptoms of AD²⁷ making tau aggregates important molecules to study to understand the role of tau misfolding and aggregation in disease progression. Tau aggregates are also promising targets for passive immunotherapy to slow disease progression.^{25,28} However, there are few options for disease-modifying treatments for tauopathies³² and there is a need for better diagnostics and research tools to study these diseases. Therapeutic conformational antibodies directed at tau could be used to neutralize or promote the clearance of toxic protein aggregates.³³ This reduction in toxic tau protein may prevent the transneuronal spreading of tau and the seeding and propagation of tau aggregation.

Conformational antibodies that selectively bind tau fibrils or tau oligomers have been developed and shown to promote tau clearance and prevent or slow the progression of AD in animal models. Tilavonemab (ABBV-8E12) is a humanized mAb that recognizes extracellular tau aggregates. HJ8.5, the mouse antibody from which tilavonemab was

derived, binds to human tau fibrils.³⁴ Treatment with HJ8.5 in P301S tau transgenic mice reduced tau pathology, insoluble tau levels, loss of motor functions, and brain atrophy compared to control mice³⁵ and blocked tau seeding in a cell-based assay³⁶. Clinical trials with tilavonemab began in January 2017 but were discontinued after phase 2 because treatment with tilavonemab did not change the decline of cognitive function or lower brain atrophy in patients with early AD.³⁷

Zagotenemab (LY3303560) is a humanized version of MC-1, a conformational mouse mAb that preferentially binds tau aggregates over tau monomer. MC-1 was developed by the immunization of mice with PHFs from Alzheimer brain tissue.³⁸ In tau transgenic mice, treatment with MC-1 reduced hyperphosphorylated insoluble tau levels and the presence of NFTs and delayed onset of symptoms associated with neurodegenerative disease.³⁹ Clinical trials with zagotenemab began in April 2016 but were also halted after phase 2.^{40,41} APNmAb005 is a humanized mAb that recognizes a conformational epitope on tau oligomers and preferentially binds early-stage oligomers over tau monomer and late-stage oligomers. In a tauopathy mouse model, rTg4510, treatment with APNmAb005 partially rescued neuronal loss. Ongoing phase I clinical trials with a humanized APNmAb005 began in May 2022.⁴²

Treatment with these conformational antibodies in tau transgenic mice have shown promising results and emphasize the therapeutic value of tau aggregate-targeting antibodies. Treatment with these antibodies in humans, however, have not yet progressed passed clinical trials. There is currently a need for novel antibodies or antibody-like molecules that target tau aggregates and could serve as therapeutics or diagnostics for tauopathies. In this work, we have taken an alternative approach to address this need and

developed conformational tau-binding nanobodies that likely interact with tau aggregates at epitopes different from the previously reported tau mAbs.

Amyloid- β is another aggregate-forming protein involved in the pathogenesis of AD. Amyloid- β is generated from the proteolytic cleavage of amyloid precursor protein, a transmembrane protein highly expressed in the synapses of neurons.⁴³ Extracellular misfolded amyloid- β monomer aggregates into oligomers, protofibrils, and fibrils.⁴³ Amyloid- β fibrils accumulate and form the primary component of amyloid plaques, a pathological hallmark of AD.⁴⁴

Like tau, conformational amyloid- β antibodies have been studied as potential disease-modifying therapies. Lecanemab is a mAb that binds specifically to large, soluble amyloid- β protofibrils and is approved by the FDA for the treatment of AD.⁴⁴ Another mAb, aducanumab, was approved by the FDA for AD treatment, but since its approval its manufacturer Biogen has announced that treatment with aducanumab will be discontinued.⁴⁵ Given the limited progress creating effective amyloid- β -targeting therapeutics, there is a need for additional safe and effective disease-modifying treatments for neurodegenerative diseases targeting amyloid- β .

1.3 COVID-19 and the SARS-CoV-2 Virus

Severe acute respiratory syndrome coronavirus 2 (SARS-CoV-2) is a single stranded, positive-sense RNA coronavirus that causes COVID-19.⁴⁶ The virus is made up of four main structural proteins: spike (S), envelope (E), membrane (M), and nucleocapsid (N) proteins. The S protein is responsible for viral attachment, fusion, and entry into host cells. The S protein is composed of two subunits, S1 and S2, on the N- and C-terminus,

respectively. Within S1 is the RBD, the location at which SARS-CoV-2 binds to the receptor angiotensin-converting enzyme 2 (ACE2) on host cell membranes.

The SARS-CoV-2 virus is rapidly evolving, and new variants are continually emerging. Mutations that occur in the S protein are largely focused in the S1 subunit, while the S2 subunit is more highly conserved across variants. These mutations can affect RBD binding to ACE2 and viral entry making many of the new variants more transmissible than the previous ones. Mutations in the S protein can also contribute to the evasion of neutralizing antibodies, which often target the RBD. The Omicron variant, first identified in November 2021,⁴⁷ and variants of its sublineages BA.1, BA.2, BA.4, and BA.5 are highly transmissible and caused a surge in COVID-19 cases in late 2021 and 2022.⁴⁸ A recombinant variant of two viruses from the Omicron sublineages, XBB, was first identified in August 2022 and rapidly spread around the world causing a wave of COVID-19 infections.⁴⁹ At the time, XBB was one of the most distant SARS-CoV-2 variants from early isolates of SARS-CoV-2. The XBB RBD has only 90.1% RBD amino acid sequence homology to ancestral SARS-CoV-2 RBD. In contrast, the Alpha, Delta, and Omicron BA.4/5 RBDs have 99.6%, 99.1%, and 92.3% sequence homology, respectively, with ancestral SARS-CoV-2 RBD.⁵⁰ These mutations allow the XBB variant to evade neutralization by many antibody therapeutics previously developed for the treatment of COVID-19.^{49,51}

As of May 2024, the most widely circulating variants in the United States are JN.1, an Omicron variant from the BA.2.86 lineage, and KP.2, a descendant of JN.1.⁵² There are currently no mAbs available to treat SARS-CoV-2 infections with XBB variants or newly emerging SARS-CoV-2 variants. Hence, there is a need for neutralizing antibodies against

XBB and variants of the XBB lineage and for broadly neutralizing antibodies to treat infections from XBB and newer variants.

In this work, we have addressed the aforementioned limitations of existing antibody-based research tools and therapeutics, namely the lack of tau oligomer and tau fibril-targeting antibodies with therapeutic and diagnostic potential and the lack of neutralizing antibodies for the XBB variant of the SARS-CoV-2 virus. In Chapter 2, we introduce a facile approach to identify nanobodies that bind to many forms of tau through the *in vitro* screening of a synthetic yeast surface display nanobody library against monomeric tau. We created multivalent versions of our lead nanobody to increase its avidity for tau aggregates and show that these nanobody constructs bind pathogenic tau from a tauopathy mouse model. In collaboration with the Tessier Lab at the University of Michigan, we characterized conformational tau fibril-selective antibody fragments which show selective binding to pathological tau aggregates from transgenic mouse brain and human tauopathy samples. We have begun work modifying these antibody fragments for improved delivery across the blood-brain barrier. Results with our tau fibril-targeting antibody fragments are discussed in Chapter 3. In Chapter 4, we describe the use of screening strategies established in Chapter 2 to develop conformational, tau oligomer-specific multivalent nanobodies. We show that these nanobodies are highly specific for tau oligomers relative to tau monomer and fibrils and bind to tau oligomers in brain samples from AD patients. We have extended this work to screen for nanobody binders to oligomers of another amyloid protein involved in AD, amyloid- β . In Chapter 5, we apply the screening methods developed in the previous chapters to develop high affinity multivalent nanobodies that neutralize the XBB variant of SARS-CoV-2. The multivalent nanobodies

that we have generated in this work could be developed into therapies for neurodegenerative or infectious diseases and are valuable reagents for the identification and characterization of amyloid proteins. The methods established here can be applied to the generation of multivalent nanobodies that target other amyloid or multivalent proteins.

CHAPTER 2. DEVELOPMENT OF A PAN-TAU MULTIVALENT NANOBODY

2.1 Introduction

With the recent development and FDA approval of therapeutics to treat Alzheimer's disease (AD)^{53,54}, discovery of new AD diagnostic biomarkers^{55,56}, and creation of amyloid- β - and tau-directed antibodies, progress has been made to treat, diagnose, and study AD and other neurodegenerative diseases. However, work still remains to develop more effective disease-modifying treatments for AD.

Antibodies directed at tau and amyloid- β have been developed as tools to study these proteins involved in AD and their aggregated forms *in vitro* and as therapeutics with the goal of neutralizing or promoting the clearance of toxic protein aggregates.³³ Much of the past research towards understanding AD and the development of disease-modifying AD treatments has focused on amyloid- β . Recently, more attention has been given to tau as a research and therapeutic target given the correlation between tau pathology and the clinical symptoms of AD.^{25,57-59}

Tau-targeting antibodies used in research and diagnostics include antibodies that target epitopes in the N-terminal region⁶⁰⁻⁶² or proline rich domain^{61,63} of tau, phospho-tau antibodies⁶⁴, and conformational aggregate-specific antibodies^{38,65-68}. Antibodies against tau have been developed using immunization^{38,62,65,66,69} as well as completely *in vitro* discovery via phage display or yeast surface display and sorting from an antibody fragment library^{67,70,71}. *In vitro* antibody discovery can be advantageous over immunization because

this allows for control of a target antigen's presentation including valency, conformation, solubility, and concentration and for control over antibody affinity and specificity through number and stringency of screens.⁷² Synthetic antibody fragment libraries are created through the mutagenesis of single-chain variable fragments (scFvs) or single-domain antibodies such as nanobodies.

Nanobodies have attracted considerable interest in recent years for use as therapeutics, diagnostic tools, and reagents for *in vitro* characterization.^{10,73,74} Like antibodies, nanobodies have high affinity and specificity for their target antigens, but their small size and extended CDR3 give them the ability to bind to epitopes inaccessible to conventional IgGs.⁹ As they are small, single chain molecules, nanobodies are easily covalently linked into multivalent constructs for enabling enhancements in avidity.

Few tau-binding nanobodies have been developed.^{66,67,70,71,75-78} Li et al. created a tau-directed nanobody-based imaging probe via the immunization of alpacas with phospho-tau enriched AD brain extracts and a phospho-tau C-terminal peptide and the creation and panning of a phage display anti-tau nanobody library.⁷⁵ Their anti-tau nanobody recognized phosphorylated tau and neurofibrillary tangle-like structures from tau transgenic mice. Zupancic et al. developed conformational nanobodies that preferentially bind tau fibrils over monomer.⁶⁶ These nanobodies were isolated from a yeast surface display immune library using flow cytometric sorting following the immunization of a llama with tau fibrils. Dupre et al. and Danis et al. identified nanobodies that bind to the C-terminal domain⁷⁰ and microtubule-binding region (MTBR)⁷¹ of tau through the screening of a synthetic phage display nanobody library against recombinant tau monomer. Despite this previous work, developing nanobodies that recognize aggregated forms of

amyloidogenic proteins, such as tau oligomers or fibrils, and ensuring they are able to bind to mouse- or human-derived pathological tau can be challenging due to the high complexity and the heterogeneity in size, conformation, and solubility, of these protein aggregates.

Here, we have taken a simplified approach to identifying nanobodies that bind to many forms of tau by screening a yeast surface display nanobody library against monomeric tau.⁷⁹ We then created multivalent versions of our lead tau-binding nanobody, MT3.1, and showed that they recognized not just tau monomer but also tau oligomers and fibrils but do not interact with other amyloid proteins including amyloid- β fibrils and α -synuclein fibrils. Epitope mapping revealed MT3.1 binds to a critical amyloidogenic motif, VQIXXK, within the MTBR and fibril core of tau. We also demonstrated binding of MT3.1 to aggregated tau in brain samples from a transgenic tauopathy mouse model. This work demonstrates the effectiveness of our antibody screening and multivalent design approach in developing antibodies that bind amyloidogenic protein aggregates. These antibodies have the potential to advance our understanding and treatment of prominent neurodegenerative diseases.¹

2.2 Materials and Methods

2.2.1 Tau monomer and oligomer expression and purification

The gene encoding full length human tau with F8W, C291A, C322A mutations and a C-terminal His-tag was synthesized and cloned into an expression plasmid for expression in BL21(DE3)pLysS *E. coli* by Gene Universal Inc. (Newark, DE). This tau was used for

¹ This chapter is based on our work published in *Biotechnology Progress*.⁷⁹

screens of the nanobody library. The plasmid containing tau was transformed into BL21(DE3)pLysS *E. coli* (Promega) following the manufacturer's protocol. Transformed cells were used to start a 5 mL culture in LB media with 100 µg/mL ampicillin and 35 µg/mL chloramphenicol. After incubating at 37 °C overnight with rotation, the 5 mL culture was used to inoculate 200 mL of LB media with 100 µg/mL ampicillin and 35 µg/mL chloramphenicol, and cells were grown at 37 °C and 225 rpm until they reached an OD₆₀₀ value between 0.6 and 0.8. Protein expression was induced with 1 mM IPTG for 3 h at 30 °C. After 3 h, the culture was heat shocked at 80 °C for 15 min and centrifuged for 20 min at 7,000 × g. The supernatant containing tau was mixed with 1.5 mL of HisPur Ni-NTA resin (Thermo Fisher Scientific) overnight at 4 °C.

The following day, tau was purified by immobilized metal affinity chromatography (IMAC). The HisPur Ni-NTA resin was loaded into a gravity flow column (G-Biosciences) and washed with 25 mL PBS (137 mM NaCl, 2.7 mM KCl, 10 mM Na₂HPO₄, 1.8 mM KH₂PO₄, pH 7.4). Tau was eluted in 9 mL of 4 M guanidine hydrochloride buffer (4 M guanidine hydrochloride, 50 mM NaCl, 3.52 mM NaH₂PO₄, pH 3.0). The tau protein was concentrated with a 10 kDa MWCO centrifugal filter (Millipore Sigma) and further purified by size exclusion chromatography (SEC) using a Superdex 200 Increase 10/300 GL column (Cytiva) in PBS. Tau concentration and purity were determined by the bicinchoninic acid (BCA) assay (Thermo Scientific) and sodium dodecyl sulfate-polyacrylamide gel electrophoresis (SDS-PAGE), respectively.

An optimized protocol for the expression of full length human F8W, C291A, C322A tau without a His-tag in BL21(DE3) *E. coli* was developed and used for tau monomer and oligomer preparation. The gene encoding full length human tau with F8W,

C291A, C322A mutations was cloned into pET-28b plasmid without a His-tag by Gene Universal Inc. (Newark, DE). This plasmid was transformed into BL21(DE3) *E. coli* (New England Biolabs) following the manufacturer's protocol. Transformed cells were used to start four 5 mL cultures in LB media with 50 µg/mL kanamycin. After incubating at 37 °C overnight with rotation, the 5 mL cultures were used to inoculate 1 L of LB media with 50 µg/mL kanamycin and cells were grown at 37 °C and 225 rpm until they reached an OD₆₀₀ value between 0.6 and 0.8. Protein expression was induced with 0.9 mM IPTG overnight at 22 °C.

The following day, cells were harvested by centrifugation at 7,000 × g for 7 min, resuspended in 20 mL lysis buffer (20 mM tris, 100 mM NaCl, 1 mM EDTA, 1 mM PMSF, protease inhibitor tablet [Sigma Aldrich]) and sonicated eight times with 40 s on and 60 s off pulses at 25% amplitude. Cell debris was separated from the lysate by centrifugation at 15,000 × g for 10 min, and the lysate was boiled in a water bath at 100 °C for 30 min. The boiled lysate was centrifuged at 15,000 × g for 10 min to remove precipitated, denatured proteins, and tau was purified from the supernatant using IMAC. The supernatant was mixed with 2.5 mL of HisPur Ni-NTA resin (Thermo Fisher Scientific) for 1 h at 4 °C. The HisPur Ni-NTA resin was then loaded into a gravity flow column (G-Biosciences) and washed with 20 mL IMAC equilibration buffer (20 mM tris HCl, 500 mM NaCl, pH 8.0). Tau was eluted in 8 mL of elution buffer (20 mM tris HCl, 500 mM NaCl, 100 mM imidazole, pH 8.0). The tau protein, containing tau monomer and oligomer, was concentrated with a 10 kDa MWCO centrifugal filter (Millipore Sigma) and SEC using a Superdex 200 Increase 10/300 GL column (Cytiva) in PBS was performed to separate tau

monomer and oligomers. Tau monomer and oligomer concentration and purity were determined by BCA assay (Thermo Scientific) and SDS-PAGE, respectively.

2.2.2 *Tau biotinylation*

Tau monomer and oligomers were biotinylated using EZ-Link Sulfo-NHS-LC-Biotin (Thermo Scientific) following the manufacturer's protocol. Excess reagent was removed by buffer exchanging into TBS (20 mM tris HCl, 100 mM NaCl, pH 7.4) with a 10 kDa MWCO centrifugal filter (Millipore Sigma). The extent of biotinylation was determined by performing SDS-PAGE with biotinylated protein and streptavidin (Rockland Immunochemicals) at 4 °C.

2.2.3 *Tau, amyloid- β , and α -synuclein fibril formation*

Tau fibrils were formed using tau monomer or biotinylated tau monomer. 5 μ M tau and 2.5 μ M heparin were mixed in PBS for a final volume of 1 mL. Fibrillization mixtures were incubated at 37 °C at 250 rpm for 3-4 days. Tau fibrils were then buffer exchanged with a 100 kDa MWCO centrifugal filter (Millipore Sigma) into HEPES buffer (20 mM HEPES, 100 mM NaCl, 1 mM EDTA, pH 7.4) to remove excess tau monomer. Tau fibril concentration was determined by BCA assay (Thermo Scientific).

To form amyloid- β fibrils, 500 μ g amyloid- β (1-42) peptide (rPeptide) were dissolved in 1100 μ L 1,1,1,3,3,3-hexafluoroisopropanol. The solution containing the dissolved peptide was separated into 25 μ L aliquots, and the liquid in each tube was allowed to evaporate. 50 μ L of 1% NH₄OH was added to each tube and the tubes were vortexed and then centrifuged for 30 s at 1,000 rpm.

To form α -synuclein fibrils, α -synuclein monomer (rPeptide) was diluted to 5 mg/mL in PBS in a 1.5 mL microcentrifuge tube. The tube was vortexed for 3 s and placed in an orbital shaker at 37 °C for 7 days at 1,000 rpm.

2.2.4 SDS-PAGE

Protein samples were diluted in Nu-PAGE lithium dodecyl sulfate (LDS) sample buffer (Invitrogen). β -mercaptoethanol was added to reduced and heated samples at a final concentration of 70 mM, and the samples were heated at 98 °C for 10 min. PageRuler Plus Prestained Protein Ladder (Thermo Scientific) and protein samples were loaded into the wells of a 4-12% Bis-Tris gel (Invitrogen) and the gel was run at 120 V for 50 min. The gel was stained with Imperial Protein Stain (Thermo Scientific), destained, and imaged using the ChemiDoc MP imaging system (Bio-Rad).

2.2.5 *Tau immunoblot characterization*

Tau monomer, oligomers, and fibrils were characterized by dot blot and western blot with Tau5 and T22 antibodies. For dot blots, 0.5 μ g tau monomer, 0.5 μ g tau oligomers, and 0.5 μ g tau fibrils in 1 μ L PBS were spotted onto a 0.2 μ m nitrocellulose membrane in triplicate. The membrane was allowed to dry for at least 30 min then stained with Ponceau S Solution (Rockland Immunochemicals) for 15 min. The membrane was imaged using the ChemiDoc MP imaging system (Bio-Rad) then the Ponceau S stain was removed by washing with TBST (20 mM Tris, 150 mM NaCl, 0.1% Tween-20, pH 7.4) 3 times for 5 min. The membrane was blocked with 10% milk in TBST for 1 h at room temperature. The membrane was washed with TBST for 5 min and then incubated with Tau5 (Invitrogen, 1:5,000) or T22⁶⁹ (1:250) in 5% milk in TBST for 2 h at room

temperature. The membrane was washed three times for 5 min with TBST and incubated with secondary antibody in 5% milk in TBST for 1 h at room temperature. For Tau5 blots, a horseradish peroxidase (HRP)-conjugated anti-mouse IgG antibody (Jackson ImmunoResearch, 1:5,000) was used, and for T22 blots, an HRP-conjugated anti-rabbit IgG antibody (Fisher Scientific, 1:5,000) was used. The membrane was washed three times for 5 min with TBST, and SuperSignal West Femto Chemiluminescent Substrate (Thermo Fisher) was added to the membrane for 30 s-2 min. The membrane was imaged using the ChemiDoc MP imaging system (Bio-Rad).

For western blots, 1 μg (for Tau5 blots) or 4 μg (for T22 blots) tau monomer and oligomers were run on an SDS-PAGE gel as described and transferred to a 0.2 μm nitrocellulose membrane using a Trans-Blot Turbo Mini 0.2 μm Nitrocellulose Transfer Pack (Bio-Rad) and Trans-Blot Turbo Transfer System (Bio-Rad). The membrane was blocked with 10% milk in TBST for 1 h at room temperature. The membrane was washed with TBST for 5 min and then incubated with Tau5 (Invitrogen, 1:5,000) or T22⁶⁹ (1:250) in 5% milk in TBST overnight at 4 °C. The membrane was then washed three times for 10 min with TBST and incubated with the secondary antibodies described above in 5% milk in TBST for 1 h at room temperature. The membrane was then washed three times for 10 min with TBST, and SuperSignal West Femto Chemiluminescent Substrate (Thermo Fisher) was added to the membrane for 30 s-2 min. The membrane was imaged using the ChemiDoc MP imaging system (Bio-Rad).

2.2.6 *Dynamic light scattering*

Tau monomer, oligomers, or fibrils were diluted to 70 $\mu\text{g/mL}$ in PBS and 100 μL was added to a ZEN0040 cuvette (Malvern) and loaded into a Zetasizer Nano ZS instrument (Malvern). Zetasizer software (Malvern) was used to record 5 size measurements per sample at 25 $^{\circ}\text{C}$ using refractive index and absorption parameters for a protein sample in PBS with a 173 $^{\circ}$ backscatter measurement angle.

2.2.7 *Yeast cell culture*

Yeast cells expressing the synthetic nanobody library⁸⁰ were cultured at 10^7 cells/mL in tryptophan deficient SD-Trp media (3.8 g/L yeast synthetic drop-out medium supplements without tryptophan, 6.7 g/L yeast nitrogen base, 20 g/L glucose, 100 U/mL penicillin-streptomycin, pH 6.0) at 30 $^{\circ}\text{C}$ and 250 rpm. Cell surface nanobody expression was induced by transferring the yeast to SG-Trp media (3.8 g/L yeast synthetic drop-out medium supplements without tryptophan, 6.7 g/L yeast nitrogen base, 20 g/L galactose, 100 U/mL penicillin-streptomycin, pH 6.0) at 10^7 cells/mL and incubating overnight at 25 $^{\circ}\text{C}$ and 250 rpm.

2.2.8 *Magnetic-activated cell sorting*

Two rounds of magnetic-activated cell sorting (MACS) were performed to select tau-binding nanobodies from the synthetic nanobody library. For each round of sorting, two negative sorts against magnetic Dynabeads Biotin Binder beads (Invitrogen) followed by one positive sort against tau-coated beads were performed. The positive sort for MACS Round 1 was conducted with 10^7 Dynabeads coated with 12.5 μg biotinylated tau

monomer, and for MACS Round 2 was conducted with 10^6 Dynabeads coated with 1.25 μg biotinylated tau monomer. Dynabeads were prepared according to the manufacturer's instructions. In brief, the beads were washed twice with PBS containing 0.1% bovine serum albumin (BSA) using a magnet and were incubated with biotinylated tau monomer in 500 μL (MACS Round 1) or 50 μL (MACS Round 2) 0.1% BSA in PBS overnight at 4 °C with rotation. Beads were also washed and incubated without biotinylated tau monomer for negative sorts against unlabeled beads.

Following the overnight incubation, the beads were washed once with 0.1% BSA in PBS and resuspended in 100 μL 0.1% BSA in PBS. Unlabeled Dynabeads were added to 10^{10} induced library cells (for MACS Round 1) or 10^9 induced MACS Round 1 cells (for MACS Round 2) and incubated for 1 h at room temperature with rotation. After 1 h, unbound yeast cells were collected with a magnet and this negative selection step was repeated once more. After the negative selections, the yeast cells were incubated with tau-coated beads for 1 h at room temperature with rotation. Unbound cells were discarded, and the beads were washed 5 times by first resuspending the beads in 1 mL 0.1% BSA in PBS, then using a magnetic tube rack, collecting the beads on the side of a 1.5 mL tube, and finally removing the 0.1% BSA in PBS and any cells in the tube not bound to the magnetic beads. The beads were transferred to 5 mL of SD-Trp media and yeast bound to the beads were cultured for 48 h at 30 °C and 250 rpm.

2.2.9 Fluorescence-activated cell sorting and individual nanobody selection

Following MACS, three rounds of fluorescence-activated cell sorting (FACS) were performed against tau monomer. Yeast cells from the previous sort were induced in SG-

Trp media and labeled for FACS. 10^7 induced cells were labeled with 300 nM, 100 nM, or 10 nM biotinylated tau monomer (for FACS Rounds 1, 2, and 3, respectively) and with an anti-HA tag rabbit antibody (Invitrogen, 1:200) in 100 μ L 0.1% BSA in PBS for 20 min at room temperature with rotation. The anti-HA antibody binds to an HA tag present in the polypeptide linker connecting the nanobody to the yeast cell wall and confirms nanobody expression on the yeast.⁸⁰ Cells were washed with 0.1% BSA in PBS and incubated with streptavidin R-phycoerythrin conjugate (Invitrogen, 1:250) and donkey anti-rabbit IgG Alexa Fluor 488 (Invitrogen, 1:500) in 100 μ L 0.1% BSA for 10 min on ice. Cells were washed with 0.1% BSA in PBS and sorted on a BD FACSAria Fusion cytometer. The selected yeast were transferred to 5 mL of SD-Trp media and cultured for 48 h.

Yeast from each FACS round were plated on SD-Trp plates (3.8 g/L yeast synthetic drop-out medium supplements without tryptophan, 6.7 g/L yeast nitrogen base, 20 g/L glucose, 100 U/mL penicillin-streptomycin, 15 g/L agar) and grown for 48 h at 30 °C. 15 colonies from each sort were randomly selected and used to inoculate 5 mL SD-Trp cultures. After 24-48 h, plasmid DNA was extracted from the yeast using a Zymoprep Yeast Plasmid Miniprep II kit (Zymo Research). The plasmids were transformed into NEB 5-alpha Competent *E. coli* cells (New England Biolabs) following the manufacturer's protocol. The *E. coli* cells were grown overnight in 5 mL LB media with 100 μ g/mL ampicillin at 37 °C with rotation. Plasmid DNA was extracted using the E.Z.N.A. Plasmid Mini Kit I (Omega Biotek) and sequenced by MCLAB (San Francisco, CA).

2.2.10 Flow cytometry

Flow cytometry was performed after MACS and FACS sorts or on individual nanobody-expressing yeast cultures to determine the extent of binding to tau monomer or tau oligomers. Yeast cells were induced in SG-Trp media and labeled for flow cytometry. 10^7 induced cells were labeled with biotinylated tau monomer or biotinylated tau oligomers and with an anti-HA tag rabbit antibody (Invitrogen, 1:200) in 100 μ L 0.1% BSA in PBS for 20 min at room temperature with rotation. Cells were washed with 0.1% BSA in PBS and incubated with streptavidin R-phycoerythrin conjugate (Invitrogen, 1:250) and donkey anti-rabbit IgG Alexa Fluor 488 (Invitrogen, 1:500) in 100 μ L 0.1% BSA for 10 min on ice. Cells were washed with 0.1% BSA in PBS and binding was analyzed on a CytoFLEX S flow cytometer (Beckman Coulter).

2.2.11 Expression and purification of bivalent and tetravalent MT3.1-Fc

Genes encoding bivalent and tetravalent MT3.1 nanobodies fused to a human IgG Fc were synthesized and cloned into the TGEX-HC plasmid (Antibody Design Labs) by Gene Universal (Newark, DE). In the tetravalent MT3.1-Fc construct, nanobodies are separated by a (GGGGS)₃ linker. These plasmids were transfected into Expi293F cells (Thermo Fisher Scientific) using the ExpiFectamine 293 Transfection Kit (Thermo Fisher Scientific) and protocol, and the Fc fusion proteins were expressed for six days. Cell cultures were then centrifuged at $5,000 \times g$ for 10 min, and the supernatant was loaded onto a 1 mL HiTrap MabSelect SuRe column (GE). Proteins were purified following the manufacturer's protocol and eluted with a 20 column volume linear gradient of 0.1 M sodium citrate, pH 3.5. These proteins were then dialyzed into PBS and their concentration

and purity were determined by BCA assay (Thermo Scientific) and SDS-PAGE, respectively.

2.2.12 Expression and purification of MT3.1, bivalent MT3.1(3) and MT3.1(10)

Genes encoding monovalent MT3.1, bivalent MT3.1(3) and bivalent MT3.1(10)—MT3.1 nanobodies connected by a (GGGGS)₃ or (GGGGS)₁₀ linker, respectively—with an N-terminal StrepTag-II and C-terminal 3x FLAG-tag and His-tag were synthesized and cloned into the pET-28b plasmid by Gene Universal (Newark, DE). These plasmids were transformed into BL21(DE3) *E. coli* (New England Biolabs) following the manufacturer's protocol. Transformed cells were used to start four 5 mL cultures in LB media with 50 µg/mL kanamycin. After incubating at 37 °C overnight with rotation, the 5 mL cultures were used to inoculate 1 L of 2xYT media with 50 µg/mL kanamycin and cells were grown at 37 °C and 225 rpm until they reached an OD₆₀₀ value between 0.6 and 0.8. Protein expression was induced with 0.5 mM IPTG overnight at 22 °C. The following day, cells were harvested by centrifugation at 7,000 × g for 7 min, resuspended in 25 mL lysis buffer (20 mM tris, 500mM NaCl, 20 mM imidazole, 5% glycerol pH 8.0 supplemented with protease inhibitor tablet [Sigma Aldrich], 0.5 mg/mL mg lysozyme, 125 units benzonase [Millipore Sigma]). Resuspended cells were kept on ice for 15 min with occasional mixing and a sodium deoxycholate solution was added to the cell slurry at a final concentration of 0.1%. Cells were sonicated for 3 min with 3 s on and 3 s off pulses at 25% amplitude. The cell suspension was centrifuged at 19,000 × g for 30 min to sediment cell debris and MT3.1 proteins of interest were purified from the supernatant with IMAC at 4 °C.

Cell lysate was loaded into a gravity flow column (G-Biosciences) with 2 mL HisPur Ni-NTA resin (Thermo Fisher Scientific) and washed with 80 mL IMAC equilibration buffer (20 mM tris, 500mM NaCl, 20 mM imidazole, 5% glycerol, pH 8.0). MT3.1 constructs were eluted with 10 mL IMAC elution buffer (20 mM tris, 500mM NaCl, 400 mM imidazole, 5% glycerol pH 8.0) and dialyzed into StrepTrap binding buffer (100 mM tris HCl, 150 mM NaCl, 1 mM EDTA, pH 8.0).

The proteins were next purified using a 1 mL StrepTrap HP (GE) column following the manufacturer protocol. MT3.1 constructs were eluted with six column volumes of elution buffer (100 mM tris, 150 mM NaCl, 1 mM EDTA, 2.5 mM desthiobiotin, pH 8.0) and concentrated with a 10 kDa MWCO centrifugal filter (Millipore Sigma). They were then further purified by SEC using a Superdex 200 Increase 10/300 GL column (Cytiva) in PBS. MT3.1 construct concentration and purity were determined by BCA assay (Thermo Scientific) and SDS-PAGE, respectively.

2.2.13 MT3.1 immunoblot characterization

Binding of MT3.1 to tau monomer, oligomers, and fibrils was characterized by dot blot and western blot. Dot blots were performed as described above with 0.5 μ g tau monomer, 0.5 μ g tau oligomers, and 0.1 μ g tau fibrils. 250 nM bivalent MT3.1-Fc in 5% milk in TBST and HRP-conjugated anti-human IgG goat secondary antibody (MP Biomedical, 1:5,000) in 5% milk in TBST were used during the primary and secondary antibody incubations, respectively.

Binding of MT3.1 to tau, amyloid- β , and α -synuclein fibrils was also characterized by dot blot. Dot blots were performed as described above with 0.3 μ g tau, amyloid- β , and

α -synuclein fibrils in 1 μ L PBS. 250 nM bivalent MT3.1-Fc in 5% milk in TBST and HRP-conjugated anti-human IgG goat secondary antibody (MP Biomedical, 1:5,000) in 5% milk in TBST were used during the primary and secondary antibody incubations, respectively.

Western blots were performed as described above with 4 μ g tau monomer or oligomers. 250 nM bivalent MT3.1-Fc in 5% milk in TBST and HRP-conjugated anti-human IgG goat secondary antibody (MP Biomedical, 1:5,000) in 5% milk in TBST were used during the primary and secondary antibody incubations, respectively.

2.2.14 MT3.1 binding epitope analysis

Epitope mapping of MT3.1 was first conducted using overlapping 15 amino acid peptides scanning the full length human tau sequence synthesized on PepSpots cellulose membranes (JPT Peptide Technologies, Berlin, Germany). Neighboring tau peptides overlapped by 11 amino acids. The peptide membrane was rinsed for 5 min with methanol and then washed three times for 3 min with TBST (50 mM tris, 137 mM NaCl, 2.7 mM KCl, 0.05% Tween-20, pH 8.0). The membrane was blocked with 5% milk in TBST at room temperature for 1 h and then incubated with 10 μ g/mL bivalent MT3.1-Fc (129 nM) in 5% milk in TBST at room temperature for 2 h. The membrane was then washed three times for 5 min with TBST, incubated with HRP-conjugated goat anti-human IgG (MP Biomedical, 1:5,000) in 5% milk in TBST at room temperature for 1 h, and then washed with TBST three times for 5 min. The membrane was incubated with SuperSignal West Femto Maximum Sensitivity Substrate (Thermo Scientific) for 1 min and imaged using the ChemiDoc MP imaging system (Bio-Rad).

To characterize the binding epitopes of MT3.1 with greater precision, an additional PepSpots membrane was manufactured with peptides based on information obtained from the initial round of epitope mapping. This membrane contained hit peptides from the original membrane as well as these peptides with glycine substitutions at either end of the peptide. Epitope mapping was performed as described above except 0.01 µg/mL bivalent MT3.1-Fc (0.129 nM) was used during the primary antibody incubation.

2.2.15 MT3.1 ELISA binding analysis

0.1 µg of tau monomer, oligomers, or fibrils in 50 µL PBS was added to the wells of a Nunc MaxiSorp 96-well flat-bottom plate (Invitrogen) and incubated overnight at 4 °C. The next day, unbound antigen was discarded, and the wells were blocked with 200 µL 5% BSA in PBST (PBS with 0.05% Tween-20) for 1 h. The wells were then washed three times with 200 µL PBST and primary antibodies tetraivalent MT3.1-Fc, bivalent MT3.1-Fc, bivalent MT3.1(3), bivalent MT3.1(10) and monovalent MT3.1 were added the wells. Three-fold dilutions of these antibodies ranging from 3 µM to 16.9 pM in 100 µL 1% BSA PBST were added to each well and incubated for 1 h. The wells were washed three times with 200 µL PBST and secondary antibodies were added for 1 h. To detect Fc fusion proteins, 100 µL HRP-conjugated goat anti-human IgG secondary antibody (MP Biomedical, 1:5,000) in 1% BSA PBST was used. To detect bivalent MT3.1(3), bivalent MT3.1(10), and MT3.1, 100 µL of an HRP-conjugated anti-6x-His-Tag secondary antibody (Invitrogen, 1:5,000) in 1% BSA PBST was used. The wells were washed three times with 200 µL PBST, and 100 µL TMB reagent (Millipore) was added to each well. Reactions were stopped with the addition of 100 µL 160 mM sulfuric acid, and absorbance at 450 nm was read with a BioTek Synergy H4 Microplate Reader and Gen5 software.

Binding data for each combination of tau antigen and MT3.1 antibody were fit to a binding isotherm using global nonlinear least squares regression.⁸¹ Maximum absorbance values for each repeat, which were used to normalize the data, and a single EC₅₀ value for each antigen and antibody combination were determined as fitted parameters across all three repeats. When binding did not near maximum binding (for His-tagged proteins bivalent MT.31(3), bivalent MT3.1(10) and MT3.1 binding to tau oligomers and MT3.1 binding to tau fibrils) and a maximum absorbance could not be fit to the data, the maximum absorbance was set as the average fitted maximum absorbance of binding by other His-tagged MT3.1 constructs.

2.2.16 Western blotting of transgenic mouse samples

Western blot analysis was conducted with hippocampus and somatosensory cortex tissue from wild-type and Tg4510 mice at 9 months old. Tissue lysates from Tg4510 mice on a FVB;B129 F1 genetic background were received from Massachusetts General Hospital. Hippocampi and somatosensory cortices were microdissected from the left hemisphere, then lysed using Bio-Plex cell lysis kit (Bio-Rad) according to the recommended protocol with the addition of one cComplete mini tablet (Roche) per 5 mL of lysis buffer solution. Lysed samples were end-over-end rotated at 4 °C for a minimum of 10 min, then centrifuged for 10 min at 13,200 rpm. Supernatant was transferred to fresh tubes and stored at -80 °C. Lysed tissue samples were thawed on ice then centrifuged at 4 °C and 13,000 × g for 10 min and total protein concentration was determined by BCA assay (Thermo Scientific). 30 µg of total protein was diluted in Laemmli Sample Buffer (Bio-Rad) and β-mercaptoethanol (BME) for a final BME concentration of 2.5% and heated at 65 °C for 5 min. PageRuler Plus Prestained Protein Ladder (Thermo Scientific) and lysate

samples were loaded into the wells of 4-12% Bis-Tris gels (Invitrogen) and the gels were run at 120 V for 50 min. The lysates were then transferred to 0.2 μ m polyvinylidene difluoride (PVDF) membranes using a Trans-Blot Turbo Mini 0.2 μ m PVDF Transfer Pack (Bio-Rad) and Trans-Blot Turbo Transfer System (Bio-Rad). The membranes were blocked with 5% BSA in TBST (20 mM tris, 150 mM NaCl, 0.1% Tween-20, pH 7.4) for 1 h at room temperature. The membranes were washed with TBST for 5 min and then incubated with Phospho-Tau (Ser202, Thr205) Monoclonal Antibody (AT8) (Invitrogen, 1:1,000) or Tau5 (Invitrogen, 1:5,000) and Tau13 (BioLegend, 1:1,000) in 5% BSA in TBST overnight at 4 °C. The membranes were washed three times for 10 min with TBST and incubated with goat anti-mouse IgG Alexa Fluor 647 (Invitrogen, 1:2,000) in 5% BSA in TBST for 1 h and washed three times again. Next, the membranes were incubated with 250 nM bivalent MT3.1-Fc in 5% BSA in TBST for 1 h at room temperature or overnight at 4 °C, washed three times, and incubated with goat anti-human IgG Alexa Fluor 488 (Invitrogen, 1:2,000) in 5% BSA in TBST. The membranes were then washed three times and imaged using the ChemiDoc MP imaging system (Bio-Rad). Next, antibodies were stripped from the membranes using Restore Western Blot Stripping Buffer (Thermo Scientific) for 1 h at 37 °C with shaking. The membranes were washed three times, blocked with 5% BSA in TBST for 1 h at room temperature, incubated with GAPDH antibody (GeneTex, 1:1,000) in 5% BSA in TBST overnight at 4 °C, washed three times, and incubated with goat anti-mouse IgG Alexa Fluor 647 (Invitrogen, 1:2,000) in 5% BSA in TBST for 1 h. The membranes were then washed three times and imaged using the ChemiDoc MP imaging system (Bio-Rad). The brightness and contrast of the fluorescent images was adjusted, and the color was inverted to provide better contrast between

fluorescent signal and background. The membranes were also stained with Ponceau S Solution (Rockland Immunochemicals) as described above.

2.3 Results and Discussion

2.3.1 Identification of tau-directed nanobodies

To develop a pan-tau nanobody, we first screened a synthetic nanobody library against full length (2N4R) human tau monomer.⁸⁰ The nanobody library was generated by the Kruse Lab at Harvard Medical School. This library consists of approximately 500 million unique nanobodies and was generated by the mutagenesis of residues within the CDRs guided by sequences of nanobodies reported in the Protein Data Bank (PDB). The framework regions of the nanobodies in the library were determined from a consensus sequence derived from llama VHH genes. These were combined with variable CDR sequences designed to recapitulate the natural amino acid composition seen in CDR residues in nanobodies of known structure in the PDB. CDR3 was designed to be 12, 16, or 20 residues long to mimic the natural CDR3 length diversity seen in nanobodies in the PDB. The nanobody library is covalently connected to the yeast cell wall through a 649-amino acid synthetic tether containing a C-terminal anchor sequence. The length of the tether was chosen to maximize accessibility of the displayed nanobody to a target antigen past cell wall glycans. The tether also contains an HA tag which is used for confirming the successful display of the nanobodies on the yeast surface.

The recombinant tau that we screened against contained three mutations, F8W, C291A, and C322A.⁸² The first mutation was introduced to increase the protein's absorbance at 280 nm and the ease of protein characterization. C291 and C322 were

mutated to alanines to prevent the formation of intra- and intermolecular disulfide bonds for improved purification of tau monomer.⁸² Tau monomer was expressed in BL21(DE3) *E. coli* and purified with immobilized metal affinity chromatography (IMAC) and size exclusion chromatography (SEC) (Figure 3a) and characterized by dynamic light scattering (Figure 3b), dot blots, and western blots (Figure 4).

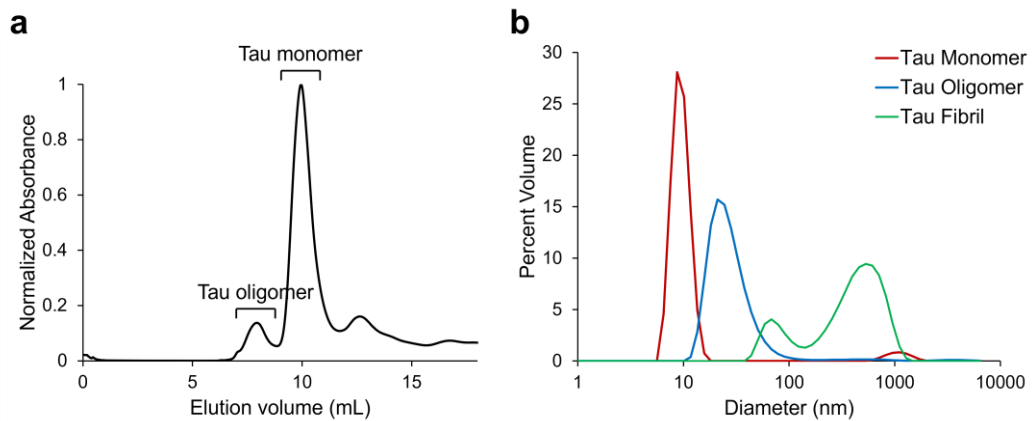


Figure 3. Size characterization of tau monomer, oligomers, and fibrils. a) Size exclusion chromatography trace for tau monomer and oligomers during purification of tau without a His-tag. b) Characterization of tau monomer, oligomers, and fibrils by dynamic light scattering.

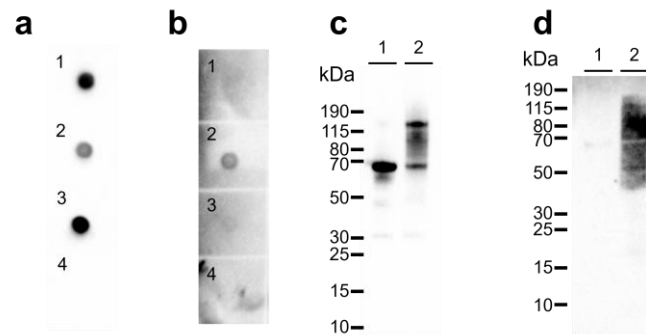


Figure 4. Immunoblot characterization of tau monomer, oligomers, and fibrils. a-b) Dot blots characterizing the binding of Tau5 antibody (a) and T22 antibody (b) to tau monomer (1), oligomers (2), fibrils (3), and BSA (4). c-d) Western blots characterizing the binding of Tau5 antibody (c) and T22 antibody (d) to tau monomer (lane 1) and oligomers (lane 2).

We performed two rounds of magnetic-activated cell sorting (MACS) and three rounds of fluorescence-activated cell sorting (FACS) of the nanobody library against tau monomer. After each sort, we performed flow cytometric analysis to evaluate the binding of the post-sort nanobody populations to tau monomer (Figure 5a). Each sort contributed to an enrichment of binding to tau. After each FACS round, 15 individual nanobodies were randomly selected and sequenced. Of the 45 nanobodies selected, only six sequences were unique (Figure 5b, Appendix Table 3). We assessed binding of a representative set of the selected nanobodies (MT2.1 or Nanobody 2, MT2.4 or Nanobody 4, and MT3.1 or Nanobody 6) to tau monomer using flow cytometry and observed much stronger binding of a lead nanobody, MT3.1, to tau monomer than the other nanobodies tested (Figure 5c). MT3.1 was also the only nanobody that was selected from FACS Round 3.

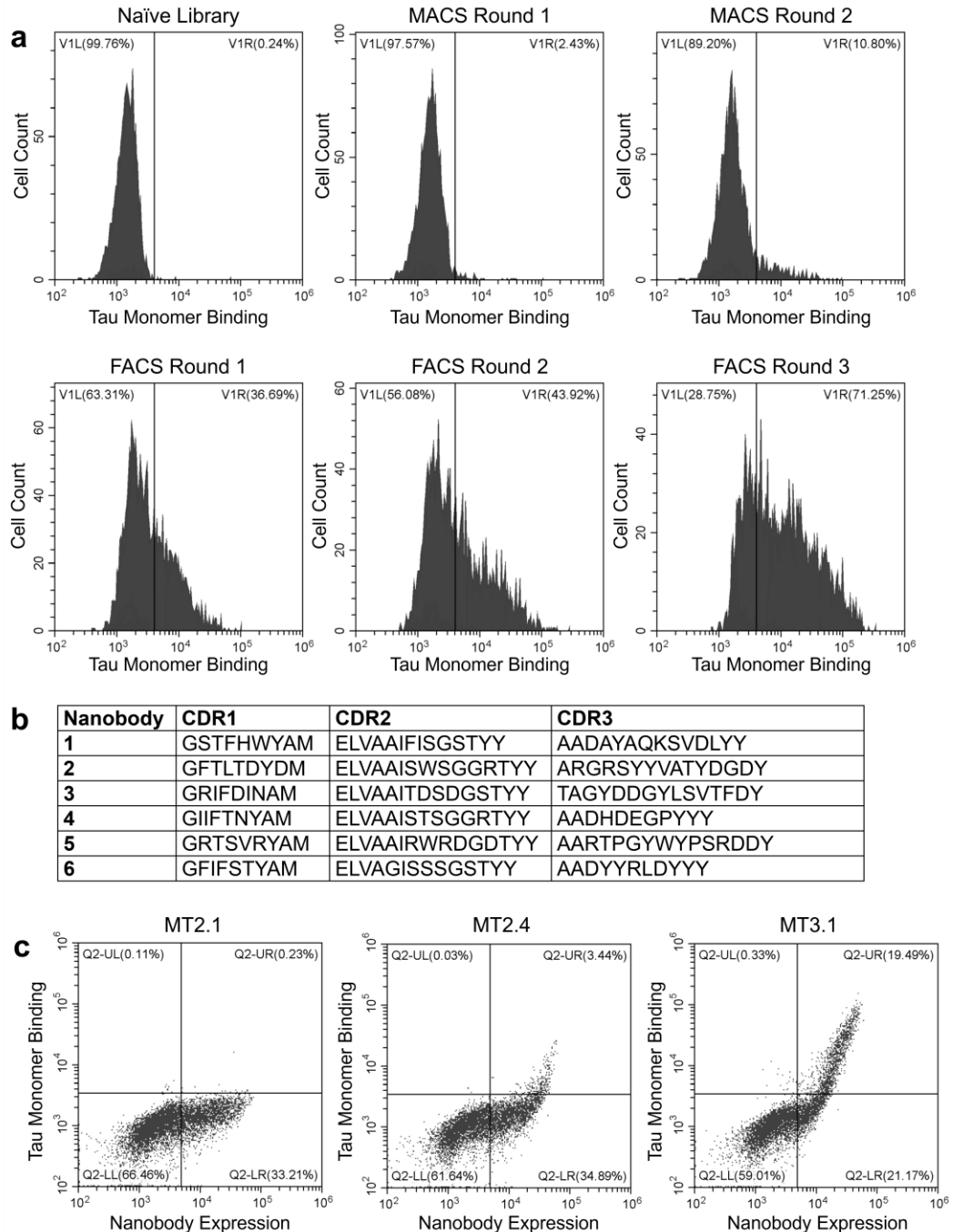


Figure 5. Selection of tau-directed nanobodies. a) A yeast surface display nanobody library was screened against tau monomer through two rounds of MACS and three rounds of FACS. After each sort, the selected yeast cells were incubated with 300 nM tau monomer and the extent of tau binding was assessed with flow cytometry. The fluorescence signal corresponding to tau binding to nanobodies displayed on yeast is plotted on the x-axis. Binding to tau above the level of the nanobody library appears on the right side of the vertical gate. b) CDR1, CDR2, and CDR3 sequences of the six nanobodies selected from sorts against tau monomer. c) Extent of tau binding to nanobodies MT2.1 (Nanobody 2),

MT2.4 (Nanobody 4), and MT3.1 (Nanobody 6) (y-axis) was assessed using flow cytometry. Yeast cells were incubated with 10 nM tau monomer. Expression levels of each nanobody on the surface of the yeast cells are shown on the x-axis.

2.3.2 Characterization of nanobody MT3.1

To facilitate characterization of MT3.1, we designed and expressed a bivalent MT3.1 fused to a human IgG Fc. To characterize binding of bivalent MT3.1-Fc to different forms of tau, we probed binding to tau monomer, oligomers, and fibrils using dot blots and western blots. Dot blots, shown in Figure 6a, demonstrated binding of bivalent MT3.1-Fc to all three forms of tau. Western blots were then performed to confirm binding to tau monomer and oligomers (Figure 6b). To further verify binding of MT3.1 to tau oligomers, we labeled yeast surface displayed MT3.1 with tau monomer and oligomers, and probed binding with flow cytometry. The results of this analysis show binding of MT3.1 to both tau monomer and oligomers (Figure 6c). To determine if MT3.1 discriminates between tau fibrils and fibrillar forms of other amyloid proteins involved in neurodegenerative diseases, we performed dot blots (Figure 6d) with tau, amyloid- β , and α -synuclein fibrils. These blots revealed that MT3.1 binds only to tau fibrils and not to the fibrils of the other amyloid proteins.

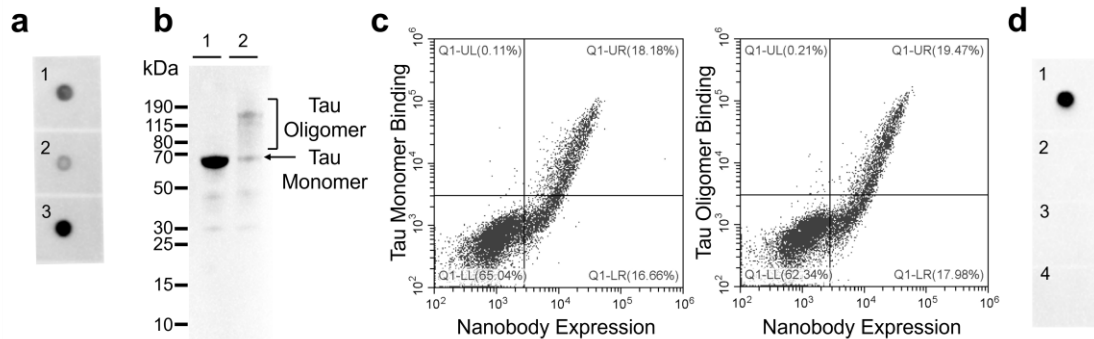


Figure 6. MT3.1 binds to recombinant tau monomer, oligomers, and fibrils. a) Dot blots with tau monomer (1), oligomers (2), and fibrils (3) reveal binding of bivalent MT3.1-

Fc to all three forms of tau. b) Characterization of the binding of MT3.1 to tau monomer (lane 1) and oligomers (lane 2) by western blot. c) Characterization of the binding of MT3.1 to 100 nM tau monomer and oligomers (y-axis) by flow cytometry. Expression level of MT3.1 on the surface of the yeast cells is shown on the x-axis. d) Dot blot with tau fibrils (1), amyloid- β fibrils (2), α -synuclein fibrils (3), and BSA (4) show binding of bivalent MT3.1-Fc to tau fibrils and not other amyloid fibrils.

Our characterization of MT3.1 demonstrated binding to monomeric tau and large and small tau aggregates with different conformations suggesting that MT3.1 may bind to an epitope within tau that is partially or fully exposed in all of these conformations. To determine precisely the epitope at which MT3.1 binds to tau, we performed epitope mapping. First, we probed the binding of bivalent MT3.1-Fc to 15-mer peptides scanning the full length human tau sequence with 11 amino acid overlaps. As shown in Figure 7a, bivalent MT3.1-Fc bound to four distinct epitopes on this membrane containing residues 117-139, 269-287, 297-319, and 381-403. To determine the minimal binding epitopes within these amino acid ranges, we performed additional epitope mapping. Binding of bivalent MT3.1-Fc to 15-mer peptides within residues 117-139, 269-287, 297-319, or 381-403 and containing glycine substitutions on either end of the peptide was evaluated (Figure 7b, c). From this analysis, we concluded minimal binding epitopes were ¹²⁵ARMVSK¹³⁰, ²⁷⁵VQIINK²⁸⁰, ³⁰⁶VQIVYK³¹¹, and ³⁹⁰AEIVYK³⁹⁵.

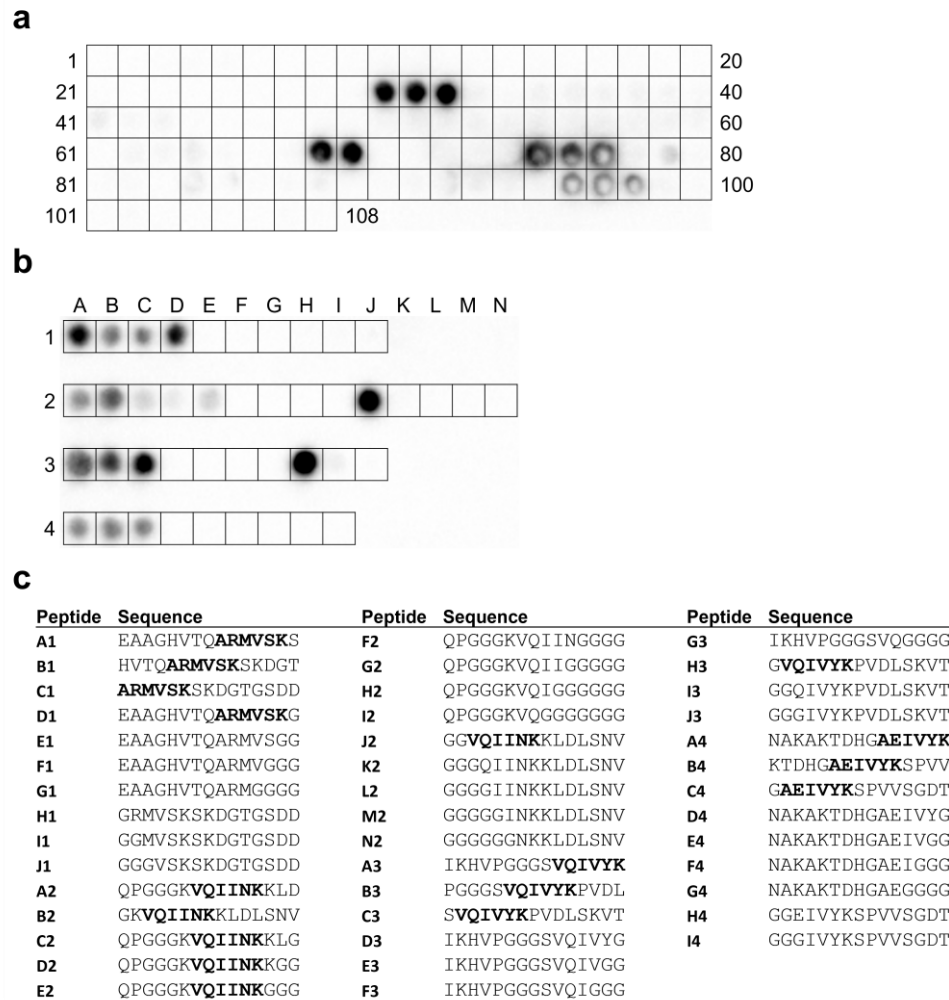


Figure 7. Identification of MT3.1 binding epitope. a) MT3.1 epitope mapping was performed with bivalent MT3.1-Fc and 108 15-mer peptides scanning the full length tau sequence. Peptides overlapped by 11 amino acids. Bivalent MT3.1-Fc bound to peptides 30-32, 68-69, 75-77, and 96-98 corresponding to tau residues 117-139, 269-287, 297-319, and 381-403. b) A second round of epitope mapping was performed. Bivalent MT3.1-Fc bound only to peptides containing the minimal binding epitopes ¹²⁵ARMVSK¹³⁰, ²⁷⁵VQIINK²⁸⁰, ³⁰⁶VQIVYK³¹¹, and ³⁹⁰AEIVYK³⁹⁵. c) Peptide sequences for the second round of epitope mapping are shown. The first three (row 1, 3, and 4) or two (row 2) peptides in each row are those that interacted with bivalent MT3.1-Fc in the first epitope mapping experiment. The following peptides in each row are glycine substitution mutants of these known binding peptides. The minimal binding epitopes identified are indicated in bold text.

Three of these epitopes, ²⁷⁵VQIINK²⁸⁰, ³⁰⁶VQIVYK³¹¹, and ³⁹⁰AEIVYK³⁹⁵, are within the MTBR of tau and close to or within the fibril core of tau.⁸³ The structured fibril core, residues 306-378, contain the amino acids that interact with each other in the core of

a tau fibril and is necessary and sufficient for the seeded assembly of tau fibrils.⁸³ Additionally, tau segments ²⁷⁵VQIINK²⁸⁰, ³⁰⁶VQIVYK³¹¹, also called PHF6* and PHF6, respectively, are known drivers of tau aggregation and seeding and mediate fibril formation.^{84,85} Our epitope mapping studies thus demonstrated that MT3.1 recognizes important aggregation-driving segments within tau.

2.3.3 *Design and characterization of multivalent pan-tau nanobodies*

To increase the binding avidity of MT3.1 towards tau aggregates, we designed and expressed additional multivalent MT3.1 constructs. In addition to our bivalent MT3.1-Fc, we created a tetravalent MT3.1-Fc, and two bivalent MT3.1 proteins without an Fc. These bivalent MT3.1 proteins were connected with a (GGGGS)₃ or (GGGGS)₁₀ linker, and we referred to them as bivalent MT3.1(3) and bivalent MT3.1(10), respectively. After expression and purification, the purity of these proteins was confirmed by SDS-PAGE (Figure 8a). Using ELISAs, EC₅₀s of binding to tau oligomers and fibrils were calculated for each construct (Figure 8b-d). The binding of the tetravalent and bivalent MT3.1 constructs was about 13- to 3300-fold stronger than the binding of the monovalent MT3.1 to tau oligomers and 170- to 1800-fold stronger than the binding of monovalent MT3.1 to tau fibrils. Tetravalent MT3.1-fc had the highest avidity to tau oligomers and fibrils with EC₅₀s of 14.2 nM and 6.94 nM, respectively. These results indicate that the increase in the valency of MT3.1 allows for increased binding to tau aggregates. We note that the barely detectable binding of monovalent MT3.1 to tau oligomers in this ELISA format contrasts with our results showing clear binding of MT3.1 to tau oligomers using flow cytometry (Figure 6c). We believe that these results reflect the greater sensitivity of detection by flow cytometry and are consistent with other reports of the detection of antibody binding using

flow cytometry at antigen concentrations multiple orders of magnitude below the dissociation constant (K_D) of their yeast surface displayed antibody fragments.^{86,87}

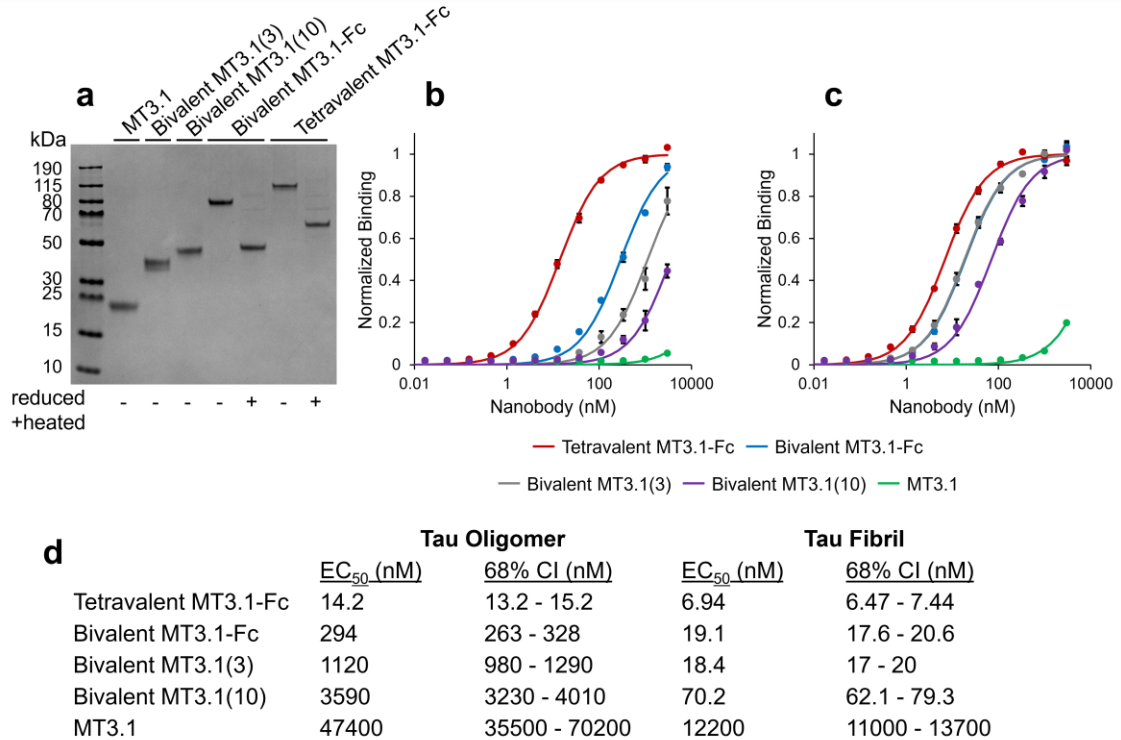


Figure 8. Characterization of multivalent MT3.1. a) Characterization of the purified monovalent and multivalent MT3.1 constructs by SDS-PAGE and stained by Coomassie blue dye. b-c) Binding of MT3.1 constructs to tau oligomers (b) and fibrils (c) was evaluated by ELISA. Data points are averages of three repeats and error bars indicate standard deviation. d) EC_{50} s for the binding of the MT3.1 constructs to tau oligomers or fibrils were calculated using a global nonlinear least squares fit of the data presented in Figure 8b and c, respectively.

2.3.4 MT3.1 detection of tau aggregates from mouse tissues

We next sought to demonstrate recognition by MT3.1 of pathological tau aggregates formed *in vivo* in a transgenic tauopathy mouse model. For this, homogenized tissue from the hippocampus and somatosensory cortex of Tg4510 mice was used. Tg4510 mice express human tau containing the P301L mutation, a mutation associated with familial frontotemporal dementia, and demonstrate tau pathology and neurodegeneration

similar to human tauopathies.⁸⁸⁻⁹⁰ Binding of phospho-tau antibody AT8 and bivalent MT3.1-Fc to the soluble fraction of homogenized brain samples from 9 month old Tg4510 and wild-type mice was evaluated (Figure 9a, b). Western blot analysis revealed strong binding of bivalent MT3.1-Fc to tau from Tg4510 mouse samples from both the somatosensory cortex and hippocampus tissues. A band at 59 kDa was stained by both AT8 and bivalent MT3.1-Fc and is seen more prominently in tissues from the Tg4510 mice compared to wild-type mice. This result indicates that although our nanobody selection was performed with unphosphorylated monomeric tau, MT3.1 recognizes aggregated, phosphorylated tau and can be used for the detection of pathological tau from mouse samples.

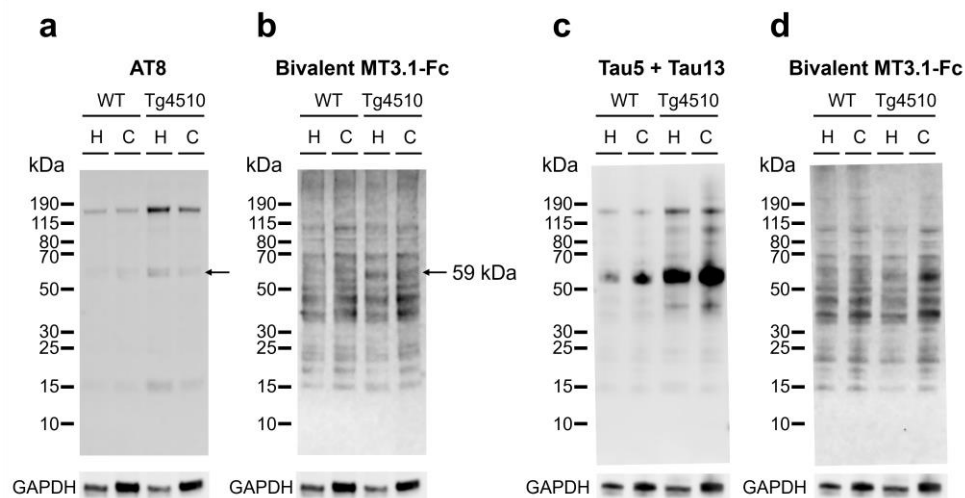


Figure 9. Western blotting of transgenic mice tissues. Characterization of binding of AT8 (a) and bivalent MT3.1-Fc (b) and Tau5 and Tau13 (c) and bivalent MT3.1-Fc (d) to hippocampus (H) and somatosensory cortex (C) tissue lysate from wild-type (WT) and Tg4510 mice was performed with western blotting. Blotting revealed a prominent band at 59 kDa in the Tg4510 samples stained by both AT8 and bivalent MT3.1-Fc.

In this western blot, we observed more binding of bivalent MT3.1 to the mouse lysates than expected, so to probe off-target binding by MT3.1 to the lysate samples, we conducted additional western blots and compared binding of bivalent MT3.1-Fc to pan-tau

antibodies Tau5 and Tau13. These blots revealed that most of the bands stained by bivalent MT3.1-Fc are also stained by Tau5 or Tau13, including tau fragments and aggregates not stained by AT8 (Figure 9c, d). This result supports the idea that MT3.1 is a pan-tau nanobody and not specific to phosphorylation status. Additionally, this result along with the specificity of MT3.1 to tau fibrils over other amyloid fibrils seen in Figure 6d, suggests that most of the bands stained by bivalent MT3.1 in the mouse lysate samples represent tau protein. In future work, the approaches used in this work could be applied for nanobody selection against tau aggregates, for instance to identify nanobodies that discriminate tau oligomers from monomer and fibrils.

2.4 Conclusions and Future Work

The development of antibodies targeting aggregate-forming proteins involved in disease has been limited by complex immunization and antibody selection strategies, antigen heterogeneity, and antigen presentation including valency and conformation.^{72,91,92} In this study, we have developed a simple approach to identifying nanobodies that bind to many forms of the aggregate-forming protein tau by first sorting a synthetic nanobody library against recombinant monomeric tau and then improving the nanobody's binding ability to tau oligomers and fibrils by creating multivalent nanobody constructs. Nanobodies are ideal candidates for development as binders to multimeric proteins, as they can be easily incorporated into multivalent constructs which allows for amplifications in binding avidity. Additionally, nanobodies are small and stable molecules that are easily expressed in bacteria and yeast.⁹

Screens of the nanobody library yielded a lead nanobody candidate, MT3.1, and binding of MT3.1 to tau monomer, oligomers, and fibrils was demonstrated. We determined MT3.1 discriminates between different amyloid fibrils and binds to only tau fibrils and not amyloid- β or α -synuclein fibrils. We found that MT3.1 binds to four epitopes on tau, three of which are close to or within the fibril core of tau. Two of these binding epitopes contain the amino acid sequence VQIXXX, which is a known motif that drives tau aggregation and seeding. We developed and characterized multivalent versions of MT3.1 and demonstrated increased binding of our multivalent MT3.1 constructs to tau oligomers and fibrils compared to the monovalent MT3.1. We assessed the binding ability of bivalent MT3.1-Fc to tissue lysate from the hippocampus and somatosensory cortex of a tauopathy mouse model. We observed strong binding of MT3.1 to the tissue lysates and an overlap between the binding of MT3.1 and phospho-tau antibody AT8 to these samples. These results indicate that our strategy to perform sorts against recombinant monomeric tau was successful in identifying a pan-tau nanobody capable of recognizing pathological and phosphorylated tau aggregates.

This work can be extended to the creation of multivalent nanobodies against other amyloid proteins including amyloid- β and α -synuclein, both of which are key proteins involved in neurodegenerative diseases. Our findings demonstrate significant progress towards the facile development of amyloid protein-directed antibodies and have the potential to guide the study, diagnosis, and treatment of tauopathies and other neurodegenerative diseases.

CHAPTER 3. MODIFICATION AND CHARACTERIZATION OF TAU FIBRIL-SELECTIVE ANTIBODIES

3.1 Introduction

Antibody- and nanobody-based discrimination between different conformations of the same protein has broad impacts, ranging from structural biology studies to the development of therapies for diseases associated with protein conformational changes. For instance, antibody fragments have frequently been generated to selectively recognize specific conformational states of membrane proteins, such as G-protein-coupled receptors^{93–102} as well as transport and channel proteins^{103–106}, stabilizing such proteins in particular states of activation or membrane orientation and allowing for elucidation of their structures and mechanisms. Nanobodies have also been generated to stabilize enzymes in various conformations to study their structural changes and better understand their mechanisms and overall functions.^{107–109} Furthermore, a limited number of nanobodies have also been developed to recognize conformational states of various proteins that undergo aggregation.^{110–112}

However, the potential of nanobodies to target aggregated antigens is relatively unexplored due to challenges involved in working with these complex, often insoluble antigens. In particular, the aggregation of amyloidogenic proteins represents a highly active area of research, and the development of nanobodies in this area has the potential to impact the understanding of a number of diseases associated with protein aggregation, especially neurodegenerative diseases such as Alzheimer's and Parkinson's diseases that are rapidly

growing in prevalence.^{113,114} Surprisingly, few nanobodies have been generated with both conformational and sequence specificity for amyloidogenic aggregates^{110–112}, and only one has been reported for a complex amyloidogenic protein (α -synuclein, 140 amino acids)¹¹⁰.

There is broad interest in developing conformational nanobodies against other complex amyloidogenic proteins, including tau, a large protein (441 amino acids for the longest isoform). However, to date no tau nanobodies have been reported with both conformational and sequence specificity, and only a few tau nanobodies have been reported that are sequence-specific^{70,71,76} or phospho-specific⁷⁵. The paucity of tau conformational nanobodies can be largely explained by the limitations of the methods used previously to generate them. The majority of previously reported nanobodies specific for amyloidogenic peptides and proteins have been isolated using either immunization followed by preparation and panning of phage libraries^{112,115,116} or direct panning of synthetic phage libraries^{70,71,111,117}. However, it is difficult to use either method, without extensive secondary screening, to routinely isolate nanobodies specific for amyloid aggregates with a combination of desirable binding properties, namely: i) high conformational specificity (i.e., strong preference for aggregates relative to monomeric protein) and ii) low off-target binding (i.e., low binding to non-tau proteins).

In this work, we, in collaboration with the Tessier Lab, have sought to address these challenges associated with generating antibody fragments with both conformational and sequence specificity for amyloid aggregates formed by large and complex proteins. To do this, the Tessier Lab used flow cytometric sorting of yeast displayed libraries to enable selection of antibody fragments that bind selectively to tau fibrils. We expressed multivalent Fc fusion versions of these antibody fragments and examined their specificity

for tau fibrils and their binding epitopes. Here, we report the results of the characterization of these conformational tau fibril-specific antibodies.²

In addition to improving sequence and conformational specificity, a critical consideration when designing tau-targeting antibody treatments for neurodegenerative diseases is the delivery of these antibodies across the blood-brain barrier (BBB) and into the brain. The BBB is a physical barrier composed of endothelial cells, pericytes, and astrocytes that restricts the passage of molecules from the blood into the extracellular fluid of the brain.¹¹⁸ The BBB allows for the entry of nutrients and signaling molecules while preventing the entry of most large proteins such as antibodies.¹¹⁹ Although a small fraction of systemically administered antibody drugs may pass through the BBB and enter the brain, a system that enhances delivery across the BBB would be beneficial to increase antibody concentration in the brain.

One method to deliver therapeutics across the BBB is receptor-mediated transcytosis (RMT). In RMT, a ligand binds to a receptor on endothelial cells lining capillaries within the brain, and the ligand and any molecules attached to it are endocytosed, transported through the cell, and released into the brain parenchyma.¹¹⁸ Drug cargos can be attached to these ligands and efficiently shuttled into the brain.

One target of RMT that has been widely and successfully used for drug delivery is the transferrin receptor (TfR). TfR imports iron bound to transferrin into cells¹²⁰ and is highly expressed on endothelial cells of the BBB¹²¹. Many antibodies and antibody

² Sections of this chapter are based on our work published in *Frontiers in Immunology*⁶⁶ and our work published as a preprint in *bioRxiv*⁶⁷.

fragments targeting TfR have been developed as molecular shuttles for drugs into the brain. For example, RO7126209 is an anti-amyloid- β antibody conjugated to an anti-TfR Fab. In a transgenic mouse model of AD, delivery of the anti-amyloid- β antibody conjugated to the TfR Fab shuttle to the brain increased by more than 50-fold compared to the anti-amyloid- β antibody alone.¹²²

In this work, we modified our tau fibril-targeting multivalent nanobodies to allow for their more efficient delivery to the brain. We have created and characterized bispecific Fc fusion constructs containing fibril-targeting and anti-TfR single-domain antibodies. We have confirmed the binding of the bispecific antibody shuttles to tau fibrils and TfR *in vitro* and discuss future work to evaluate the delivery and efficacy of these bispecific nanobodies in tau mouse models.

3.2 Materials and Methods

3.2.1 Expression and purification of bivalent and tetravalent P8.A1.A21

Genes encoding bivalent and tetravalent P8.A1.A21 nanobodies fused to a human IgG Fc were synthesized and cloned into the TGEX-HC plasmid (Antibody Design Labs) by Gene Universal (Newark, DE). In the tetravalent MT3.1-Fc construct, nanobodies are separated by a (GGGGS)₃ linker. These plasmids were transfected into Expi293F cells (Thermo Fisher Scientific) using the ExpiFectamine 293 Transfection Kit (Thermo Fisher Scientific) and protocol, and the Fc fusion proteins were expressed for six days. Cell cultures were then centrifuged at $5,000 \times g$ for 10 min, and the supernatant was loaded onto a 1 mL HiTrap MabSelect SuRe column (GE). Proteins were purified following the manufacturer's protocol and eluted with a 20 column volume linear gradient of 0.1 M

sodium citrate, pH 3.5. These proteins were then dialyzed into PBS and their concentration and purity were determined by BCA assay (Thermo Scientific) and SDS-PAGE, respectively.

3.2.2 *Competition ELISA*

0.05 μ g P301S tau fibrils (StessMarq) in 50 μ L PBS were coated onto a Nunc MaxiSorp 96-well plate (Invitrogen) overnight at room temperature. The next day, unbound antigen was discarded, and the wells were blocked with 5% BSA in PBST (PBS with 0.05% Tween-20) for 1 h then washed with PBST. 10 nM multivalent P8.A1.A21 constructs were preincubated with 0.1-1,000 nM tau monomer for 1 h in 1% BSA PBST, added to the 96-well plate, and incubated at room temperature for 1 h. The plate was washed with PBST, and HRP-conjugated goat anti-human IgG secondary antibody (MP Biomedical, 1:5,000) in 1% BSA PBST was added and allowed to incubate at room temperature for 1 h. Binding was quantified after the addition of TMB reagent (Millipore) and 160 mM sulfuric acid with a BioTek Synergy H4 Microplate Reader and Gen5 software.

3.2.3 *Antibody epitope analysis*

Peptide scanning of the epitope of bivalent WA2.22, ATA1.459.3, and P8.A1.A21 Fc fusion proteins was first performed using overlapping 15 amino acid peptides scanning the full length tau sequence synthesized on PepSpots cellulose membranes (JPT Peptide Technologies). Neighboring tau peptides had 11 overlapping amino acids. The peptide membranes were rinsed with methanol for 5 min and washed with TBST (50 mM Tris, 137 mM NaCl, 2.7 mM KCl, 0.05% Tween-20, pH 8.0) three times for 3 min. Membranes were

blocked with 5% milk in TBST at room temperature for 1 h. The membrane containing tau peptides was incubated with 0.1 $\mu\text{g}/\text{mL}$ WA2.22, 0.01 $\mu\text{g}/\text{mL}$ ATA1.459.3, or 0.02 $\mu\text{g}/\text{mL}$ P8.A1.A21 in 5% milk in TBST at room temperature for 2 h. Membranes were then washed with TBST three times for 5 min. Membranes were incubated with HRP-conjugated goat anti-human IgG (1:5,000) in 5% milk in TBST at room temperature for 1 h and were washed with TBST three times for 5 min. Membranes were incubated with SuperSignal West Femto Maximum Sensitivity Substrate (Thermo Scientific) for 1 min and imaged using the ChemiDoc MP imaging system (Bio-Rad).

To characterize the binding epitopes of these antibody fragments with greater precision, additional PepSpots membranes were manufactured with peptides based on information obtained from the initial rounds of epitope mapping. Epitope mapping with these membranes was performed as described above except 0.05 $\mu\text{g}/\text{mL}$ WA2.22, 0.005 $\mu\text{g}/\text{mL}$ ATA1.459.3, or 0.005 $\mu\text{g}/\text{mL}$ P8.A1.A21 was used during the primary incubation.

3.2.4 Expression and purification of bispecific antibody shuttles

Genes encoding the bispecific antibody shuttles or TfR only-binding constructs were synthesized and cloned into the TGEX-HC plasmid (Antibody Design Labs) by Gene Universal (Newark, DE). In the bispecific constructs, single-domain antibodies were separated by a (GGGGS)₃ linker. These Fc fusion proteins were expressed in Expi293F cells and purified as described above.

3.2.5 SDS-PAGE

0.5 μg of each protein sample was diluted in Nu-PAGE LDS sample buffer (Invitrogen). β -mercaptoethanol was added to reduced and heated samples at a final concentration of 70 mM, and the samples were heated at 98 $^{\circ}\text{C}$ for 10 min. PageRuler Plus Prestained Protein Ladder (Thermo Scientific) and protein samples were loaded into the wells of a 4-12% Bis-Tris gel (Invitrogen) and the gel was run at 120 V for 50 min. The gel was stained with Imperial Protein Stain (Thermo Scientific), destained, and imaged using the ChemiDoc MP imaging system (Bio-Rad).

3.2.6 ELISA

0.1 μg recombinant mouse TfR ectodomain (Sino Biological) and 0.1 μg P301S tau fibrils (StessMarq) in 50 μL PBS were coated onto a Nunc MaxiSorp 96-well plate (Invitrogen) overnight at 4 $^{\circ}\text{C}$ (TfR) or room temperature (tau fibrils). The next day, unbound antigen was discarded, and the wells were blocked with 5% BSA in PBST (PBS with 0.05% Tween-20) for 1 h then washed with PBST. 10 nM Fc fusion proteins in 1% BSA PBST were added to the 96-well plate and incubated at room temperature for 1 h. The plate was washed with PBST, and HRP-conjugated anti-mouse IgG antibody (Jackson ImmunoResearch, 1:5,000) in 1% BSA PBST was added and allowed to incubate at room temperature for 1 h. Binding was quantified after the addition of TMB reagent (Millipore) and 160 mM sulfuric acid with a BioTek Synergy H4 Microplate Reader and Gen5 software.

3.3 Results and Discussion

3.3.1 *Characterization of tau conformational nanobody WA2.22 specific for pathological aggregates*

To generate tau conformational nanobodies, our collaborators in the Tessier Lab first immunized a llama with tau fibrils and from the antibodies elicited, generated a yeast display immune nanobody library.⁶⁶ They then performed sorts using human tau fibrils immobilized on quantum dots (QD). From these sorts, nanobodies were selected and a lead clone, WA2.22, was identified (Appendix Table 4). WA2.22 was cloned as an Fc fusion protein, expressed, and purified. Using flow cytometry-based assays, the Tessier lab analyzed the affinity of WA2.22 (EC_{50} of 10.1 ± 1.5 nM) and the conformational specificity of WA2.22.⁶⁶ Their results revealed that WA2.22 displayed conformational specificity for tau aggregates over tau monomer.⁶⁶

We next examined the epitope of WA2.22 using epitope mapping (Figure 10). We first performed a scan of the WA2.22 epitope using a peptide array consisting of 15-mer peptides scanning the full length human tau sequence with 11 amino acid overlaps. This initial scanning identified a region near the C-terminus of tau that was recognized by WA2.22 (Figure 10a). We performed additional epitope mapping to identify the minimal binding epitope in this region. These results revealed that the minimal binding epitope was 425-LATLADEVSASL-436 (Figure 10b-d).

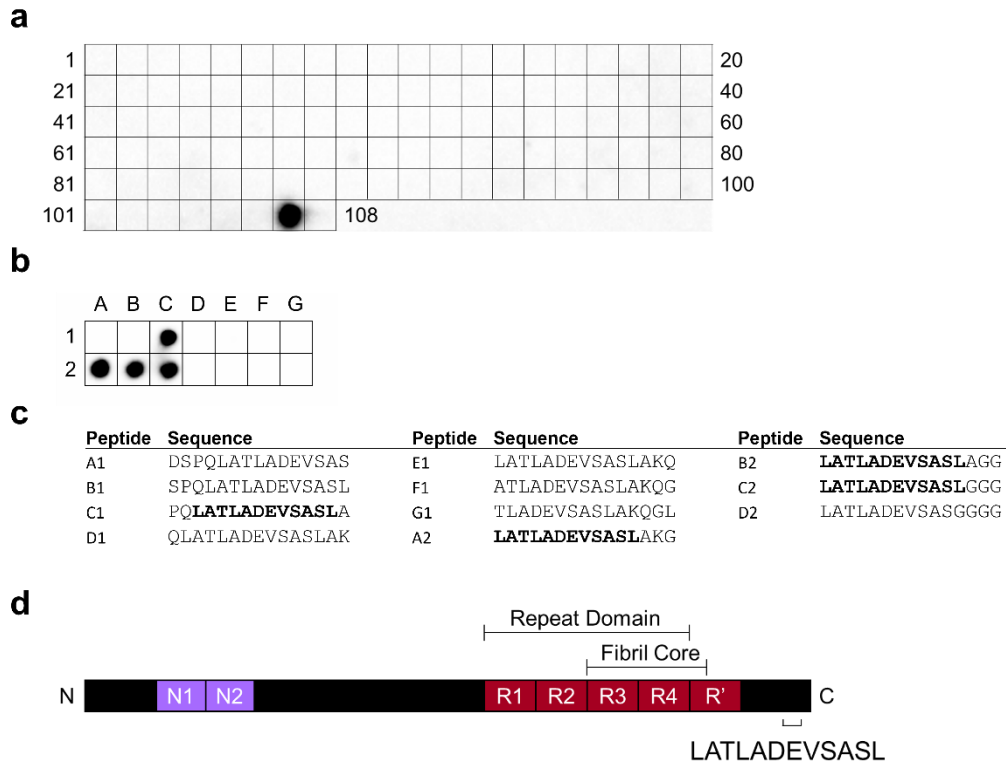


Figure 10. Identification of WA2.22 binding epitope. a) WA2.22 epitope mapping was performed with 108 15-mer peptides scanning the full length tau sequence. Peptides overlapped by 11 amino acids. b) A second round of epitope mapping was performed with the peptides listed in Figure 10c. This membrane contained peptides scanning the C-terminal region identified as the WA2.22 binding epitope in the first round of epitope mapping shifting by 1 amino acid (Peptides A1-G1) and contained glycine substitution mutants of the identified epitope from the first round of mapping (Peptides A2-D2). c) Peptide sequences for the second round of epitope mapping. Residues within the identified epitope are bolded for peptides in which WA2.22 binding was observed. d) A schematic of the 2N4R human tau sequence with the minimal binding epitope 425-LATLADEV SASL-436 indicated.

The Tessier Lab conducted additional analysis to show that WA2.22 selectively recognizes tau aggregates formed *in vivo* in both a transgenic mouse model and human tauopathies, and that WA2.22 has favorable biophysical properties such as low non-specific binding and a moderate melting temperature.⁶⁶

3.3.2 Characterization of tau fibril conformational antibody ATA1.459.3

To generate a second set of tau conformational nanobodies, our collaborators in the Tessier Lab took a simpler, alternative approach than the one taken to develop WA2.22.⁶⁷ This involved the *in vitro* screening of a single-chain (scFv) antibody library¹²³ against tau fibrils without the need for animal immunization. This scFv library was sorted against human tau fibrils immobilized on QD and from these sorts, a lead antibody was selected. Next, affinity maturation was performed on the lead clone and additional sorts were completed. The Tessier Lab evaluated the affinity and conformational specificity of scFv-Fc fusion proteins generated from these screens. One antibody which showed high conformational specificity for tau fibrils over tau monomer, ATA1.459.3 (EC₅₀ of 0.5 ± 0.1 nM), was chosen for further characterization (Appendix Table 4).⁶⁷

We next examined the epitope of ATA1.459.3 using peptide scanning (Figure 11). We first performed a coarse scan of the ATA1.459.3 epitope using a peptide array that consisted of 15 amino acid tau peptides—which were offset from each other by 4 amino acids—and covered the entire full length tau sequence (Figure 11a). This initial scanning identified a region near the N-terminus of tau that was recognized by ATA1.459.3. We further refined the epitope with a more detailed peptide scan, which revealed that tau residues 16-TYGL-20 are necessary for binding of ATA1.459.3 (Figure 11b-d).

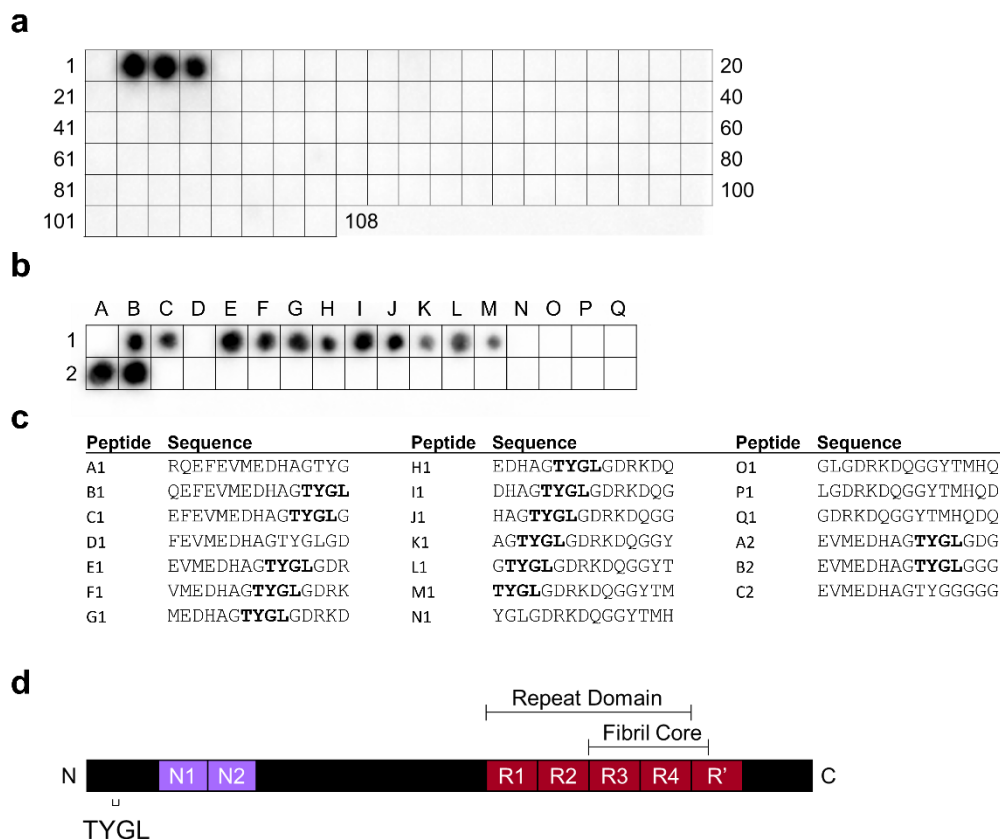


Figure 11. Peptide scanning analysis of ATA1.459.3 epitope. a) The epitope of ATA1.459.3 was first probed using a membrane containing 15-mer overlapping peptides for the full length 2N4R tau protein, which are shifted in an interval of four amino acids. The epitope was identified as an N-terminal region using this first array. b) A focused array containing overlapping tau 15-mer peptides from this N-terminal region, which differ by one amino acid, (Peptides A1-Q1) and glycine substitution mutants of the identified epitope from the first round of mapping (Peptides A2-C2) was then probed. These peptides are listed in Figure 11c. This refined scanning identified a more focused epitope containing residues 16-TYGL-20 of the tau protein. c) Peptide sequences for the second round of epitope mapping. Residues within the identified epitope are bolded for peptides in which ATA1.459.3 binding was observed. d) A schematic of the 2N4R human tau sequence with the minimal binding epitope 17-TYGL-20 indicated.

The Tessier Lab conducted additional analysis to show that ATA1.459.3 selectively recognizes tau aggregates formed *in vivo* in P301S mice and human tauopathies and that ATA1.459.3 has favorable biophysical properties such as low non-specific binding and a high melting temperature.⁶⁷

3.3.3 *MACS-based development and characterization of tau fibril-specific nanobody*

P8.A1.A21

A third antibody fragment, P8.A1.A21, was developed by our collaborators in the Tessier Lab using another unique method to identify tau fibril-specific binders. This method included only MACS-based positive selections against tau fibrils as traditional FACS-based selections with insoluble antigens, such as amyloid fibrils, are difficult to perform due to their particulate and insoluble nature.^{66,67,72,91} P8.A1.A21 was developed by the screening of a synthetic nanobody library created by the Tessier Lab against recombinant full length human tau fibrils. Initially six positive MACS screens and one negative FACS screen against tau monomer were performed. From the enriched library, a lead clone P8.HT40.5 was identified. Two rounds of affinity maturation of P8.HT40.5 and subsequent screens were performed to identify higher affinity nanobody P8.A1.A21 (Appendix Table 4).

We expressed, purified, and characterized bivalent and tetravalent Fc fusion versions of P8.A1.A21. We assessed the specificity of these constructs for tau fibrils relative to tau monomer using competition ELISAs. Binding of the P8.A1.A21 constructs to tau fibrils in the presence of up to 100-fold molar excess of tau monomer was measured and normalized to the binding of the multivalent nanobodies to fibrils in the absence of tau monomer. Figure 12 shows that the bivalent and tetravalent P8.A1.A21 constructs retained 92% and 100%, respectively, of their ability to bind to fibrils in the presence of 10-fold excess tau monomer and their binding only decreased to 71% and 99%, respectively, with 100-fold excess tau monomer. In comparison, the binding of Tau5, a non-conformational sequence-specific tau antibody, begins to decrease at equimolar concentrations of tau monomer and

fibrils. At 10- and 100-fold excess tau monomer, the binding of Tau5 to tau fibrils decreases to 35% and 16%, respectively. These results demonstrate the specificity of the multivalent P8.A1.A21 constructs for tau fibrils over tau monomer and suggest that P8.A1.A21 may bind to a conformational epitope on tau fibrils not present on tau monomer. Additionally, these results indicate that an increase in valency from two to four nanobodies contributes to increased specificity for tau fibrils over monomer.

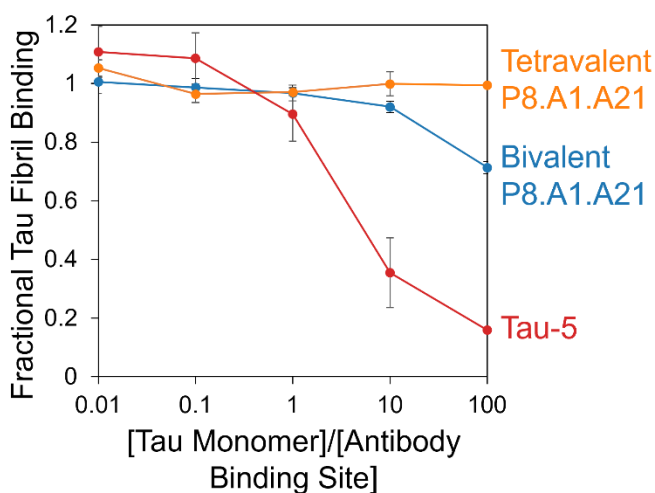


Figure 12. Conformational specificity of P8.A1.A21. Competition ELISAs with tau fibrils (immobilized antigen) and tau monomer (soluble competitor) were conducted to investigate the specificity of bivalent and tetravalent P8.A1.A21 Fc fusion proteins for tau fibrils over tau monomer. Tau fibril binding in the presence of tau monomer is shown relative to tau fibril binding in the absence of tau monomer. Tau5, a sequence-specific antibody, was used as a negative control for selectivity. Error bars show standard error; n = 4 technical repeats from 2 independent assays.

We next determined the epitope of P8.A1.A21 using epitope mapping (Figure 13). We first performed a scan of the P8.A1.A21 epitope using a peptide array consisting of 15-mer peptides scanning the full length human tau sequence with 11 amino acid overlaps. This initial scanning identified a region near the C-terminus of tau that was recognized by P8.A1.A21 (Figure 13a). We performed additional epitope mapping to identify the minimal binding epitope in this region. These results revealed that the minimal binding epitope was

424-QLATLADEV-432 (Figure 13b-d). This is an almost exact match of the minimal binding epitope of conformational fibril-specific nanobody WA2.22 (425-LATLADEV SASL-436) suggesting that P8.A1.A21 may interact with tau fibrils in a manner very similar to WA2.22 and also conformationally and selectively recognize tau aggregates formed *in vivo* in both a transgenic mouse model and human tauopathies.

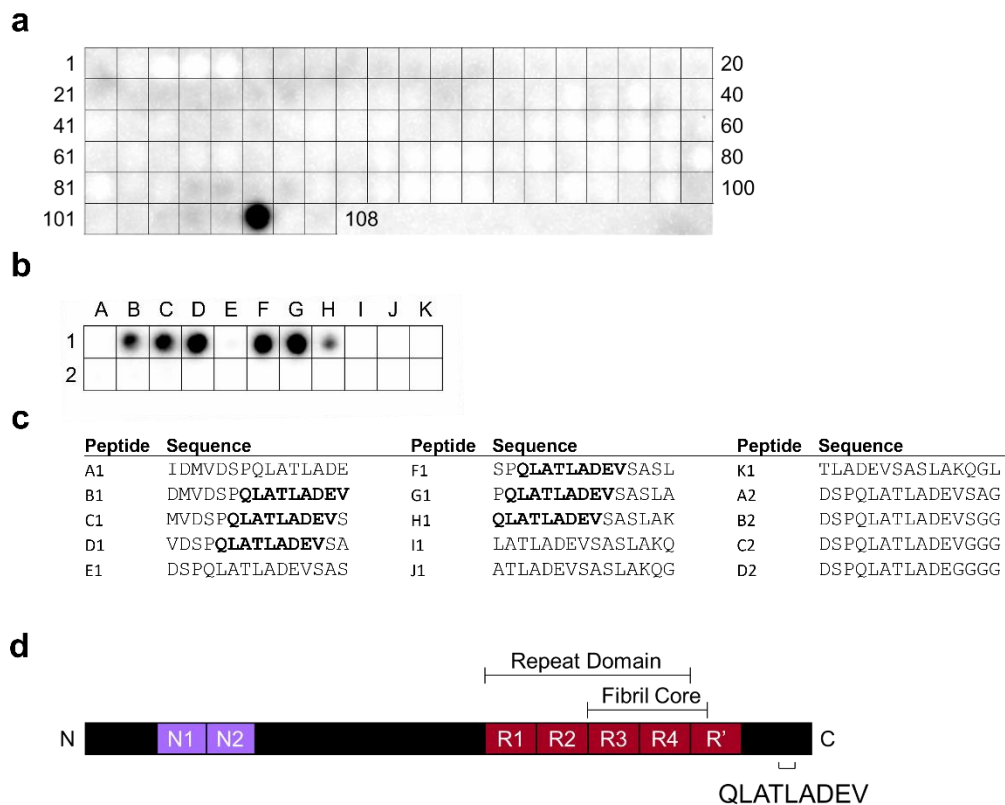


Figure 13. Identification of P8.A1.A21 binding epitope. a) P8.A1.A21 epitope mapping was performed with 108 15-mer peptides scanning the full length tau sequence. Peptides overlapped by 11 amino acids. b) A second round of epitope mapping was performed with the peptides listed in Figure 13c. This membrane contained peptides scanning the C-terminal region identified as the P8.A1.A21 binding epitope in the first round of epitope mapping shifting by 1 amino acid (Peptides A1-K1) and contained glycine substitution mutants of the identified epitope from the first round of mapping (Peptides A2-D2). c) Peptide sequences for the second round of epitope mapping. Residues within the identified epitope are bolded for peptides in which P8.A1.A21 binding was observed. d) A schematic of the 2N4R human tau sequence with the minimal binding epitope 424-QLATLADEV-432 indicated.

3.3.4 Modification of fibril-specific nanobodies to improve their delivery across the BBB

To increase the delivery of our multivalent tau fibril-specific nanobodies WA2.22 and P8.A1.A21 across the BBB, we have modified them through the addition of a TfR-targeting single-domain antibody. These bispecific antibody shuttles contain two copies of a fibril-binding nanobody and two copies of a TfR-binding single-domain antibody arranged in different orientations and genetically fused to a mouse Fc domain (Figure 14a, b). High affinity TfR-directed VNAR F02, developed by Häsler et al.¹²⁴, and lower affinity nanobody VHHA, developed by Cohen et al.¹²⁵, were incorporated into our bispecific antibodies (Appendix Table 5). We have expressed, purified, and characterized bispecific antibodies WA2.22-F02-Fc, F02-WA2.22-Fc, WA2.22-VHHA-Fc, VHHA-WA2.22-Fc, and P8.A1.A21-F02-Fc as well as control antibodies F02-Fc and VHHA-Fc containing only a TfR-targeting single-domain antibody (Figure 14c). Characterization of these purified constructs by SDS-PAGE is shown in Figure 15a.

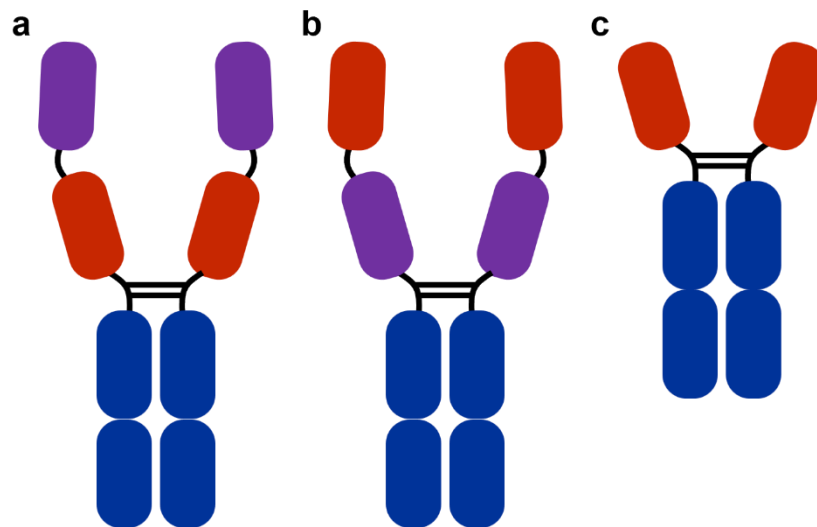


Figure 14. Design of bispecific antibody shuttles. a) A depiction of bispecific antibody shuttles WA2.22-F02-Fc, WA2.22-VHHA-Fc, and P8.A1.A21-F02-Fc with tau fibril-binding nanobodies (purple), TfR-binding single-domain antibodies (red), and a mouse Fc

(blue). b) A depiction of bispecific antibody shuttles F02-WA2.22-Fc and VHHA-WA2.22-Fc with TfR-binding single-domain antibodies (red), tau fibril-binding nanobodies (purple), and a mouse Fc (blue). c) A depiction of TfR only-binding constructs F02-Fc and VHHA-Fc with TfR-binding single-domain antibodies (red) and a mouse Fc (blue).

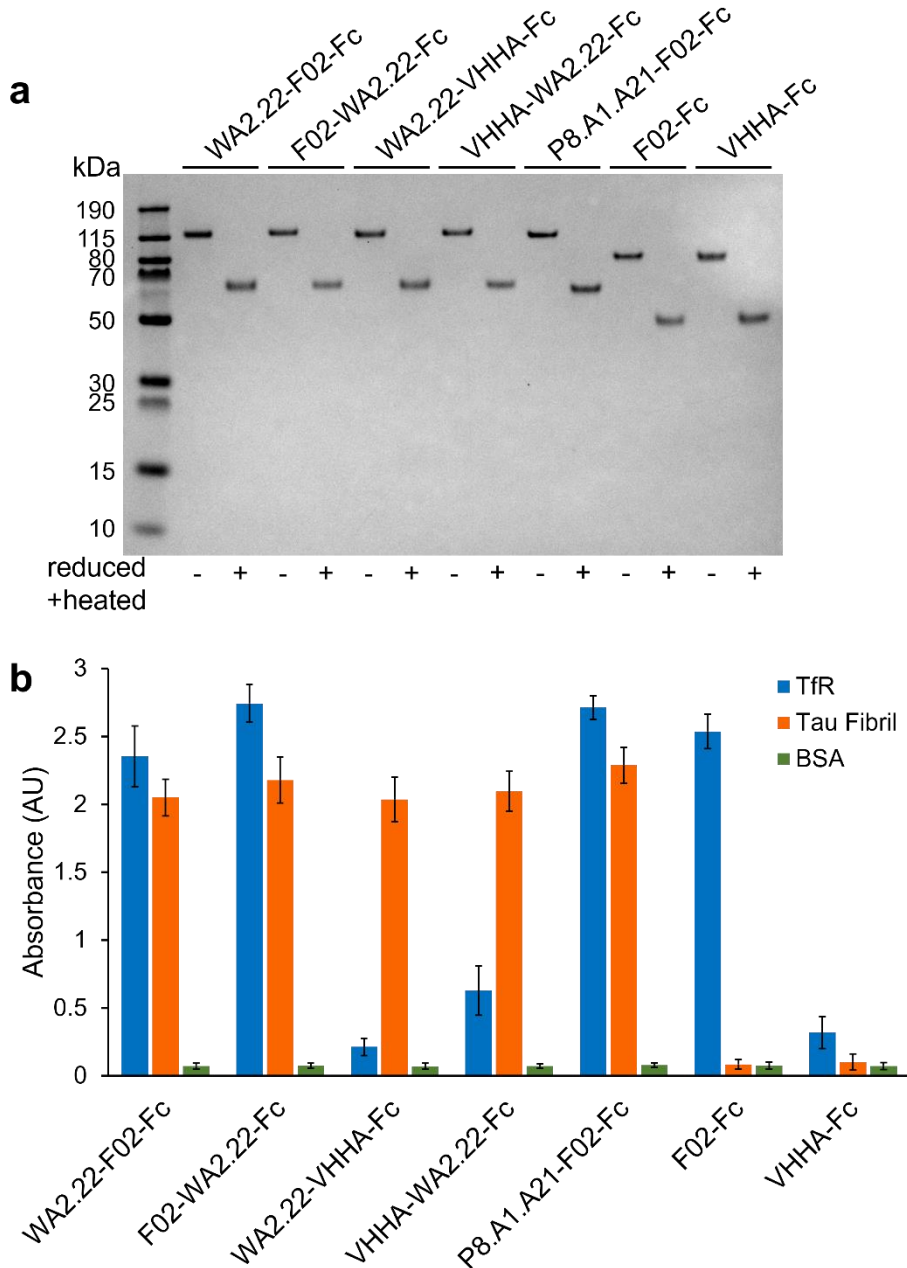


Figure 15. Bispecific antibody shuttle characterization. a) The purified bispecific antibody shuttles and TfR-binding constructs were analyzed by SDS-PAGE. b) ELISAs were conducted to assess the binding of the bispecific antibody shuttles and TfR-binding constructs to recombinant mouse TfR ectodomain, full length human tau fibrils, and BSA.

Data points are averages from six repeats from two independent assays and error bars indicate standard deviation.

ELISA binding analysis revealed that all bispecific antibody shuttles bound to their two target antigens, TfR and tau fibrils (Figure 15b). These results also demonstrated that i) binding to either antigen is not affected by the order of the single-domain antibodies fused to the Fc and ii) the addition of a tau-binding nanobody did not reduce the ability of F02 or VHHA to bind to TfR. This suggests that these bispecific shuttles may be good candidates for improved delivery of tau fibril nanobodies across the BBB and motivates future *in vivo* studies to investigate this idea further.

3.4 Conclusions and Future Work

In this chapter we describe the characterization of three conformational tau fibril-specific antibody fragments WA2.22, ATA1.459.3, and P8.A1.A21, isolated through three different methods: i) llama immunization with tau fibrils and subsequent FACS-based screening using tau fibrils captured on QD; ii) *in vitro* FACS-based screening of an scFv library against tau fibrils captured on QD without the need for animal immunization; and iii) *in vitro* screening using only MACS selections against tau fibrils immobilized on magnetic beads, respectively.

Specificity analysis with all three antibodies revealed that they demonstrate high conformational specificity for tau fibrils relative to tau monomer. Epitope mapping revealed that nanobodies WA2.22 and P8.A1.A21 bind to almost identical epitopes on tau, suggesting that P8.A1.A21 may also conformationally and selectively recognize tau aggregates formed *in vivo* in transgenic mouse and human tauopathies and have similar biophysical properties to WA2.22. To the best of our knowledge, these nanobodies,

WA2.22 and P8.A1.A21, are the first reported conformational nanobodies that recognize tau fibrils.

Due to the favorable binding and biophysical properties of these reported antibody fragments, they have the potential to be critical in studying differences in tau fibril morphology present in different tauopathies, understanding the progression of tau aggregation, and testing the effects of targeting tau aggregates using *in vivo* models of neurological disease.

In the last part of this work, we developed bispecific antibody shuttles with our tau fibril-targeting nanobodies WA2.22 and P8.A1.A21 to improve their delivery across the BBB. To these Fc fusion nanobody constructs, we added single-domain antibodies that bind to TfR, which is abundant on endothelial cells of the BBB. We show that these bispecific antibody shuttles bind to TfR ectodomain and tau fibrils in an ELISA format. Future work can be conducted to evaluate the delivery of our antibody shuttles and their ability to bind to pathological tau fibrils after an intravenous administration in P301S tau mice. These experiments would involve the measurement of antibody shuttle concentration in the brain and blood to determine an optimal dose and treatment frequency to maintain nanomolar concentrations of the shuttles in the brain. Additionally, binding to tau fibrils in the brain would be assessed by immunostaining of mouse brain sections. The antibody shuttles that show the best binding to tau fibrils and least off-target binding in the brain would then be tested for their ability to inhibit tau seeding following the injection of tau fibrils and subsequent ability to reduce tau pathology and cognitive decline in P301S tau mice.

CHAPTER 4. GENERATION OF NANOBODIES WITH CONFORMATIONAL SPECIFICITY FOR AMYLOID OLIGOMERS

4.1 Introduction

Neurodegenerative diseases that involve the misfolding and deposition of aggregates of the protein tau, termed tauopathies, are among the most common neurodegenerative diseases and include Alzheimer's disease (AD) and other less widespread disorders such as progressive supranuclear palsy, Pick's disease, and corticobasal degeneration.²⁴ Despite the growing burden of tauopathies, there are few options for safe and effective disease-modifying treatments for them.³² In addition to the lack of effective therapies for tauopathies, there is a need for better diagnostics and research tools to study these diseases. Conformational antibodies that target aggregates of the amyloidogenic proteins involved in neurodegenerative diseases, namely tau, amyloid- β , and α -synuclein, are promising candidates for treatments to slow the progression of neurodegenerative diseases and are useful as reagents to understand the aggregation of amyloid proteins and the role of aggregation in disease progression.^{65,126–129}

In AD, tau becomes hyperphosphorylated and undergoes other post-translational modifications leading to its dissociation from microtubules, misfolding, and aggregation into oligomers and larger fibrils, the primary component of neurofibrillary tangles (NFTs).¹³⁰ Many studies have indicated that soluble tau oligomers, and not fibrils, are the most toxic form of tau.^{31,130–134} Prefibrillar soluble aggregates or oligomers and protofibrils

of tau, not NFTs, correlate with cognitive deficits in transgenic mice models of AD and in humans.^{132,133} Additionally, small, soluble oligomers, rather than fibrils, are prion-like in nature, display seeding behavior, and are responsible for the spread of tau pathology throughout the brain.^{31,133} Finally, oligomers, not fibrils, propagate or induce toxic effects *in vivo*.¹³⁴ For example, when administered to wild-type mice, tau oligomers, not monomer or fibrils, induce synaptic damage, mitochondrial dysfunction, and cognitive deficits.¹³⁴ This evidence suggests that tau oligomers are an attractive target for passive immunotherapy.

Many groups have developed antibodies that interact with tau oligomers, but few antibodies are available that conformationally and specifically target tau oligomers.^{38,62,68,135} Castillo-Carranza et al. report the development of a tau oligomer-specific monoclonal antibody (TOMA), via the immunization of mice with tau oligomers formed spontaneously from recombinant tau monomer.¹²⁷ They found that a single injection of TOMA in P301L tau (JNPL3) mice, a mouse model of tauopathy, or in htau mice (over-expressing human tau) along with the administration of brain-derived tau oligomers, conferred protection against the accumulation of tau oligomers and locomotor and memory deficits.^{65,127} TOC1, a mAb that binds dimeric and larger tau oligomers but not fibrils, was developed by Patterson et al. by immunization of mice with cross linked tau dimers and oligomers.¹³⁶ When used to stain human tissue from an AD patient, TOC1 colocalizes with Tau pS422, an early marker of tau pathology, and not with NFT markers.¹³⁶ Tai et al. describe the development of APNmAb005, a mAb that preferentially binds early-stage oligomers over tau monomer and late-stage oligomers through the immunization of mice with tau aggregates encapsulated in artificial vesicles.⁴² In a

tauopathy mouse model, rTg4510, treatment with APNmAb005 partially rescued neuronal loss.⁴² Ongoing phase I clinical trials with a humanized APNmAb005 began in May 2022.

The success of these approaches emphasizes the diagnostic and therapeutic value of antibodies targeting tau oligomers. In this work, we have taken a different approach focused on nanobodies or single-domain antibodies. Specifically, we have generated conformational, tau oligomer-specific nanobodies through the screening of a synthetic yeast surface display nanobody library against recombinant tau oligomers. Nanobodies display high binding affinity and selectivity towards a target antigen, high thermal stability, and can be expressed in bacteria and yeast cells.⁹ Because of their single-domain nature, they are easily engineered in a multivalent format to enhance avidity. Their small size and extended CDR3 loop allow them to bind concave or less accessible epitopes on antigens.¹³⁷

While a few tau-targeting nanobodies have been developed^{66,67,70,71,75–79,138}, to our knowledge, there are no reports of conformational tau oligomer-specific nanobodies. A few nanobodies specific for oligomers of the small amyloidogenic peptide amyloid- β have been identified^{112,139,140}; however, no conformational nanobodies specific for oligomers of α -synuclein, another large amyloidogenic protein, have been developed either. The development of amyloid oligomer-specific nanobodies is thus a relatively unexplored field.

Here, we establish a method to develop conformational nanobodies that bind specifically to tau oligomers over monomer or fibrils and identify and characterize two of these tau oligomer-specific nanobodies. We show that our nanobodies bind to nonoverlapping epitopes on tau, which are exposed and properly folded only in the oligomeric conformation. Our nanobodies bind to tau oligomers of various sizes present in

the brains of older adults and AD patients. Because of their smaller size and the shape of their paratope, these single-domain antibodies likely interact with tau oligomers at three-dimensional epitopes different from the previously reported tau oligomer monoclonal antibodies. We have begun work to show that our *in vitro* discovery method for identifying oligomer-specific nanobodies is generalizable to other amyloid proteins by screening the same yeast surface display nanobody library against amyloid- β oligomers. The nanobodies generated in this study could be developed into disease-modifying treatments for AD and other tauopathies and are valuable reagents for the identification and characterization of tau oligomers.

4.2 Materials and Methods

4.2.1 Expression and purification of tau monomer and oligomers

The gene encoding 2N4R human tau with mutations F8W, C291A, C322A was synthesized and cloned into the pET-28b plasmid without a His-tag by Gene Universal Inc. (Newark, DE). This mutant 2N4R tau was expressed and purified as described previously.⁷⁹ The tau-containing plasmid was transformed into BL21(DE3) *E. coli* (New England Biolabs) according to the manufacturer's protocol. Four 5 mL cultures of LB media with 50 $\mu\text{g}/\text{mL}$ kanamycin were inoculated with the transformed *E. coli*. The culture was incubated overnight at 37 °C with rotation. The next day, the four 5 mL cultures were used to inoculate 1 L of LB media with 50 $\mu\text{g}/\text{mL}$ kanamycin. The culture was grown until it reached an OD_{600} value between 0.6 and 0.8 at 37 °C and 225 rpm. 0.9 mM IPTG was added to the culture to induce protein expression, and the culture was incubated with rotation at 225 rpm overnight at 22 °C.

The next day, the cells were pelleted by centrifugation at $7,000 \times g$ for 7 min and resuspended in 20 mL lysis buffer (20 mM tris, 100 mM NaCl, 1 mM EDTA, 1 mM PMSF, protease inhibitor tablet [Sigma Aldrich]). The cell slurry was sonicated eight times at 25% amplitude with 40 s on and 60 s off pulses, and centrifugation at $15,000 \times g$ for 10 min was used to separate the cell debris from the lysate. The lysate was boiled in a water bath at 100 °C for 30 min, and then the boiled lysate was centrifuged at $15,000 \times g$ for 10 min. The pellet containing precipitated, denatured proteins was discarded, and tau was purified from the supernatant using immobilized metal affinity chromatography (IMAC). 2.5 mL of HisPur Ni-NTA resin (Thermo Fisher Scientific) was mixed with the tau-containing supernatant for 1 h at 4 °C. The resin slurry was then loaded into a gravity flow column (G-Biosciences), and the resin was washed with 20 mL IMAC equilibration buffer (20 mM tris HCl, 500 mM NaCl, pH 8.0). Tau was eluted in 8 mL of imidazole-containing elution buffer (20 mM tris HCl, 500 mM NaCl, 100 mM imidazole, pH 8.0) and then concentrated with a 10 kDa MWCO centrifugal filter (Millipore Sigma). To separate tau monomer from spontaneously forming tau oligomers, size exclusion chromatography (SEC) with a Superdex 200 Increase 10/300 GL column (Cytiva) in PBS (137 mM NaCl, 2.7 mM KCl, 10 mM Na₂HPO₄, 1.8 mM KH₂PO₄, pH 7.4) was conducted. Tau monomer and oligomer concentrations were determined by BCA assay (Thermo Scientific) and protein purity was confirmed by SDS-PAGE.

4.2.2 *Tau biotinylation*

EZ-Link Sulfo-NHS-LC-Biotin (Thermo Scientific) was used to biotinylate tau monomer and oligomers according to the manufacturer's protocol. The biotinylated protein was buffer exchanged into TBS (20 mM tris HCl, 100 mM NaCl, pH 7.4) with a 10 kDa

MWCO centrifugal filter (Millipore Sigma) to remove excess biotin reagent. The extent of biotinylation was measured by characterizing mixtures of streptavidin (Rockland Immunochemicals) and biotinylated tau monomer or oligomers with SDS-PAGE at 4 °C.

4.2.3 *Tau fibril formation*

To form tau fibrils, 5 μ M tau monomer, 2.5 μ M heparin, and PBS were mixed in a final volume of 1 mL. This mixture was incubated at 37 °C at 250 rpm for 3-4 days. To remove leftover tau monomer, the tau fibrils were buffer exchanged with a 100 kDa MWCO centrifugal filter (Millipore Sigma) into HEPES buffer (20 mM HEPES, 100 mM NaCl, 1 mM EDTA, pH 7.4), and fibril concentration was determined by the BCA assay (Thermo Scientific).

4.2.4 *Dynamic light scattering*

100 μ L of tau monomer, oligomers, or fibrils at 70 μ g/mL were added to a ZEN0040 cuvette (Malvern) and loaded into a Zetasizer Nano ZS instrument (Malvern). Zetasizer software (Malvern) was used to record 5 size measurements per sample at 25 °C using refractive index and absorption parameters for a protein sample in PBS with a 173° backscatter measurement angle.

4.2.5 *SDS-PAGE*

1 μ g of protein was diluted in Nu-PAGE LDS sample buffer (Invitrogen). β -mercaptoethanol was added to reduced and heated samples at a final concentration of 70 mM, and the samples were heated at 98 °C for 10 min. Protein samples and PageRuler Plus Prestained Protein Ladder (Thermo Scientific) were loaded onto a 4-12% Bis-Tris gel

(Invitrogen) and the gel was run for 50 min at 120 V. Gels that were not transferred onto a membrane for western blots were rinsed with water, stained with Imperial Protein Stain (Thermo Scientific), destained in water, and imaged using the ChemiDoc MP imaging system (Bio-Rad).

4.2.6 *Tau immunoblot characterization*

Dot blots and western blots with Tau5 and T22⁶⁹ antibodies were used to characterize tau monomer, oligomers, fibrils, and biotinylated tau monomer and oligomers. Dot blots were conducted by spotting 0.1 µg of tau protein or BSA in 1.3 µL PBS onto a 0.2 µm nitrocellulose membrane in triplicate. The membrane was allowed to dry for 30 min and then blocked with 5% BSA in TBST (20 mM tris, 150 mM NaCl, 0.1% Tween-20, pH 7.4) for 1 h at room temperature. The membrane was next incubated with Tau5 primary antibody (Invitrogen, 1:5,000) in 5% BSA in TBST for 2 h at room temperature. The membrane was washed with TBST three times for 5 min and incubated with goat anti-mouse IgG Alexa Fluor 647 (Invitrogen, 1:2,000) secondary antibody in 5% BSA in TBST for 1 h at room temperature. The membrane was washed with TBST three times for 5 min and imaged with the ChemiDoc MP imaging system (Bio-Rad). With the same membrane, primary and secondary antibody incubations were repeated with T22 (1:250) and donkey anti-rabbit IgG Alexa Fluor 488 (Invitrogen, 1:2,000), respectively, and the membrane was imaged with the ChemiDoc MP imaging system (Bio-Rad).

Western blots were conducted with tau monomer, oligomers, and biotinylated tau monomer and oligomers. 1 µg of protein was run on an SDS-PAGE gel as described and proteins were transferred to a 0.2 µm nitrocellulose membrane using a Trans-Blot Turbo

Mini 0.2 μm Nitrocellulose Transfer Pack (Bio-Rad) and Trans-Blot Turbo Transfer System (Bio-Rad). The membrane was rinsed with TBST and then to confirm protein transfer, was stained with Ponceau S Solution (Rockland Immunochemicals) for 15 min. The membrane was rinsed with water, then imaged with the ChemiDoc MP imaging system (Bio-Rad). The membrane was washed with TBST three times for 5 min to remove the Ponceau S Solution and then blocked with 5% BSA in TBST for 1 h at room temperature. Antibody incubations and membrane imaging was conducted as described for dot blots.

4.2.7 *Yeast cell culture*

Yeast cells expressing the synthetic nanobody library⁸⁰ were grown overnight in tryptophan deficient SD-Trp media (3.8 g/L yeast synthetic drop-out medium supplements without tryptophan, 6.7 g/L yeast nitrogen base, 20 g/L glucose, 100 U/mL penicillin-streptomycin, pH 6.0) at 30 °C, 225 rpm, and 10^7 cells/mL. Nanobody expression on the surface of the cells was induced by culturing the yeast in SG-Trp media (3.8 g/L yeast synthetic drop-out medium supplements without tryptophan, 6.7 g/L yeast nitrogen base, 20 g/L galactose, 100 U/mL penicillin-streptomycin, pH 6.0) overnight at 25 °C and 250 rpm.

4.2.8 *Magnetic-activated cell sorting*

Magnetic-activated cell sorting (MACS) was performed as described previously.⁷⁹ Two rounds of MACS were conducted to select tau oligomer-binding nanobodies. In each round, negative selections were followed by a positive selection against tau oligomer-coated magnetic Dynabeads Biotin Binder beads (Invitrogen).

Dynabeads were prepared following the manufacturer's protocol. For MACS Round 1, to prepare oligomer-coated beads for positive selection, 10^7 beads were first washed twice using a magnet and PBS with 0.1% BSA and then incubated with 12.5 μg biotinylated tau oligomers in 500 μL 0.1% BSA in PBS overnight at 4 $^{\circ}\text{C}$ with rotation. 10^7 beads for negative sorts containing no tau protein were washed and incubated in 0.1% BSA in PBS overnight at 4 $^{\circ}\text{C}$ with rotation. The following day, the beads were washed with 0.1% BSA in PBS and resuspended in 100 μL 0.1% BSA in PBS. 10^{10} nanobody-expressing library cells were mixed with the unlabeled Dynabeads and incubated for 1 h at room temperature with rotation. Unbound yeast were then collected with a magnet, and this negative selection step against unlabeled beads was repeated once. After the negative selections, the remaining yeast cells were incubated with tau oligomer-coated beads for 1 h at room temperature with rotation. Unbound cells were discarded, and the beads were washed 5 times with 1 mL 0.1% BSA in PBS using a magnetic tube rack. The beads were transferred to 5 mL of SD-Trp media and yeast bound to the beads were grown for 48 h at 30 $^{\circ}\text{C}$ and 250 rpm.

During MACS Round 2, two sets of selections starting with 10^9 nanobody-expressing MACS Round 1 yeast cells were performed in parallel. Negative selections against unlabeled Dynabeads were first performed as described with both sets of yeast. After negative selections against the unlabeled Dynabeads, one set of yeast underwent a negative selection against 10^6 Dynabeads coated with 1.25 μg biotinylated tau monomer. Finally, a positive selection with both sets of yeast against tau oligomer-coated beads was performed as described. Oligomer-coated beads for the positive selection were prepared by

mixing 10^6 Dynabeads with 1.25 μg biotinylated tau oligomers in 50 μL 0.1% BSA in PBS overnight at 4 °C with rotation.

4.2.9 *Fluorescence-activated cell sorting*

Two rounds of fluorescence-activated cell sorting (FACS) were conducted with yeast from each of the two MACS Round 2 sorts—one without a negative selection against tau monomer and one with a negative selection against tau monomer. Induced yeast cells from the previous MACS or FACS rounds were labeled for FACS as described previously.⁷⁹ 10^7 yeast cells were labeled with 10 nM biotinylated tau oligomers and with an anti-HA tag rabbit antibody (Invitrogen, 1:200) to check for nanobody expression in 100 μL 0.1% BSA in PBS for 20 min at room temperature with rotation. Yeast cells were washed with 0.1% BSA in PBS and then incubated with streptavidin R-phycoerythrin conjugate (Invitrogen, 1:250) and donkey anti-rabbit IgG Alexa Fluor 488 (Invitrogen, 1:500) in 100 μL 0.1% BSA for 10 min on ice. Cells were washed with 0.1% BSA in PBS and sorted on a BD FACSAria Fusion cytometer. Selected yeast were added to 5 mL of SD-Trp media and cultured for 48 h.

4.2.10 *Individual nanobody selection*

Yeast from each of the four FACS rounds were plated on SD-Trp agar plates (SD-Trp media supplemented with 15 g/L agar) and grown for 48 h at 30 °C. 15 colonies from each round of sorting were randomly selected and used to inoculate 5 mL SD-Trp cultures. The cultures were allowed to grow for 24-48 h, and then plasmid DNA was extracted from the yeast using a Zymoprep Yeast Plasmid Miniprep II kit (Zymo Research). The extracted plasmids were transformed into NEB 5-alpha Competent *E. coli* cells (New England

Biolabs) according to the manufacturer's protocol. The transformed *E. coli* was grown in 5 mL LB media with 100 µg/mL ampicillin overnight at 37 °C with rotation. Plasmid DNA was extracted from the *E. coli* using the E.Z.N.A. Plasmid Mini Kit I (Omega Biotek) and sequenced by MCLAB (San Francisco, CA).

4.2.11 Flow cytometry

10⁷ nanobody-expressing yeast cells were labeled with biotinylated tau oligomers or biotinylated tau monomer and with an anti-HA tag rabbit antibody (Invitrogen, 1:200) in 100 µL 0.1% BSA in PBS for 20 min at room temperature with rotation. Yeast cells were washed once with 0.1% BSA in PBS and incubated in 100 µL 0.1% BSA for 10 min on ice with streptavidin R-phycoerythrin conjugate (Invitrogen, 1:250) and donkey anti-rabbit IgG Alexa Fluor 488 (Invitrogen, 1:500). Cells were washed with 0.1% BSA in PBS and tau binding was evaluated on a CytoFLEX S flow cytometer (Beckman Coulter).

4.2.12 Expression and purification of bivalent OT2.4-Fc, OT2.6-Fc, and MT3.1-Fc

Genes encoding bivalent OT2.4 fused to a rabbit IgG Fc and bivalent OT2.6 fused to a mouse IgG Fc (used for epitope mapping analysis) and bivalent OT2.4 or bivalent OT2.6 fused to a human IgG Fc (used for all other immunoblot analysis) were synthesized and cloned into the TGEX-HC plasmid (Antibody Design Labs) by Gene Universal (Newark, DE). These plasmids and a TGEX-HC plasmid for the expression of bivalent MT3.1-Fc fused to a human IgG Fc were transfected into Expi293F cells (Thermo Fisher Scientific) using the ExpiFectamine 293 Transfection Kit (Thermo Fisher Scientific) and protocol. The Fc fusion proteins were expressed for six days in the Expi293F cells and purified as previously described.⁷⁹ Cell cultures were centrifuged at 5,000 × g for 10 min

to pellet out the Expi293F cells, and the supernatant was loaded onto a 1 mL HiTrap MabSelect SuRe column (GE). Fc fusion proteins were purified according to the manufacturer's protocol. Protein elution was conducted with a 20 column volume linear gradient of 0.1 M sodium citrate, pH 3.5 and the purified Fc fusion proteins were dialyzed into PBS. Protein concentrations were determined using the BCA assay (Thermo Scientific) and purity was confirmed by SDS-PAGE.

4.2.13 OT2.4 and OT2.6 western blot characterization

Western blots with 1 μ g of tau monomer and oligomers were conducted as described above to probe binding of OT2.4 and OT2.6 to tau monomer and oligomers. 50 nM bivalent OT2.4-Fc or bivalent OT2.6-Fc were used as primary antibodies and goat anti-human IgG Alexa Fluor 488 (Invitrogen, 1:2,000) was used as the secondary antibody.

4.2.14 OT2.4 and OT2.6 dot blot characterization

Two-fold serial dilutions of tau monomer, oligomers, or fibrils starting at 256 ng/ μ L in 1 μ L PBS were spotted onto a 0.2 μ m nitrocellulose membrane in triplicate. Dot blots were probed as described above with 50 nM bivalent OT2.4-Fc or bivalent OT2.6-Fc. Goat anti-human IgG Alexa Fluor 647 (Invitrogen, 1:2,000) was used as the secondary antibody.

4.2.15 Binding epitope analysis

Epitope mapping with OT2.4 and OT2.6 was performed using a membrane containing overlapping 15 amino acid peptides scanning the full length 2N4R human tau sequence. The peptides were synthesized on a PepSpots cellulose membrane (JPT Peptide Technologies, Berlin, Germany). Peptides overlapped by 11 amino acids. The peptide

membrane was rinsed with methanol for 5 min and washed three times with TBST (50 mM tris, 137 mM NaCl, 2.7 mM KCl, 0.05% Tween-20, pH 8.0) for 3 min. The membrane was blocked with 5% BSA in TBST at 4 °C overnight and then incubated with 1 µg/mL bivalent OT2.4 fused to a rabbit Fc (12.8 nM) in 5% BSA in TBST at 4 °C overnight. The membrane was washed three times with TBST for 5 min and incubated with HRP-conjugated donkey anti-rabbit IgG (Cytiva, 1:5,000) in 5% BSA in TBST for 1 h at room temperature. The membrane was washed three times with TBST for 5 min and then incubated with SuperSignal West Femto Maximum Sensitivity Substrate (Thermo Scientific) for 30 s and imaged using the ChemiDoc MP imaging system (Bio-Rad).

The membrane was also incubated with 1 µg/mL bivalent OT2.6 fused to a mouse Fc (12.5 nM) in 5% BSA in TBST at 4 °C overnight. The membrane was washed three times with TBST for 5 min and incubated with a goat anti-mouse IgG Alexa Fluor 546 (Invitrogen, 1:2,000) in 5% BSA in TBST for 1 h at room temperature. The membrane was washed three times with TBST for 5 min and imaged using the ChemiDoc MP imaging system (Bio-Rad).

4.2.16 Western blotting of human tissue lysates

Postmortem brain tissue from human subjects with AD (n = 5) and control subjects (n = 5), obtained from the Goizueta Alzheimer's Disease Center at Emory University, were lysed in PBS (137 mM NaCl, 2.7 mM KCl, 10 mM Na₂HPO₄, 1.8 mM KH₂PO₄, pH 7.4). Sections approximately 100 mg were cut from frozen tissues and placed into 300 µL ice cold PBS containing cOmplete™, Mini Protease Inhibitor Cocktail (Roche, 1 tablet/5 mL). Tissues were lysed using a TissueLyser II (Qiagen) and one 5 mm stainless steel bead

(Qiagen) per sample for 4 min at 30 Hz. The stainless steel beads were removed, and the lysates were centrifuged at 13,000 rpm and 4 °C for 10 min. The pellet was discarded, and a BCA assay (Thermo Scientific) was performed with the supernatant to determine total protein concentration. The tissue lysate was aliquoted and stored at -80 °C.

Frozen lysates were thawed on ice and 15 µg of total protein was diluted in Laemmli Sample Buffer (Bio-Rad) and run on two identical western blots as described above. First, 5 nM bivalent OT2.4-Fc (membrane 1) or 5 nM bivalent OT2.6-Fc (membrane 2) primary antibodies and goat anti-human IgG Alexa Fluor 488 (Invitrogen, 1:2,000) secondary antibodies were used to probe OT2.4 and OT2.6 binding to the tissue samples. Both membranes were then incubated with 3 nM Phospho-Tau (Ser202, Thr205) Monoclonal Antibody (AT8) (Invitrogen) primary antibody, washed with TBST (20 mM tris, 150 mM NaCl, 0.1% Tween-20, pH 7.4), and incubated with goat anti-mouse IgG Alexa Fluor 647 (Invitrogen, 1:2,000) secondary antibody. Membrane 2 was incubated with T22 (1:250) primary antibody, washed with TBST, and incubated with HRP-conjugated donkey anti-rabbit IgG (Cytiva, 1:5,000) to confirm the presence of tau oligomers. Next, antibodies were stripped from both membranes using Restore Western Blot Stripping Buffer (Thermo Scientific) for 30 min at 37 °C with shaking. The membranes were washed three times for 5 min with TBST, blocked with 5% BSA in TBST for 1 h at room temperature, incubated with GAPDH primary antibody (GeneTex, 1:1,000), washed with TBST, and incubated with goat anti-mouse IgG Alexa Fluor 647 (Invitrogen, 1:2,000) secondary antibody. All images were taken using the ChemiDoc MP imaging system (Bio-Rad).

4.2.17 Sorting against amyloid- β oligomer

Our collaborators in the Rosenberry Lab generated ~150 kDa amyloid- β oligomers incorporating 10% biotinylated amyloid- β monomer (AnaSpec) and 90% unlabeled amyloid- β monomer as previously described.¹⁴¹ Sorts of the synthetic yeast surface display nanobody library⁸⁰ included two MACS screens and one FACS screen and were performed as described above for tau oligomers. In MACS Round 1 and 2, the nanobody library was sorted against 12.5 μ g and 1.25 μ g of amyloid- β oligomers, respectively, immobilized on magnetic Dynabeads Biotin Binder beads (Invitrogen). A negative screen against monomeric protein was not conducted during MACS Round 2. FACS Round 1 was performed against 50 nM amyloid- β oligomers. Flow cytometric analysis of binding after each sort was conducted as described above for tau oligomer-binding nanobodies.

4.3 Results and Discussion

4.3.1 Identification of tau oligomer-specific nanobodies

To identify tau oligomer-specific nanobodies, we screened a synthetic yeast surface display nanobody library against recombinant tau oligomers.⁸⁰ Our recombinant oligomers form spontaneously during the expression and purification of the 2N4R isoform of human tau in *E. coli*. We separated oligomeric tau from monomeric tau using SEC and characterized their sizes using dynamic light scattering. Additionally, we characterized our tau proteins via dot blot (Figure 16a, b) and western blot (Figure 16c-f). We verified the conformation of our tau oligomers using a tau oligomer-specific polyclonal antibody, T22, in these immunoblots (Figure 16b, f).⁶⁹

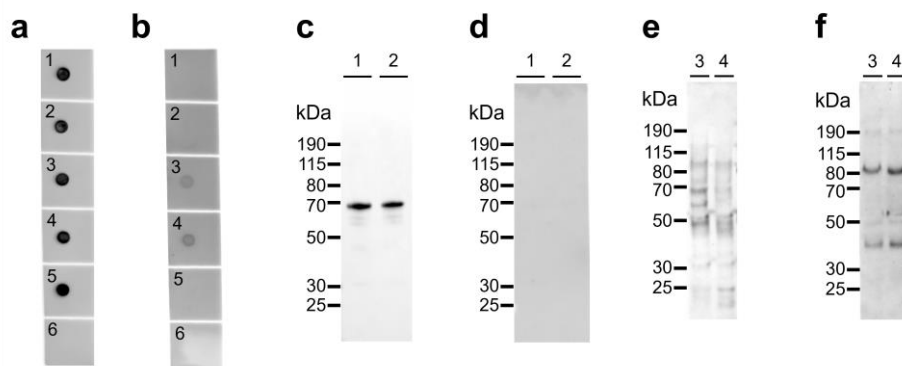


Figure 16. Tau immunoblot characterization. (a-b) Characterization of (1) tau monomer, (2) biotinylated tau monomer, (3) tau oligomers, (4) biotinylated tau oligomers, (5) tau fibrils, and (6) BSA by dot blot with (a) Tau5 antibody and (b) T22 antibody. (c-f) Characterization of (1) tau monomer, (2) biotinylated tau monomer, (3) tau oligomers, and (4) biotinylated tau oligomers by western blot with (c, e) Tau5 antibody and (d, f) T22 antibody.

We performed MACS and FACS to select for our nanobodies. During MACS Round 2, two sets of screens were performed in parallel. The first included a positive selection against tau oligomers, and the second included a negative selection against tau monomer and a positive selection against tau oligomers. FACS screens after MACS Round 2 were conducted with identical conditions on both the yeast from the MACS screen without and with the negative selection against tau monomer. After each round of sorting, yeast cells were labeled with tau oligomers (Figure 17) and monomer (data not shown) to monitor the enrichment of binding to tau oligomers and the level of undesired binding to tau monomer. Over the course of the screens, binding to tau oligomers was greatly enriched.

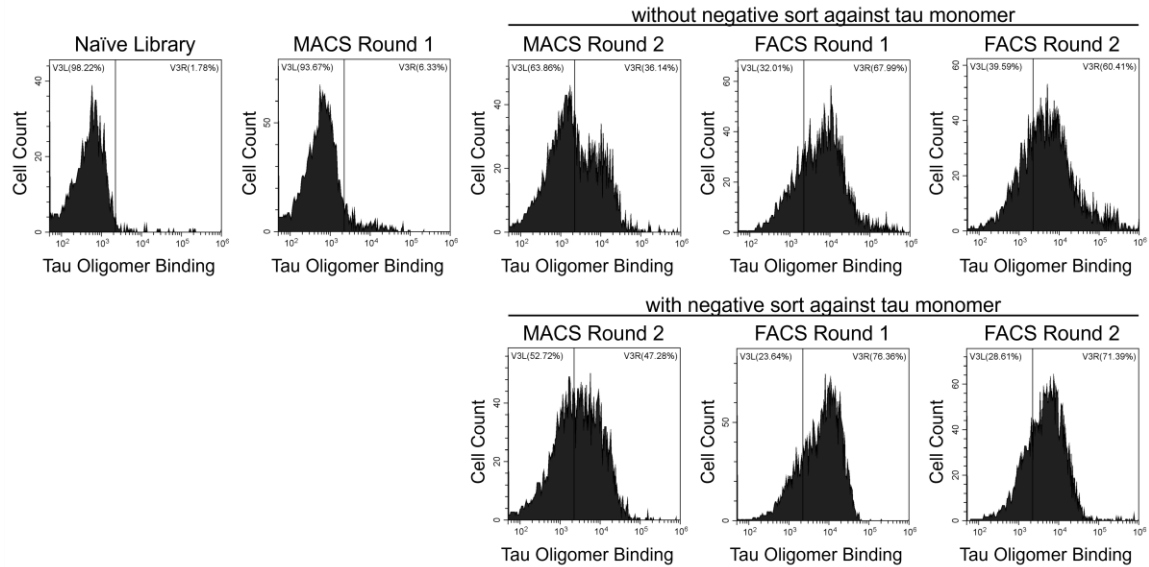


Figure 17. Selection of tau oligomer-specific nanobodies. Yeast cells from the naïve nanobody library or after each MACS or FACS screen were labeled with 30 nM tau oligomers, and the extent of binding was assessed with flow cytometry. Fluorescence signal corresponding to tau oligomer binding to yeast surface displayed nanobodies is shown on the on the x-axis. Binding to tau oligomers above the level of the nanobody library appears on the right side of the vertical gate.

After FACS Round 2, 15 nanobodies from each of the four FACS screens were selected and sequenced. From the 60 nanobodies sequenced, ten unique tau oligomer-binding nanobodies were identified (Table 1, Appendix Table 6). Yeast expressing these nanobodies were labeled with a range of concentrations of tau oligomers (1 nM-10 nM) and of tau monomer (10 nM-1,000 nM) and the extent of binding was assessed with flow cytometry (Figure 18a, b). All ten nanobodies showed binding to tau oligomers and much less binding to tau monomer. Two of the nanobodies OT2.4 and OT2.6, appeared to be either stronger binders to tau oligomers or more specific binders to tau oligomers relative to tau monomer compared to the other selected nanobodies. These nanobodies were chosen for further characterization.

Table 1. Sequences of CDR1, CDR2, and CDR3 of the ten selected nanobodies.

Nanobody	CDR1	CDR2	CDR3
1 (OT2.6)	GRTFRYNAM	ELVAAITVRTGSTYY	AVDRDYLVRYSQLYREYGY
2	GITFRSYAM	EFVAAITSGGASTYY	AARRPYKPYDY
3	GRTFYRYTM	ELVAAISFRAGRTYY	AADQYLSADYDY
4	GSIFRANAM	ELVAAITTSRSTYY	ARRALYLPQRINYSAMDY
5	GYTFGRNTM	EFVAAITQSGGNTYY	NARLRPPYGWKYGY
6	GFTFGGANVM	ELVAAITYGGGSTYY	AARSYRYWTQILYDY
7	GRTFTSYTM	ELVAAITDRGGRTYY	NTWVGYPHGGDEVVDH
8	GRTFVWNAM	ELVAAITYRGASTYY	NARKYVTLKYDY
9	GRTFGRNAM	ELVAAITGGSTNY	AATRWRKWYYY
10 (OT2.4)	GIISNNNAM	EFVAAISTSGGSTYY	NRRVVERYWRGYWYREDGY

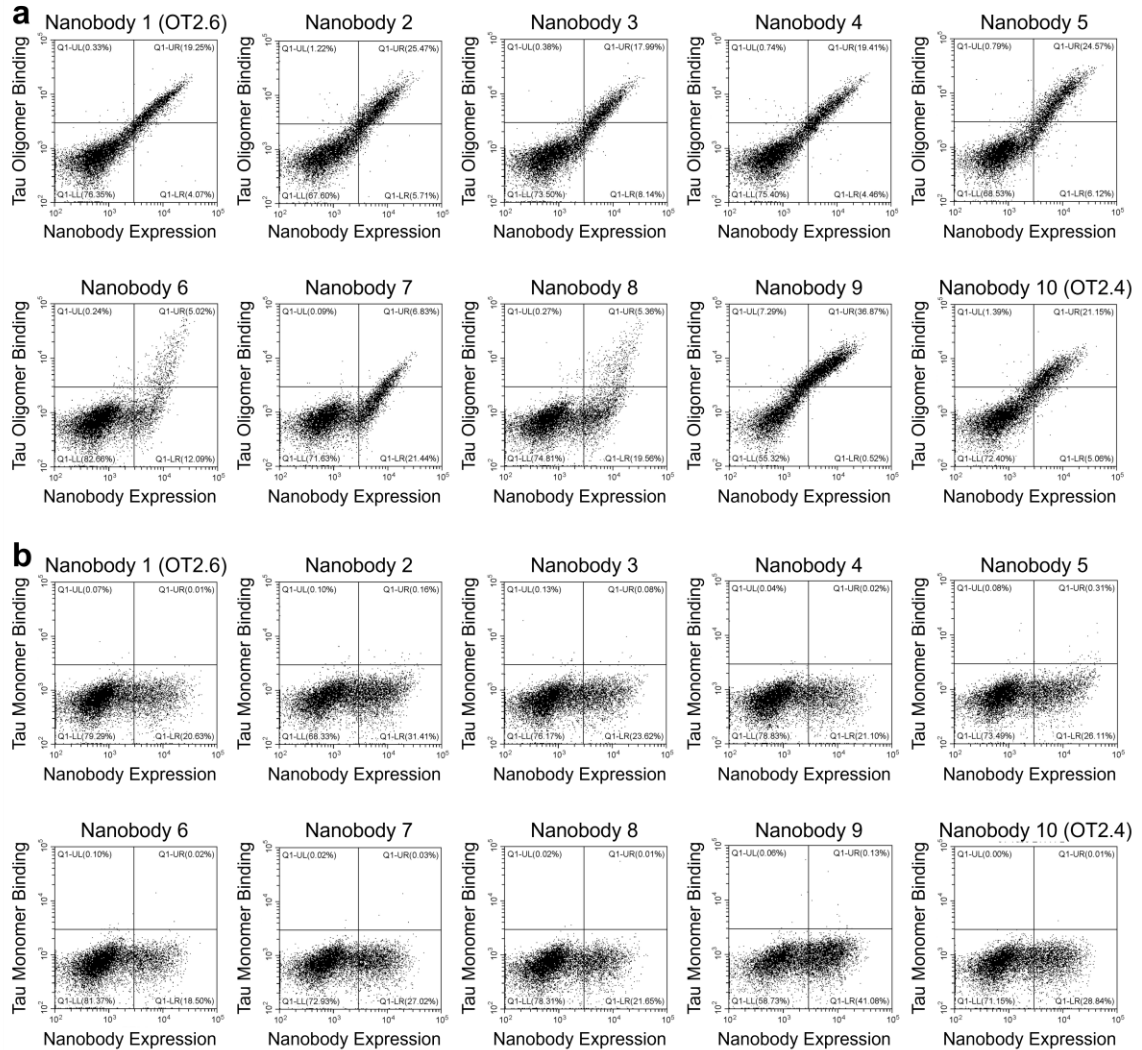


Figure 18. Single clone analysis of selected nanobodies. a-b) Yeast cells expressing copies of one of the ten selected nanobodies were labeled with (a) 10 nM tau oligomers or

(b) 100 nM tau monomer, and the extent of binding was assessed with flow cytometry. Plots display fluorescent signal corresponding to tau binding on the y-axis and fluorescent signal corresponding to the expression level of the nanobodies on the x-axis.

4.3.2 *Characterization of nanobodies confirms specificity to tau oligomers*

We designed, expressed, and purified bivalent versions of the nanobodies OT2.4 and OT2.6 fused to a human IgG Fc (Figure 19). These Fc fusion constructs were used to confirm and further examine the specificity of the nanobodies to tau oligomers over tau monomer and fibrils using western blots and dot blots. Western blots with recombinant tau monomer and tau oligomers show binding of bivalent OT2.4-Fc and bivalent OT2.6-Fc to the oligomers and not monomer (Figure 20), verifying the specificity seen in flow cytometry experiments. Next, we probed the binding of bivalent OT2.4-Fc, bivalent OT2.6-Fc, and bivalent MT3.1-Fc to serial dilutions of tau monomer, oligomers, and fibrils on dot blots (Figure 21). MT3.1 is a pan-tau nanobody developed by our lab that binds to tau monomer, oligomers, and fibrils.⁷⁹ These dot blots showed high levels of specificity for bivalent OT2.4-Fc and bivalent OT2.6-Fc to tau oligomers over both monomer and fibrils. In contrast, bivalent MT3.1-Fc preferentially binds tau fibrils, and to some extent, tau monomer, over tau oligomers. Bivalent OT2.4-Fc, in particular, was extremely selective towards tau oligomers relative to monomer and fibrils.

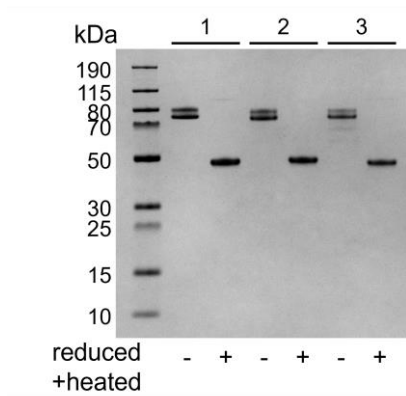


Figure 19. Bivalent Fc fusion proteins. An SDS-PAGE gel containing (1) bivalent OT2.4-Fc, (2) bivalent OT2.6-Fc, and (3) bivalent MT3.1-Fc. Reduced and heated samples are indicated with “+” and samples that are not reduced or heated are indicated with “-”.

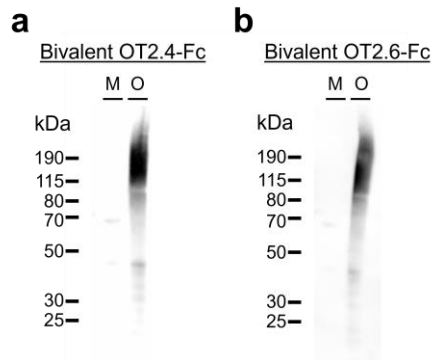


Figure 20. Western blotting with OT2.4 and OT2.6. a-b) Specific binding of (a) bivalent OT2.4-Fc and (b) bivalent OT2.6-Fc was evaluated with western blots containing recombinant tau monomer (M) and recombinant tau oligomers (O).

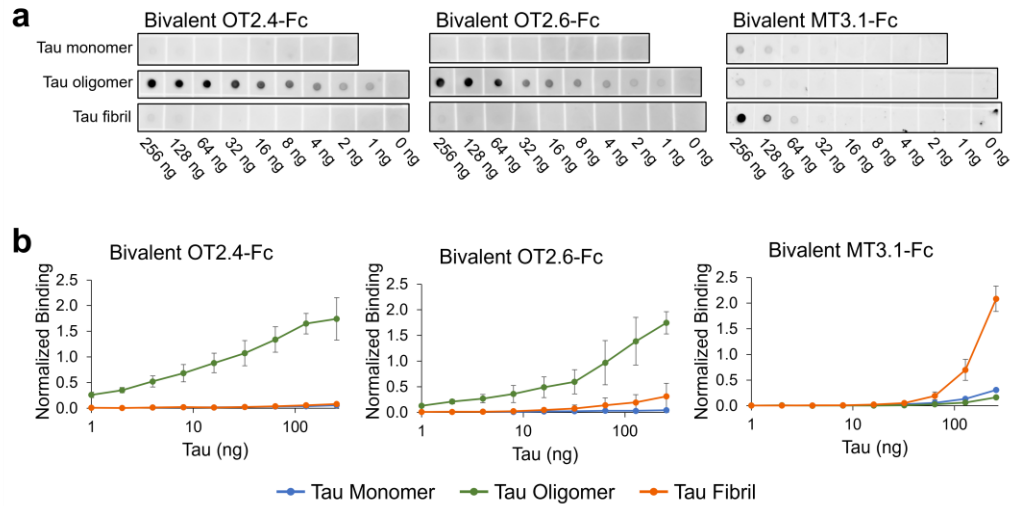


Figure 21. Analysis of OT2.4 and OT2.6 specificity towards tau oligomers. a) Dot blots containing serial dilutions of tau monomer, tau oligomers, and tau fibrils were probed with bivalent OT2.4-Fc, bivalent OT2.6-Fc, and bivalent MT3.1-Fc. Shown are representative images from six repeats from two independent assays. b) Binding of bivalent OT2.4-Fc, bivalent OT2.6-Fc, and bivalent MT3.1-Fc to tau monomer (blue), tau oligomers (green), and tau fibrils (orange) on dot blots was quantified and plotted. Data points are averages from six repeats from two independent assays and error bars indicate standard deviation.

4.3.3 Epitope mapping reveals that nanobodies interact with tau oligomers via multiple non-overlapping epitopes

To determine the epitopes at which OT2.4 and OT2.6 bind to tau, we performed epitope mapping. To conduct this mapping, we used a membrane containing 15-mer peptides spanning the full length of the 2N4R tau isoform with 11 amino acid overlaps. Incubation of the membrane with bivalent OT2.4-Fc and bivalent OT2.6-Fc revealed that both nanobodies bind to multiple discontinuous epitopes on tau (Figure 22). OT2.4 bound to peptides containing residues 133-147, 177-195, 343-367, and 413-427 (Figure 22a, c). OT2.6 bound to peptides containing residues 121-139, 149-163, 209-223, 373-391 (Figure 22b, c). Discontinuous, or conformational, epitopes are epitopes that contain multiple groups of residues essential to antibody binding that are separated in the antigen's primary

are found in the brains of humans with AD and can be detected at early stages of the disease.^{30,69,132} Additionally, tau oligomers are present in the brain tissue and serum of older adults without neurodegenerative diseases and appear during the aging process.^{143,144} Kolarova et al. reports that in healthy older adults, tau oligomers are present in serum and tau oligomer levels correlate with aging.¹⁴³ In a study by Maeda et al., tau oligomers were detected in the brains of older adults with Braak stage I neuropathology, a stage before the onset of clinical symptoms of AD and the presence of NFTs in the frontal cortex.¹⁴⁴ They found no significant difference between tau oligomer levels in Braak I, II, and V stage frontal cortex samples.¹⁴⁴

We conducted western blots with brain samples from five individuals with AD (ages 77 to 87, Braak stage VI) and from five control individuals with primary age-related tauopathy (ages 70 to >89, Braak stages I, II, or III) (Appendix Table 7). We detected tau oligomers with bivalent OT2.4-Fc (Figure 23a) and bivalent OT2.6-Fc (Figure 23b) in all of the AD tissues and non-AD (control) tissues. We note that the detection of tau oligomers in tissues of older adults without AD is expected and consistent with the studies described above. Staining of these tissues with phospho-tau antibody AT8 (Figure 23c, d) overlapped with bivalent OT2.4-Fc and bivalent OT2.6-Fc staining at 150 kDa and higher molecular weight bands. To confirm that the bands stained by bivalent OT2.4-Fc and bivalent OT2.6-Fc are tau oligomers, we probed binding with T22, an antibody that has previously been shown to bind to tau oligomers present in AD brain tissue⁶⁹, and saw an overlap of staining at bands at 50 kDa and 150 kDa (Figure 23e).

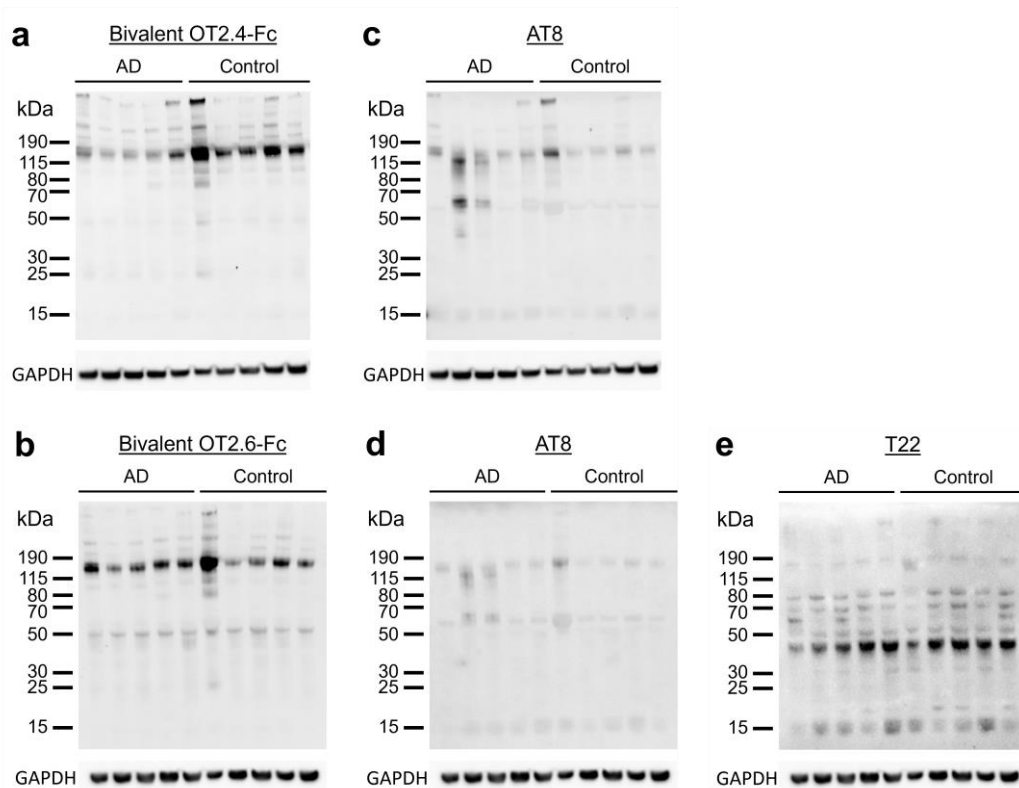


Figure 23. Binding of OT2.4 and OT2.6 to tau oligomers from human brain samples. a-b) Lysates of human brain tissue samples from five patients with AD and five controls were run on western blots and binding with (a) bivalent OT2.4-Fc and (b) bivalent OT2.6-Fc was assessed. c-e) These membranes were also stained with phospho-tau antibody AT8 (c-d) and tau oligomer-specific antibody T22 (e).

4.3.5 Sorting of a nanobody library against amyloid- β oligomers

To demonstrate that our *in vitro* discovery approach to identifying conformational oligomer-specific nanobodies is generalizable to other amyloid or aggregate-forming proteins, we have begun conducting MACS and FACS screens of the yeast surface display nanobody library⁸⁰ against amyloid- β oligomers. Two MACS and one FACS screen have been performed against biotinylated amyloid- β oligomers generated by our collaborators in the Rosenberry Lab. After each sort, we labeled the enriched libraries with 1 nM amyloid- β oligomers and used flow cytometry to monitor binding. As depicted in Figure 24, we see an enrichment in binding to amyloid- β oligomers after every MACS or FACS

screen and after one round of FACS, we are seeing very high levels of binding to only 1 nM amyloid- β oligomers. We are currently moving forward with additional FACS screens, and then we will select individual amyloid- β oligomer-binding nanobodies and characterize them as we have done with OT2.4 and OT2.6.

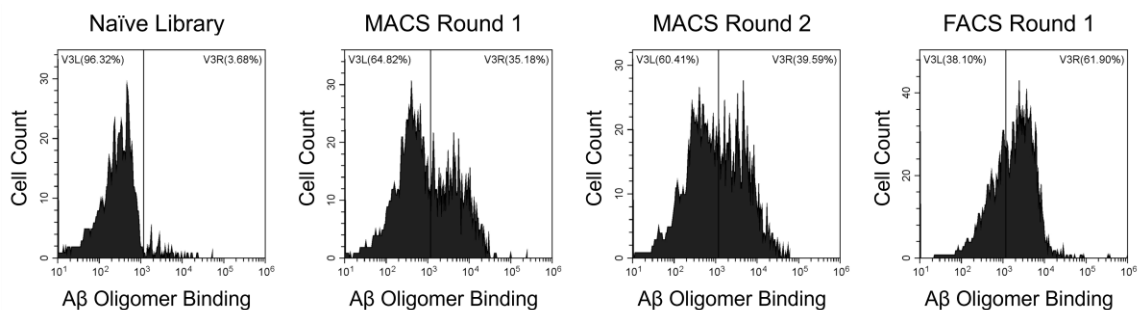


Figure 24. Selection of amyloid- β oligomer-targeting nanobodies. Yeast cells expressing nanobodies from the naïve library or enriched libraries after MACS and FACS screens were labeled with 1 nM amyloid- β oligomers and flow cytometry was used to measure the extent of binding. Fluorescence signal corresponding to amyloid- β oligomer binding to yeast surface displayed nanobodies is shown on the x-axis. Binding to amyloid- β oligomers above the level of the nanobody library appears on the right side of the vertical gate.

4.4 Conclusions and Future Work

There is a need for more effective disease-modifying treatments, diagnostics, and research tools for tauopathies like AD. Conformational antibodies that target tau oligomers, suspected to be the most toxic form of tau present in AD, are promising candidates for passive immunotherapy and diagnostic reagents. Nanobodies, in particular, are exciting options for tau oligomer-specific binders as they can target concave or hidden epitopes inaccessible to traditional IgG antibodies. Therefore, a conformational tau oligomer-specific nanobody may interact with tau oligomers differently than the few available tau oligomer-specific antibodies. Other benefits of nanobodies include their single-domain

nature which make them inexpensive to produce in yeast or bacteria cells and easy to link together in multivalent or Fc fusion formats.

In this work, we report the development and characterization of the first conformational, tau oligomer-specific nanobodies, OT2.4 and OT2.6. These nanobodies were identified through the screening of a yeast surface display nanobody library⁸⁰ against recombinant tau oligomers. We have demonstrated the specificity of these nanobodies towards tau oligomers over monomer and fibrils with western blot and dot blot analysis. With epitope mapping, we have confirmed that OT2.4 and OT2.6 bind to discontinuous epitopes on tau making them conformational binders. Finally, we have shown that OT2.4 and OT2.6 recognize tau oligomers of different sizes present in the brains of AD patients and healthy older adults with primary age-related tauopathy.

Future work will be conducted to study if and how these nanobodies interact with tau present in the brains of younger, healthy adults and towards their development into viable therapeutic or diagnostic tools for AD and other tauopathies. Additional ongoing and future work will be performed to complete screens of the nanobody library against amyloid- β oligomers and characterize the resulting nanobodies. Overall, this work demonstrates significant progress in developing conformational, amyloid oligomer-specific antibodies and antibody fragments that have great potential in the diagnosis and treatment of neurodegenerative diseases.

CHAPTER 5. DEVELOPMENT OF POTENT NANOBODIES THAT PROTECT AGAINST THE SARS-COV-2 XBB VARIANT

5.1 Introduction

Since the emergence of the severe acute respiratory syndrome coronavirus 2 (SARS-CoV-2) Omicron variant in 2021, its high mutation rate and transmissibility have been major clinical concerns.^{145,146} The SARS-CoV-2 spike (S) protein is an immunodominant surface glycoprotein that contains the receptor-binding domain (RBD). The RBD binds to the host cell receptor angiotensin-converting enzyme 2 (ACE2) upon infection and is a primary target of neutralizing antibodies isolated from sera of infected or vaccinated individuals.¹⁴⁷ Due to the aforementioned function of the RBD, mutations in the RBD may result in increased immune evasion.^{148,149} A recombinant variant of two viruses from the Omicron sublineages, XBB, was first identified in August 2022 and rapidly spread around the world causing a wave of COVID-19 infections.⁴⁹ This variant and others from the Omicron sublineages, possess amino acid substitutions in the RBD that enhance evasion of pre-Omicron neutralizing antibodies.¹⁵⁰

Conventional monoclonal antibodies serve as an important class of therapeutics for various diseases and viral infections. Since the beginning of the COVID-19 pandemic, antibody treatments have been studied and several were approved in the United States for emergency usage.^{151–153} However, the newly emerging Omicron variants have been found to be resistant to existing monoclonal antibodies.^{150,154,155} All antibody treatments approved in the United States prior to 2024 for treatment against SARS-CoV-2 possess greatly

reduced or no neutralization activity against Omicron variants including XBB, and because of this limited neutralization, their Emergency Use Authorizations have been rescinded.¹⁵⁶ One of these monoclonal antibodies, sotrovimab, retains low levels of neutralization against XBB and XBB.1.5, but no neutralization towards other variants including BA.2.¹⁵⁶ A new monoclonal antibody, Pemivibart, was given EUA for the prevention of COVID-19 by the FDA in March 2024.¹⁵⁷

Non-immunoglobulin binding proteins and peptides, such as designed ankyrin repeat proteins (DARPs)^{158,159}, monobodies^{160–165}, knottins¹⁶⁶, defensins¹⁶⁶, and affibodies¹⁶⁷ have also been developed to target and neutralize the SARS-CoV-2 virus. Like antibodies, these molecules can be engineered to have high binding affinity and specificity. Other favorable characteristics of these binding molecules are their small size and single-domain quality, high stability, good tissue permeability, and low immunogenicity.^{168,169} Rothenberger et al. created a trispecific DARPin, Ensovibep, that targets the trimetric spike protein of SARS-CoV-2 and neutralizes SARS-CoV-2 Omicron variants BA.1 and BA.2 *in vitro*.^{158,170} Ensovibep successfully completed phase II clinical trials and demonstrated a reduction in viral load, hospitalization, and death in COVID-19 patients.^{170,171} Other trimeric DARPins, FSR16m and FSR22, were developed by Chonira et al. and show protection against the B.1.617.2 variant in a transgenic mouse model of COVID-19.¹⁵⁹ Monomeric and dimeric monobodies, synthetic proteins based on a human fibronectin type III domain, that target the SARS-CoV-2 RBD were created by Kondo et al. and show high neutralizing activity against SARS-CoV-2.¹⁶⁰

In addition to conventional monoclonal antibodies and synthetic non-immunoglobulin binding proteins, single-domain antibodies, or nanobodies, have also

gained attention as alternative therapeutics to SARS-CoV-2. Nanobodies are heavy chain-only antibody fragments that are derived from the variable domain of camelid antibodies.¹⁷² Similar to non-immunoglobulin binding proteins, nanobodies possess several desirable properties over traditional antibodies such as high thermal and chemical stability, modularity, and ease of production.^{9,173,174}

Due to the immune evasive characteristics of the newly emerging SARS-CoV-2 Omicron variants, the ability of various antibody-based therapeutics, including nanobody constructs, to combat recent Omicron variant infections has been studied. Modhiran et al. constructed a human Fc-fused nanobody, W25, derived from alpacas immunized with ancestral SARS-CoV-2 strain and saw protection against the Beta and BA.1 variants as well as subnanomolar binding affinity to XBB.1.5 S (0.1 nM).¹⁷⁵ High affinity nanobodies are more likely to outcompete the ACE2 receptor and remain bound to the S protein, inhibiting the interaction between the spike and ACE2. Yao et al. engineered a trivalent construct with nanobodies acquired from screening a phage display library against BA.1 and with it demonstrated protection against BA.1.1, BA.2.3, and BA.5 in mice as well as neutralization against XBB.1.5 ($IC_{50} = 50$ nM).¹⁷⁶ A bispecific nanobody dimer constructed by Ma et al. completely reduced lung and trachea viral titers in hamsters challenged with BA.1, but the RBD-binding interface analysis proved its ineffectiveness against BA.2.75, BA.2.3.20, and XBB variants.¹⁷⁷ Solodkov et al. conducted sequential screenings of llama-derived phage libraries against various strains of SARS-CoV-2 and constructed an Fc-fused nanobody that had neutralization activity ($IC_{50} = 0.4$ nM) against the XBB lineage.¹⁷⁸ Amongst the numerous antibody-based therapeutics developed as treatments for the Omicron variants, none of them have undergone *in vivo* studies against the currently

circulating XBB variants for their anti-viral potency. Additionally, many of the identified nanobodies were derived from immunized camelid animals.^{175,177–185} Immunization of camelid animals are low throughput and expensive, which sets a high barrier for developing nanobody-based therapeutics.⁹ Using *in vitro* antibody discovery and a surface display method such as yeast surface display or phage display can help overcome these challenges.

Here, we describe the development of three Fc-fused nanobody constructs, XNb 4.13, XNb 4.14, and XNb 4.15, through the screening of a yeast surface display nanobody library against XBB RBD. We show that these nanobody constructs bind with subnanomolar affinity to the XBB S protein. Two of the nanobodies, XNb 4.13 and XNb 4.14 demonstrate neutralizing activity against XBB and reduce viral lung titers in mice challenged with XBB. We discuss future work that will be conducted to improve the neutralization and breadth of protection provided by treatment with these nanobodies.

5.2 Materials and Methods

5.2.1 XBB RBD and S expression and purification

DNA sequences encoding XBB strain SARS-CoV-2/human/USA/CA-CDC-STM-MV7TMMQMB/2022 RBD and S proteins with C-terminal His-tags were synthesized and cloned into the pcDNA3.1(-) expression vector by Gene Universal Inc. (Newark, DE). These plasmids were transfected into Expi293F cells (Thermo Fisher Scientific) using the ExpiFectamine 293 Transfection Kit (Thermo Fisher Scientific) and the manufacturer's protocol. Proteins were expressed over 6 days and then the cell culture was centrifuged at $6,000 \times g$ for 10 min to harvest the cell supernatant. The RBD and S proteins were purified by Ni-NTA chromatography using HisPur Ni-NTA resin (Thermo Fisher Scientific). First,

the cell supernatant was mixed with 1 mL of resin overnight at 4 °C. The next day, the resin slurry was loaded into a gravity flow column (G-Biosciences) and then washed with 90 mL IMAC equilibration buffer (100 mM tris HCl, 150 mM NaCl, 20 mM imidazole, pH 8.0). RBD and S proteins were eluted in 9 mL of elution buffer (100 mM tris HCl, 150 mM NaCl, 400 mM imidazole, pH 8.0) and the eluate was then concentrated with a 10 kDa MWCO centrifugal filter (Millipore Sigma). RBD and S proteins were further purified via SEC using a Superdex 200 Increase 10/300 GL column (Cytiva) in PBS. Protein concentration and purity were determined by BCA assay (Thermo Scientific) and SDS-PAGE, respectively.

5.2.2 *XBB RBD and S biotinylation*

XBB RBD and S proteins were biotinylated using the EZ-Link Sulfo-NHS-LC-Biotin reagent (Thermo Scientific) following the manufacturer's protocol. Excess reagent was removed by buffer exchanging with a 10 kDa MWCO centrifugal filter (Millipore Sigma) into TBS (20 mM tris HCl, 100 mM NaCl, pH 7.4). The extent of biotinylation was determined by running an SDS-PAGE gel with streptavidin at 4 °C.

5.2.3 *SDS-PAGE*

Proteins were diluted in Nu-PAGE LDS sample buffer (Invitrogen). β -mercaptoethanol was added to reduced and heated samples at a final concentration of 70 mM, and the samples were heated at 98 °C for 10 min. Protein samples and PageRuler Plus Prestained Protein Ladder (Thermo Scientific) were loaded into wells of a 4-12% Bis-Tris gel (Invitrogen) and the gel was run for 50 min at 120 V. The gel was stained with Imperial

Protein Stain (Thermo Scientific), destained, and then imaged using the ChemiDoc MP imaging system (Bio-Rad).

5.2.4 *Yeast cell culture*

Yeast cells expressing the nanobody library⁸⁰ were cultured at a density of 10^7 cells/mL in tryptophan deficient SD-Trp media (3.8 g/L yeast synthetic drop-out medium supplements without tryptophan, 6.7 g/L yeast nitrogen base, 20 g/L glucose, 100 U/mL penicillin-streptomycin, pH 6.0) at 250 rpm and 30 °C. Expression of nanobodies on the yeast cell surface was induced by incubation of the yeast in SG-Trp media (3.8 g/L yeast synthetic drop-out medium supplements without tryptophan, 6.7 g/L yeast nitrogen base, 20 g/L galactose, 100 U/mL penicillin-streptomycin, pH 6.0) at 10^7 cells/mL and by incubating overnight at 250 rpm and 25 °C.

5.2.5 *Magnetic-activated cell sorting*

Two rounds of MACS were conducted to identify XBB RBD-binding nanobodies. For both MACS screens, two negative selections against magnetic Dynabeads Biotin Binder beads (Invitrogen) followed by one positive selection against XBB RBD-coated beads were performed. For the MACS Round 1 positive sort, 10^7 Dynabeads coated with 12.5 µg biotinylated XBB RBD were prepared, and for the MACS Round 2 positive sort, 10^6 Dynabeads coated with 1.25 µg biotinylated XBB RBD were prepared. The manufacturer's protocol was used to prepare the Dynabeads. In brief, the beads were washed twice with PBS containing 0.1% BSA using a magnet and were incubated with the appropriate amount of biotinylated XBB RBD in 500 µL (MACS Round 1) or 50 µL

(MACS Round 2) 0.1% BSA in PBS overnight at 4 °C with rotation. Dynabeads were washed and incubated in just 0.1% BSA in PBS for negative sorts against unlabeled beads.

The next day, the Dynabeads were washed with 0.1% BSA in PBS and resuspended in 100 µL 0.1% BSA in PBS. Unlabeled Dynabeads for the first negative selection were added to 10^{10} induced library cells (for MACS Round 1) or 10^9 induced MACS Round 1 cells (for MACS Round 2) and incubated at room temperature for 1 h with rotation. Next, unbound yeast cells were collected with a magnet and bound yeast cells and the Dynabeads were discarded. This negative selection was repeated once more with unlabeled beads. To perform the positive selection, the yeast cells were incubated with XBB RBD-coated beads for 1 h at room temperature with rotation. Unbound cells were collected and discarded, and the beads were washed 5 times with 0.1% BSA in PBS and a magnetic tube rack to completely remove unbound yeast cells. The yeast immobilized on the beads were transferred to 5 mL of SD-Trp media and were cultured at 30 °C and 250 rpm for 48 h.

5.2.6 *Fluorescence-activated cell sorting*

Four rounds of FACS were conducted with XBB RBD. 10^7 Nanobody-expressing yeast cells were labeled with 100 nM, 50 nM, 50 nM, or 5 nM biotinylated XBB RBD for FACS Rounds 1, 2, 3, or 4, respectively. Cells were also labeled with an anti-HA tag rabbit antibody (Invitrogen, 1:200) and incubated at room temperature with rotation for 20 min. The cells were washed with 0.1% BSA in PBS and then labeled with streptavidin R-phycoerythrin conjugate (Invitrogen, 1:250) and donkey anti-rabbit IgG Alexa Fluor 488 (Invitrogen, 1:500) for 10 min on ice. Cells were washed with 0.1% BSA in PBS and sorted

on a BD FACSAria Fusion cytometer. The selected yeast were cultured for 48 h in 5 mL SD-Trp media at 30 °C and 250 rpm.

5.2.7 *Individual nanobody selection*

Yeast cells from FACS Rounds 4.1 and 4.2 were plated on SD-Trp plates (3.8 g/L yeast synthetic drop-out medium supplements without tryptophan, 6.7 g/L yeast nitrogen base, 20 g/L glucose, 100 U/mL penicillin-streptomycin, 15 g/L agar) and incubated for 48 h at 30 °C. 12 colonies from each culture were used to inoculate 5 mL SD-Trp media and cultured for 48-36 h at 30 °C and 250 rpm. From each culture, plasmid DNA was extracted using the Zymoprep Yeast Plasmid Miniprep II kit (Zymo Research) following the manufacturer's protocol. The extracted DNA was used to transform NEB 5-alpha Competent *E. coli* cells (New England Biolabs) according to the manufacturer's protocol. The *E. coli* was cultured in 5 mL LB media with 100 µg/mL ampicillin at 37 °C with rotation. Plasmid DNA was extracted from each culture using the E.Z.N.A. Plasmid Mini Kit I (Omega Biotek) and sequenced by MCLAB (San Francisco, CA).

5.2.8 *Flow cytometry*

Induced yeast cells were labeled with a range of concentrations of biotinylated XBB RBD or S protein, anti-HA tag rabbit antibody, streptavidin R-phycoerythrin conjugate, and donkey anti-rabbit IgG Alexa Fluor 488 as described above. Binding was quantified on a CytoFLEX S flow cytometer (Beckman Coulter).

5.2.9 *Expression and purification of bivalent Fc fusion XNb nanobodies*

Genes encoding XNb 4.13, XNb 4.14, and XNb 4.15 fused to a mouse IgG Fc were synthesized and cloned into the TGEX-HC plasmid (Antibody Design Labs) by Gene Universal (Newark, DE). Plasmids were transfected into Expi293F cells, expressed, and harvested as described above. Fc fusion proteins were purified using a 1 mL HiTrap MabSelect SuRe column (GE) and the manufacturer's protocol. The cell supernatant was loaded into the HiTrap MabSelect SuRe column, washed with 10 column volumes of binding buffer (20 mM sodium phosphate, 0.15 M NaCl, pH 7.2) and eluted with a 20 column volume linear gradient of elution buffer (0.1 M sodium citrate, pH 3.5). Fc fusion proteins were then dialyzed into PBS and their concentration and purity were determined by BCA assay (Thermo Scientific) and SDS-PAGE, respectively.

5.2.10 *XNb ELISA binding analysis*

0.2 µg of XBB S protein in 100 µL of PBS was coated onto each well of a Nunc MaxiSorp 96-well flat-bottom plate (Invitrogen). After incubation overnight at 4 °C, the wells were blocked for 1 h with 200 µL of PBST (PBS with 0.05% Tween-20) containing 5% BSA. Following three washes with PBST, a 1 in 3 serial dilution was performed across the rows of the 96-well plate starting with 1,000 nM of Fc fused XNb 4.13, XNb 4.14, or XNb 4.15 in 1% BSA in PBST. One hour later, the wells were washed three times with PBST and horseradish peroxidase (HRP)-conjugated goat anti-mouse IgG antibody (Rockland, 1:5,000) in 1% BSA in PBST was added to each well for another 1 h incubation at room temperature. Following the incubation, the plate was washed three times with PBST. Then, 100 µL of TMB substrate solution (Thermo Scientific) was added to each

well for 2.5 min and the reactions were quenched with 100 μ L of 160 mM sulfuric acid. The absorbance of each well at 450 nm was measured.

Binding data were fit to a binding isotherm using global nonlinear least squares regression.⁸¹ Maximum absorbance values for each repeat were used to normalize the data. A single EC₅₀ value for each nanobody was determined as a fitted parameter across all six repeats.

5.2.11 Competition ELISAs

Each well of a Nunc MaxiSorp 96-well flat-bottom plate (Invitrogen) was coated with 0.2 μ g of XBB S protein in 100 μ l of PBS and incubated overnight at 4 °C. After the incubation, the plate was washed three times with PBST. Samples (100 μ L per well) of 1% BSA in PBST containing 10 nM of Fc fused XNb 4.13, XNb 4.14, or XNb 4.15 mixed with 1 in 3 serial dilutions (initial concentration of 1,000 nM) of S309, CR3022 (two RBD-binding mAbs), or ACE2-Fc were prepared. These pre-mixed samples were transferred to corresponding wells of the 96-well plate and were incubated for 1 h at room temperature. Following three washes with PBST, HRP-conjugated goat anti-mouse IgG antibody (Rockland, 1:5,000) in 1% BSA in PBST was added to each well. After 1 h incubation, the plate was washed three times with PBST before adding 100 μ L of TMB substrate solution (Thermo Scientific). After 2.5 min, the reactions were stopped with 100 μ L of 160 mM sulfuric acid and the absorbance at 450 nm was measured.

5.2.12 Neutralization assays

Neutralization assays were performed by the Kawaoka Lab. Briefly, serial dilutions of the Fc fusion proteins starting at 50 µg/mL were mixed with vesicular stomatitis virus pseudotyped with the XBB S protein and incubated for 1 h at 37 °C. The virus and antibody mixtures were inoculated onto Vero E6/TMPRSS2 cells cultured in a 96-well plate and then incubated for 1 h at 37 °C. Cells were fixed and stained and foci were quantified.

5.2.13 Challenge experiments

Challenge experiments were performed by the Kawaoka Lab. Briefly, 100 µg (5 mg/kg) of XNb 4.13, XNb 4.14, or BiMT3.1-Fc, were administered intraperitoneally to K18-hACE2 mice (n = 5/group) 24 hours prior to their infection with 10⁵ plaque-forming units (pfu) of XBB virus. Three days after infection, lung tissue was collected, and viral lung titers were measured.

5.3 Results and Discussion

5.3.1 Identification of nanobodies targeting the XBB spike protein

To identify nanobodies that target the spike protein of the XBB SARS-CoV-2 variant, we screened a synthetic yeast surface display nanobody library against recombinant XBB RBD.⁸⁰ These screens contained two rounds of MACS against XBB RBD immobilized on magnetic beads and then four rounds of FACS against decreasing concentrations of XBB RBD. During FACS Round 4, two populations of yeast expressing RBD-binding nanobodies were sorted (indicated as 4.1 and 4.2) to ensure selection of a variety of unique nanobody mutants. After each sort, yeast cells were labeled with XBB

RBD (Figure 25) to evaluate binding. Throughout our rounds of screening, we observed an enrichment of binding to XBB RBD.

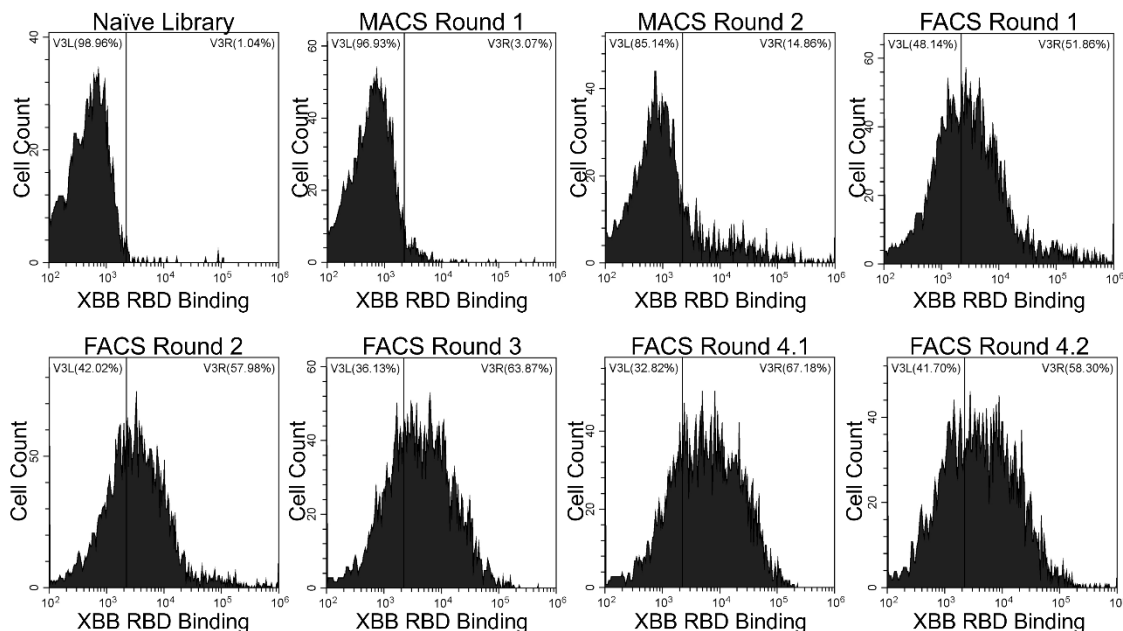


Figure 25. Enrichment of nanobody binding to XBB RBD. Yeast cells from the naïve nanobody library or enriched libraries after MACS or FACS screens were labeled with 30 nM XBB, and the extent of binding was evaluated with flow cytometry. Fluorescence signal corresponding to XBB RBD binding to yeast displayed nanobodies is shown on the x-axis. Binding to XBB RBD above the level of the nanobody library appears on the right side of the vertical gate.

From the enriched libraries resulting from FACS Round 4.1 and 4.2 sorts, 12 nanobodies were randomly selected and sequenced. Of the 24 nanobodies selected, ten had unique sequences (Table 2, Appendix Table 8). Flow cytometric binding analysis was performed to assess binding of these ten yeast displayed nanobodies to XBB RBD (Figure 26a). All ten nanobodies showed binding to XBB RBD, however nanobodies 3, 4, 5, 6, 9, and 10 demonstrated stronger binding than the others. Next, binding of these six nanobodies to XBB S protein was evaluated with flow cytometry (Figure 26b). This was done to check if the binding we observed to the RBD translated to S protein binding and to

investigate if any of these nanobodies bound to epitopes on the RBD that are inaccessible on the S protein. Interestingly, we observed a wide range of binding of these nanobodies to the XBB S protein. Nanobody 3 demonstrated no binding to XBB S suggesting that its binding epitope was hidden in the full S protein. Nanobodies 4 and 10 showed good binding to XBB S, however nanobodies 5, 6, and 9 showed the highest levels of binding to XBB S. These three lead nanobodies, called XNb 4.13, XNb 4.14, and XNb 4.15, were chosen for further characterization.

Table 2. Sequences of CDR1, CDR2, and CDR3 of the ten selected nanobodies.

Nanobody	CDR1	CDR2	CDR3
1	GITFNGNAM	ELVAAISSGGSTNY	NAESAVYTYVSWGRWSKTEYNY
2	GTAYDM	EFVADITWSDGSTYY	NRSYYWFTGYAYDY
3	GFIFDDYAM	ELVAAISWSGDRTY	VSWSPERFDY
4	GLIFDTNAM	ELVAAISLDGTSTYY	ARDDQLFRLYYGSWYGEYDS
5 (XNb 4.13)	GIIFVYTM	ELVASISSDGSTNY	AARDVDYFDLYDY
6 (XNb 4.15)	GLIFYVYDM	ELVAAITSNGDSTYY	AKLREAYYDPQTAGKIDY
7	GSTFATNAM	ELVAAINYSGGSTYY	AAEAQLAIYYGDSVDYDY
8	GITFSEYVM	ELVAAISSSGGSTYY	AKDVYTIYGGYPYGYDY
9 (XNb 4.14)	GLIFLEYAM	ELVAAISSNGDSTYY	AAEDWAPYYGGVADYDY
10	GRIFYANDM	EFVADIRWSSGGSTYY	ARRAQAYGGRYDY

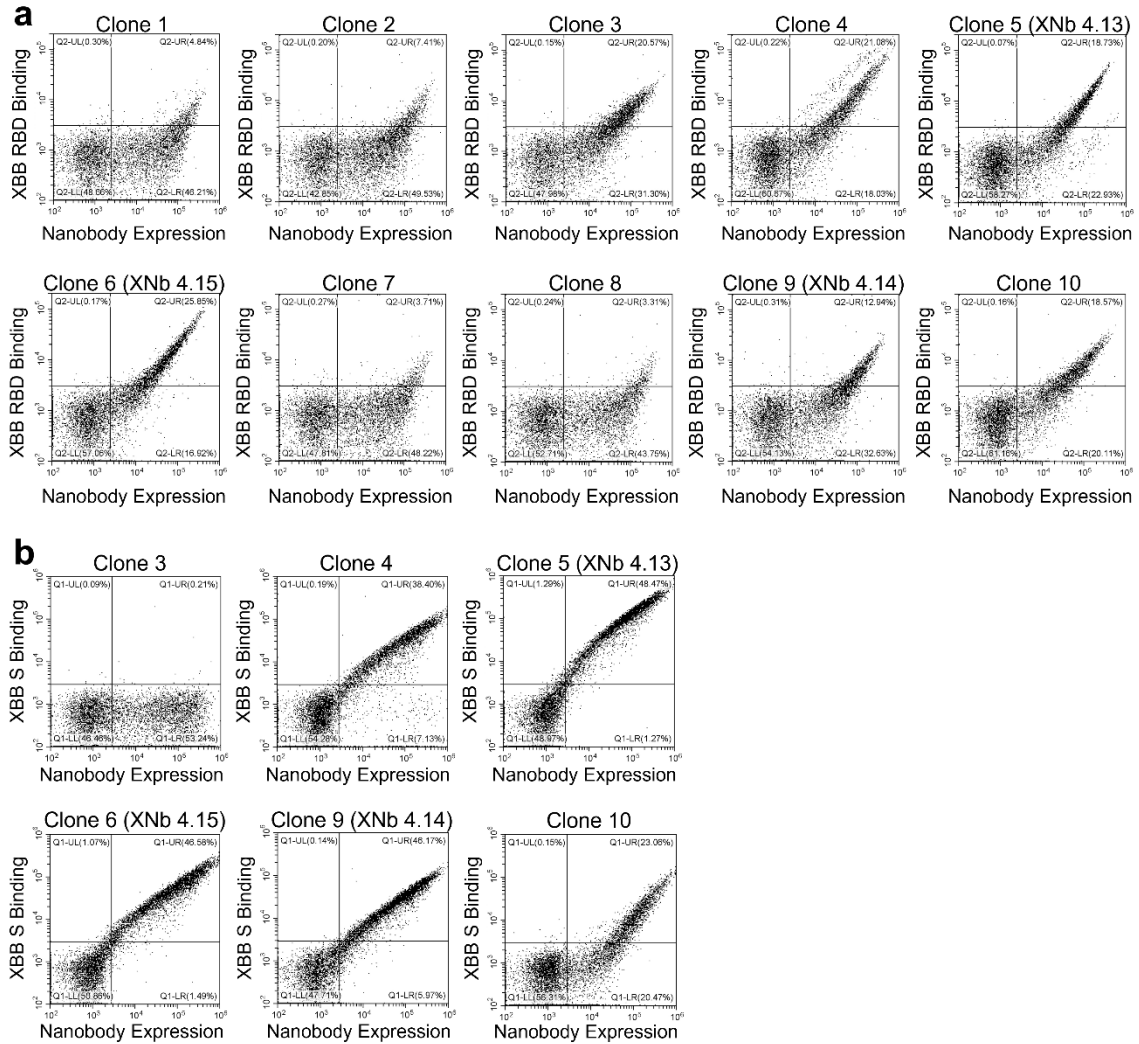


Figure 26. Single clone analysis of selected nanobodies. a-b) Yeast cells expressing multiple copies of one of the selected nanobodies were labeled with (a) 10 nM XBB RBD or (b) 1 nM XBB S, and the extent of binding was assessed with flow cytometry. Plots display fluorescent signal corresponding to binding on the y-axis and fluorescent signal corresponding to the expression level of the nanobodies on the x-axis.

5.3.2 Nanobodies bind with high affinity to the XBB spike protein

We next designed, expressed, and characterized bivalent versions of XNb 4.13, XNb 4.14, and XNb 4.15 fused to a mouse IgG Fc (Figure 27a). To measure binding affinity to XBB S protein, we performed titration ELISAs with a wide range of concentrations of our nanobodies (Figure 27b). This analysis revealed that XNb 4.13, XNb

4.14, and XNb 4.15 were high affinity binders with subnanomolar EC_{50} s (194, 483, and 329 pM, respectively). Our nanobodies bound to the XBB S with similar affinities or more strongly than an ACE2 Fc fusion protein (ACE2-Fc).

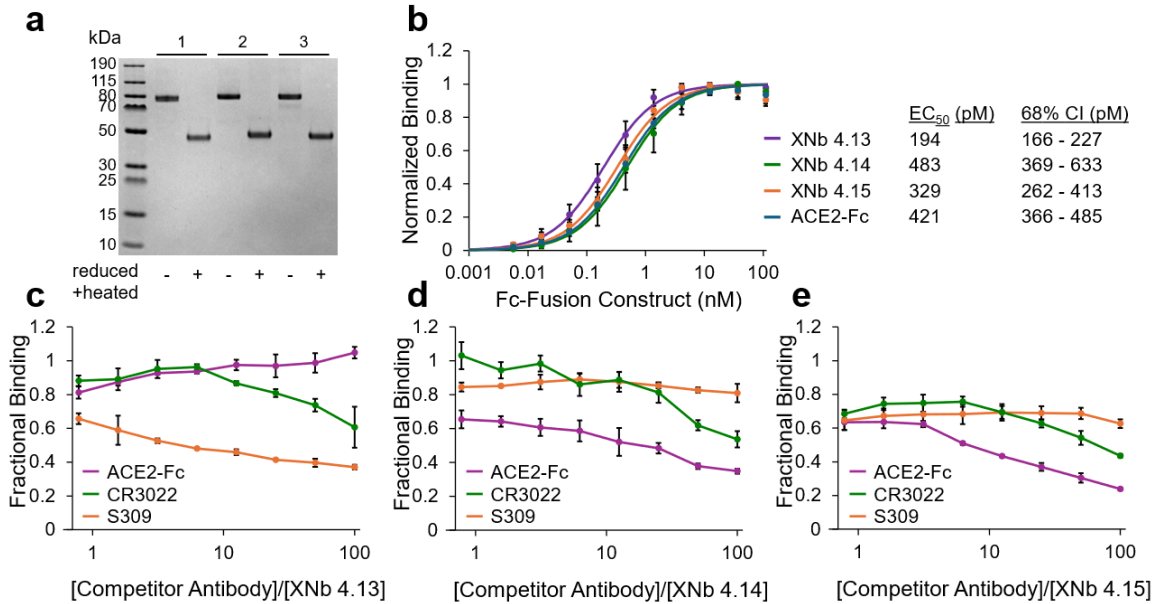


Figure 27. *In vitro* analysis of XBB S-binding nanobodies. a) An SDS-PAGE gel with bivalent Fc fusion constructs containing nanobodies (1) XNb 4.13, (2) XNb 4.14, and (3) XNb 4.15. b) Binding of XNb 4.13, XNb 4.14, XNb 4.15, and ACE2-Fc to XBB S was assessed by ELISA. Data points are averages of six repeats from two independent assays and error bars indicate standard deviation. EC_{50} s were calculated using a global nonlinear least squares fit of the ELISA data. c-d) Competition ELISAs with XBB S (immobilized antigen) and ACE2-Fc, CR3022, and S309 antibodies (soluble competitor) were conducted to investigate the binding epitopes of (c) XNb 4.13, (d) XNb 4.14, and (e) XNb 4.15 on XBB S. XNb nanobody binding in the presence of the competitor antibodies is shown relative to binding in the absence of competitor antibodies. Data points are averages of three repeats and error bars indicate standard deviation.

To further investigate how our nanobodies interact with XBB S, we performed competition ELISAs with ACE2-Fc and RBD-binding antibodies CR3022 and S309 (Figure 27c-e). CR3022 is a conformation-dependent antibody isolated from a SARS-CoV-1 patient that also binds to the SARS-CoV-2 S protein.¹⁸⁶ S309 (the parent mAb of sotrovimab) was also isolated from a SARS-CoV-1 patient and neutralizes SARS-CoV-1

and SARS-CoV-2 viruses.¹⁸⁷ The binding sites of both antibodies on the RBD are distinct from the ACE2 binding site or the receptor-binding motif (RBM).^{186,187} For these experiments, a constant concentration of our nanobodies (10 nM) was mixed with a range of concentrations of the competitor antibody (ACE2-Fc, CR3022, or S309), and then the nanobody's ability to bind to XBB S was assessed.

The binding of XNb 4.13 was greatly reduced but not completely blocked by S309 and reduced to a lesser extent by CR3022 (Figure 27c). At 100-fold molar excess S309 or CR3022, XNb 4.13 retained only 37% or 61% of its binding to XBB S. These results suggest that XNb 4.13 and S309 have similar but not completely overlapping binding epitopes. The binding of XNb 4.13 to XBB S was not impacted by ACE2-Fc indicating that its epitope is distinct from the RBM. Competition experiments with XNb 4.14 and XNb 4.15 produced very similar results revealing that these two nanobodies bind to the XBB S at similar epitopes (Figure 27d, e). The binding of both nanobodies was greatly inhibited by ACE2-Fc and slightly inhibited by CR3022 suggesting that their binding epitope is at least partially within the RBM. XNb 4.14 and XNb 4.15 retained 35% and 24% binding to XBB S, respectively, in the presence of 100-fold molar excess ACE2-Fc and 54% and 44% binding to XBB S, respectively, in the presence of 100-fold molar excess CR3022. Binding of XNb 4.14 and XNb 4.15 were not impacted by S309 in a concentration-dependent manner.

5.3.3 Nanobodies neutralize XBB and protect against an XBB challenge

To evaluate the ability of XNb 4.13, XNb 4.14, and XNb 4.15 to neutralize XBB pseudovirus, our collaborators in the Kawaoka Lab conducted virus neutralization assays

on VeroE6/TMPRSS2 cells. XNb 4.13 and XNb 4.14, but not XNb 4.15, neutralized XBB pseudovirus. Neutralization EC₅₀s with XNb 4.13 and XNb 4.14 were 46 nM and 109 nM, respectively.

Based on these results, we proceeded with *in vivo* characterization of XNb 4.13 and XNb 4.14 nanobodies with XBB challenge experiments in mice. 100 µg (5 mg/kg) of XNb 4.13, XNb 4.14, or a control bivalent nanobody Fc fusion protein, BiMT3.1-Fc⁷⁹, were administered intraperitoneally to K18-hACE2 mice (n = 5/group) 24 hours prior to XBB infection by the Kawaoka Lab. Three days after infection, viral lung titers were measured. Treatment with XNb 4.13 or XNb 4.14 significantly reduced viral titers in challenged mice compared to the control antibody (Figure 28). The mean viral titers in the lungs of mice treated with XNb 4.13 or XNb 4.14 were 65- or 19-fold lower than that of mice treated with the control Fc fusion protein, respectively. While these reductions in viral titers are modest, they may be enough to provide protection and improve survival after a challenge with the XBB SARS-CoV-2 variant. Modhiran et al. demonstrated that their Fc-fused nanobody W25, when given intraperitoneally, did not significantly reduce viral titers compared to control treated mice after an Omicron BA.1 infection, but W25-Fc treatment improved survival from 25% to 62.5% compared to control treated mice.¹⁷⁵ When given intranasally, W25-Fc also did not significantly reduce viral titers compared to control treated mice, yet W25-Fc treatment improved survival from 12.5% to 75% compared to control treated mice.¹⁷⁵ This result also suggests the potential benefit of treating intranasally as opposed to intraperitoneally.

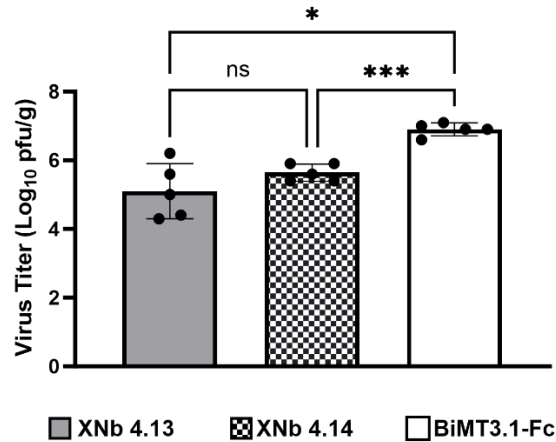


Figure 28. XNb 4.13 and XNb 4.14 protect against XBB challenges. K18-hACE2 mice were treated with XNb 4.13 and XNb 4.14 and infected with XBB virus. Three days later, viral lung titers were calculated. Shown are means and standard deviations from 5 mice per group. *** $P < 0.001$, * $P < 0.05$, ns: not significant, determined by Brown-Forsythe and Welch ANOVA tests.

5.4 Conclusions and Future Work

In this work, we have identified three XBB S protein-binding nanobodies, two of which neutralize the XBB variant *in vitro* and significantly reduce viral load in the lungs of mice challenged with XBB, a result that has not been shown before with SARS-CoV-2-targeting nanobodies. XNb 4.13, XNb 4.14, and XNb 4.15 were developed through the *in vitro* screening of a synthetic nanobody library⁸⁰ and demonstrate subnanomolar levels of binding towards the XBB S protein. Competition ELISAs suggest that the binding epitopes of our two neutralizing nanobodies, XNb 4.13 and XNb 4.14, are distinct and motivate our future work to create a bispecific Fc fusion protein containing both nanobodies. The geometry of these nanobodies will be similar to the bispecific BBB shuttles developed in Chapter 3—two copies of XNb 4.13 connected with a (GGG)₁₀ linker to XNb 4.14 fused to a mouse Fc. We will repeat neutralization and XBB challenge studies with this new

bispecific nanobody to assess potential synergistic effects of combining XNb 4.13 and XNb 4.14.

To evaluate the breadth of protection offered by XNb 4.13, XNb 4.14, and the bispecific nanobody we will be conducting neutralization experiments with EG.5.1, an XBB subvariant¹⁸⁸, and JN.1, a recent Omicron variant from the BA.2.86 lineage that is the mostly widely circulating variant in the United States as of May 2024⁵². If our nanobodies neutralize these viruses, challenge studies with these strains could be explored in future work.

To alter the binding ability of XNb 4.13 and XNb 4.14 to improve affinity and XBB neutralization or breadth of protection to circulating variants, mutagenesis of these nanobodies and additional screening against SARS-CoV-2 RBDs can be conducted. Other considerations for future studies include analyzing different methods of nanobody administration including intranasal administration and performing a dose response study to identify the optimal nanobody dosage for *in vivo* challenge studies.

Overall, this work demonstrates the utility of using a completely *in vitro* method for the development of high affinity XBB-targeting nanobodies that neutralize the SARS-CoV-2 XBB variant. These results will guide future work to rapidly and easily develop mono- or multispecific nanobodies that target the newest SARS-CoV-2 variants of concern.

CHAPTER 6. CONCLUSION AND FUTURE DIRECTIONS

In this work, we developed and characterized multivalent nanobody constructs with specificity for amyloid proteins involved in neurodegenerative diseases and a multivalent viral surface protein involved in infectious disease. There is a lack of disease-modifying treatments and effective diagnostic and research tools for these complex and widespread diseases, particularly neurodegenerative diseases such as Alzheimer's disease. mAbs that target proteins involved in neurodegenerative diseases, especially conformational antibodies that are specific for different aggregate forms of these pathogenic proteins, have shown promise as disease-modifying therapeutics and as diagnostic or research tools. However, the development of conformational mAbs for these complex proteins is limited by traditional *in vivo* antibody development techniques and the heterogeneity of amyloid antigens including their valency, conformation, and solubility. Here, we describe an entirely *in vitro* method for generating conformational nanobodies that target amyloid and multivalent proteins through the screening of a synthetic yeast surface display nanobody library. Due to their small size and the shape of their paratope, nanobodies can interact with these target antigens at epitopes not accessible to traditional IgG antibodies.

We began with the development of a facile *in vitro* screening approach to generate nanobodies with specificity for tau protein relative to other amyloid proteins including amyloid- β and α -synuclein. We created bivalent and tetravalent versions of our lead tau-targeting nanobody, MT3.1, to improve its avidity towards tau aggregates. We show that MT3.1 binds to a critical amyloidogenic motif within the fibril core of tau and to pathogenic tau found in the brains of tau transgenic mice.

In collaboration with the Tessier Lab, we characterized conformational nanobodies that recognize tau fibrils. These nanobodies show conformational specificity towards tau fibrils over tau monomer and have broad impacts towards the study of different tau fibril conformations present in tauopathies and understanding the involvement of tau fibrils in disease progression. To improve their delivery across the BBB, we have modified these tau fibril-targeting nanobodies through the addition of an anti-TfR single-domain antibody. We are excited about the future directions with these bispecific antibody shuttle constructs. To date, we have confirmed the binding of these bispecific shuttles to tau fibrils and TfR *in vitro*. Future work can be conducted to evaluate their delivery and efficacy *in vivo*. These experiments would involve the intravenous administration of our bispecific shuttles in P301S tau mice. Measurement of the antibody shuttle concentration in the brain and blood would help us determine the best dose and frequency for treatment, and immunostaining of mouse brain sections would allow us to evaluate the targeting of these shuttles to tau fibrils in the brain. Longer term experiments in mice would allow us to investigate the ability of our bispecific antibody shuttles to reduce tau pathology and cognitive decline in P301S tau mice.

Tau oligomers are attractive targets for tauopathy immunotherapy as their presence in the brain correlates well with cognitive deficits seen in AD. Here, we report the development of the first conformational tau oligomer-specific nanobodies. We constructed bivalent versions of these nanobodies, OT2.4 and OT2.6, and showed that they specifically bind tau oligomers over tau monomer and fibrils and target multiple discontinuous epitopes on the tau protein. We showed that these nanobodies recognize tau oligomers in brain lysates from human patients with AD and healthy older adults with primary age-related

tauopathy. As tau oligomers are detected in the brains of humans with early-stage AD and in the brains of older adults without neurodegenerative diseases, one limitation of this study is the lack of a negative control for OT2.4 and OT2.6 staining of human tissue samples. Future work would include western blotting with young adult brain samples that do not contain tau oligomers or other pathogenic tau aggregates as confirmed by T22 and AT8 staining. Young adult human brain samples are difficult to obtain, so an alternative experiment would include the western blotting of samples from the brains of young (1 month old) and old (9 months old) wild-type and transgenic mouse models of tauopathy.

Another important direction for future work would involve functional assays to characterize OT2.4 and OT2.6 such as cell-based experiments to investigate our nanobodies' ability to stop the spread of tau oligomers from cell to cell or reduce tau oligomer-induced cytotoxicity. We have begun to perform cytotoxicity experiments in our lab with SH-SY5Y human neuroblastoma cells (Figure 29). SH-SY5Y cells were plated in a 96-well plate and cultured overnight. Tau oligomers or monomer (250 nM) were added to the cells and the plate was incubated for 24 h. Cell proliferation was then measured with an MTT assay. As seen in Figure 29, the application of our tau oligomers resulted in cytotoxic effects in the SH-SY5Y cells. The Kaye group has previously shown that TOMA (at a 1-, 2-, or 4- fold molar excess over tau oligomers) was able to reduce cytotoxicity by tau oligomers in SH-SY5Y cells.⁶⁵ In future work, we could further optimize our experimental setup and test the inhibitory efficacy of our tau oligomer nanobodies as well as TOMA (positive control).

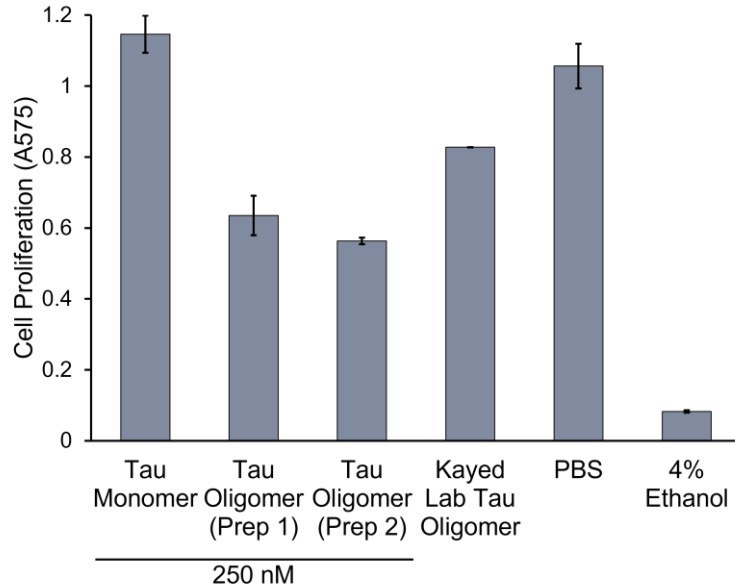


Figure 29. Tau oligomer-induced cytotoxicity in SH-SY5Y neuroblastoma cells. SH-SY5Y cells were treated with 250 nM tau monomer, 250 nM tau oligomers, PBS (negative control for cell toxicity), and a solution of 4% ethanol in PBS (positive control for cell toxicity) for 24 h and cell proliferation was measured using an MTT assay. Two individual preparations of tau oligomers from our lab and one from the Kayed lab were used. $n = 2$; error bars correspond to standard deviation.

There are many other future directions with the oligomer-specific nanobodies OT2.4 and OT2.6 that would be interesting to explore. One is the development of bispecific antibody shuttles containing one of these tau oligomer nanobodies and a BBB receptor-targeting single-domain antibody such as F02 or VHHA. The development, characterization, and future mouse studies with these constructs would mirror those performed and proposed for our tau fibril-targeting bispecific shuttles. An antibody construct that could efficiently pass through the BBB, even when administered at low concentrations, and target soluble tau oligomers in the brain would have great potential as a disease-modifying tauopathy therapeutic. These antibodies could bind to extracellular tau oligomers to promote their clearance or prevent the transneuronal spreading of tau oligomers and propagation of tau oligomerization.

We have begun applying the screening strategies we have developed in Chapter 2 and Chapter 4 towards screens of oligomers of the amyloid- β protein. To date, three sorts of the nanobody library against amyloid- β oligomers have been conducted. Future work will include completing these screens with one or two additional FACS selections. Then individual nanobodies from the enriched library will be selected and using flow cytometry, binding to amyloid- β oligomers and off-target binding to amyloid- β monomer will be assessed. The highest performing nanobodies in terms of overall affinity and specificity will be selected and expressed as bivalent Fc fusion proteins similar to MT3.1, OT2.4, and OT2.6. Characterization of these nanobody constructs will be conducted to confirm their specific binding to amyloid- β oligomers, determine their binding epitope on amyloid- β , and assess their ability to bind pathogenic oligomeric amyloid- β in mouse or human brain samples.

In the last chapter of this work, we described the use of *in vitro* antibody discovery to develop high affinity nanobodies XNb 4.13, XNb 4.14, and XNb 4.15 that target the S protein of the XBB SARS-CoV-2 variant. We showed that two of these nanobodies, XNb 4.13 and XNb 4.14, neutralized the XBB variant and provided protection during an XBB challenge in mice. We are currently developing a bispecific Fc fusion protein that contains both nanobodies XNb 4.13 and XNb 4.14, which bind to the XBB S protein in different locations. In neutralization assays and challenges in mice, we will evaluate how this bispecific nanobody performs against XBB. Future work could explore neutralization and challenge studies with XNb 4.13, XNb 4.14, and the bispecific nanobody against more recently circulating Omicron variants EG.5.1 and JN.1 to assess the breadth of protection provided by these nanobodies. In future work, we also can use directed evolution to

improve the binding affinity and neutralization or breadth of protection offered by XNb 4.13 and XNb 4.14. These nanobodies could be mutated using error-prone PCR in the CDRs, CDR swapping, or a combination of these techniques, and new nanobody libraries could be constructed. MACS and FACS screens would then be conducted against XBB RBD or RDBs of different SARS-CoV-2 variants to select nanobodies with the desired binding properties.

In summary, this work has explored the development and characterization of multivalent nanobodies that specifically target different forms of amyloid proteins involved in neurodegenerative diseases and a surface protein on the SARS-CoV-2 virus. We demonstrate the utility of using a completely *in vitro* process for the discovery of nanobodies that bind to complex or heterogeneous multimeric proteins. The multivalent nanobodies developed here can be used to study amyloid protein morphology and understand the involvement of these proteins in neurodegenerative disease progression or can be engineered into potent and effective therapeutics. We are excited about the future directions of these projects and their impact on the field of antibody engineering and antibody-based therapeutics.

APPENDIX. SUPPLEMENTARY TABLES

Table 3. Selected nanobody sequences from screens against tau monomer.

Nanobody	Sequence
1	QVQLVESGGGLVQAGGSLRLSCAASGSTFHWYAMGWYRQAPGKER ELVAAIFISGSTYYADSVKGRFTISRDNKNTVYLMNSLKPEDTAVYYC AADAYAQKSVLDLYYWGQGTQVTVSS
2 (MT2.1)	QVQLVESGGGLVQAGGSLRLSCAASGFTLTDYDMGWYRQAPGKERE LVAAISWSSGRTYYADSVKGRFTISRDNKNTVYLMNSLKPEDTAVY YCARGRSYYVATYDGDYWGQGTQVTVSS
3	QVQLVESGGGLVQAGGSLRLSCAASGRIFDINAMGWYRQAPGKEREL VAAITSDSGSTYYADSVKGRFTISRDNKNTVYLMNSLKPEDTAVYYC TAGYDDGYLSVTFDYWGQGTQVTVSS
4 (MT2.4)	QVQLVESGGGLVQAGGSLRLSCAASGIIFTNYAMGWYRQAPGKEREL VAAISTSGGRTYYADSVKGRFTISRDNKNTVYLMNSLKPEDTAVYY CAADHDEGPYYYWGQGTQVTVSS
5	QVQLVESGGGLVQAGGSLRLSCAASGRTSVRYAMGWYRQAPGKERE LVAAIRWRDGDYYADSVKGRFTISRDNKNTVYLMNSLKPEDTAVY YCAARTPGYWYPSRDDYWGQGTQVTVSS
6 (MT3.1)	QVQLVESGGGLVQAGGSLRLSCAASGFIFSTYAMGWYRQAPGKEREL VAGISSSGSTYYADSVKGRFTISRDNKNTVYLMNSLKPEDTAVYYC AADYYRLDYYYYLGQGTQVTVSS

Table 4. Tau fibril-binding nanobody and scFv sequences.

Nanobody	Sequence
WA2.22	PAMADVQLQASGGGLVQPGGSLRLSCAASGRIVSLGNMAWYRQAPG KQRELVASVGRGGNTYYADSVKGRSTISRDDAKKMLEMNSLKPED TAVYNCFVLVQPTYDPYWGQGTQVTVSSEPKTPKPQP
ATA1.459.3 V_H	QVQLQQSGPGLLKPSETLSLTCVISGDSVSSNSVTWNWIRQSPSRGL EWLGRTYFRRRWYNDYAVSVKSRTINPDTSKNQFSLQLNSATPEDTA VYYCARQMDKGVGFDFWGQGTQVTVSS
ATA1.459.3 V_L	EIVLTQSPATLSLSPGERATLSCRASQSVSSYLAWYQQKPGQAPRLLIY DASNRATGIPARFSGSGSDFTLTISLLEPEDFAVYYCQQRHNWPPT FGQGTREIK
P8.A1.A21	QVQLVESGGGLVQAGGSLRLSCAASGRTFSHYSMGWYRQAPGKQRE LVAAITNSGRNTYVDSVKGRFTISKDNKNTVYLMNSLKPEDTADYFC NLIGYHDMYYAFWGQGTQVTVSS

Table 5. Tfr-binding single-domain antibody sequences.

Nanobody	Sequence
F02	ARVDQTPQTITKETGESLTINCVLRDNDCTLSSTHWYRKKSGSTNEERI SKGGRYVETVNSGSKSFLRINDLTVEDSGTYRCNVYAMTRNWWCD VYGGGTVVTVNAASGA
VHHA	EVQLVESGGGVVQPGGSLKLSVASGTDGFSINFIRWYRQAPGKQREF VAGFTATGNTNYADSMKGRFTISRDNKNAVYLVQIDSLKPEDTAVYYCY MLDKWGQGTQVTVSS

Table 6. Selected nanobody sequences from screens against tau oligomer.

Nanobody	Sequence
1 (OT2.6)	QVQLVESGGGLVQAGGSLRSLCAASGRTFRYNAMGWYRQAPGKERE LVAAITVRTGSTYYADSVKGRFTISRDNKNTVYLVQMNSLKPEDTAVYYC AVDRDYLVRYSQLYREYGYWGQGTQVTVSS
2	QVQLVESGGGLVQAGGSLRSLCAASGITFRSYAMGWYRQAPGKERE VAAITSGGASTYYADSVKGRFTISRDNKNTVYLVQMNSLKPEDTAVYYC AARRPYKPYDYWGQGTQVTVSS
3	QVQLVESGGGLVQAGGSLRSLCAASGRTFYRYTMGWYRQAPGKEREL VAAISFRAGRYYADSVKGRFTISRDNKNTVYLVQMNSLKPEDTAVYYC AADQYLSADYDYWGQGTQVTVSS
4	QVQLVESGGGLVQAGGSLRSLCAASGSIFRANAMGWYRQAPGKEREL VAAITGSRYYADSVKGRFTISRDNKNTVYLVQMNSLKPEDTAVYYCA RRALYLPQRINYSAMDYWGQGTQVTVSS
5	QVQLVESGGGLVQAGGSLRSLCAASGYTFGRNTMGWYRQAPGKERE FVAAITQSGGNTYYADSVKGRFTISRDNKNTVYLVQMNSLKPEDTAVYY CNARLRPPYGWKYGYWGQGTQVTVSS
6	QVQLVESGGGLVQAGGSLRSLCAASGFTFGGANVMGWYRQAPGKER ELVAAITYGGGSTYYADSVKGRFTISRDNKNTVYLVQMNSLKPEDTAVY YCAARSYRYWTQILYDYWGQGTQVTVSS
7	QVQLVESGGGLVQAGGSLRSLCAASGRTFTSYTMGWYRQAPGKEREL VAAITDRGGRTYYADSVKGRFTISRDNKNTVYLVQMNSLKPEDTAVYYC NTVWGYHGGDEVDHWGQGTQVTVSS
8	QVQLVESGGGLVQAGGSLRSLCAASGRTFVWNAMGWYRQAPGKERE LVAAITYRGASTYYADSVKGRFTISRDNKNTVYLVQMNSLKPEDTAVYY CNARKYVTLKYDYWGQGTQVTVSS
9	QVQLVESGGGLVQAGGSLRSLCAASGRTFGRNAMGWYRQAPGKERE LVAAITGGSTNYADSVKGRFTISRDNKNTVYLVQMNSLKPEDTAVYYC AATRWRKYYYYWGQGTQVTVSS
10 (OT2.4)	QVQLVESGGGLVQAGGSLRSLCAASGIISNNAMGWYRQAPGKERE VAAISTSGGSTYYADSVKGRFTISRDNKNTVYLVQMNSLKPEDTAVYYC NRRVVERYWRGYWYREDGYWGQGTQVTVSS

Table 7. Sample data. PART = primary age-related tauopathy, ABC = Activities of Daily Living, Behavioral and Psychological Symptoms of Dementia, and Cognitive Function Dementia Scale, CERAD = Consortium to Establish a Registry for Alzheimer's Disease score.

Subject #	Primary Neuropathologic Diagnosis	Other Neuropathologic Diagnosis - Tau	Frontal NFT	Braak Stage	ABC	CERAD	Age at Death (yrs)	PMI (h)	Race	Sex
1	AD		frequent	VI	3	3	87	13	w	f
2	AD		frequent	VI	3	3	77	6.5	w	m
3	AD		frequent	VI	3	3	82	22.5	w	m
4	AD		frequent	VI	3	3	87	5	w	m
5	AD		frequent	VI	3	3	82	4.5	w	f
6	Control	PART	0	II	0	0	78	11.5	w	f
7	Control	PART	0	II	0	0	>89	5.5	w	m
8	Control	PART	0	III	1	1	>89	6	w	f
9	Control	PART	0	I	1	0	70	2.5	b	m
10	Control	PART	0	I	0	0	72	7	w	m

Table 8. Selected nanobody sequences from screens against XBB RBD.

Nanobody	Sequence
1	QVQLVESGGGLVQAGGSLRLSCAASGITFNGNAMGWYRQAPGKEREL VAAISSGGSTNYADSVKGRFTISRDNKNTVYLQMNSLKPEDTAVYYCN AESAVYTYVSWGRWSKTEYNYWGQGTQVTVSS
2	QVQLVESGGGLVQAGGSLRLSCAASGTAYDMGWYRQAPGKEREFVAD ITWSDGSTYYADSVKGRFTISRDNKNTVYLQMNSLKPEDTAVYYCNR YYWFTGYAYDYWGQGTQVTVSS
3	QVQLVESGGGLVQAGGSLRLSCAASGFIFDDYAMGWYRQAPGKEREL VAAISWSDRYYADSVKGRFTISRDNKNTVYLQMNSLKPEDTAVYYV SWSPEPRFDYWGQGTQVTVSS
4	QVQLVESGGGLVQAGGSLRLSCAASGLIFDTNAMGWYRQAPGKEREL VAAISLDGTSTYYADSVKGRFTISRDNKNTVYLQMNSLKPEDTAVYYC ARDDQLFRLLYYGSWYGEYDSWGQGTQVTVSS
5 (XNb 4.13)	QVQLVESGGGLVQAGGSLRLSCAASGIIFVYTMGWYRQAPGKERELV ASISSDGSTNYADSVKGRFTISRDNKNTVYLQMNSLKPEDTAVYYCAA RDVDYFDLYDYWGQGTQVTVSS
6 (XNb 4.15)	QVQLVESGGGLVQAGGSLRLSCAASGLIFYVDMGWYRQAPGKEREL VAAITSNVDSTYYADSVKGRFTISRDNKNTVYLQMNSLKPEDTAVYYC AKLREAYYDPQTAGKIDDYWGQGTQVTVSS
7	QVQLVESGGGLVQAGGSLRLSCAASGSTFATNAMGWYRQAPGKEREL VAAINYSGGSTYYADSVKGRFTISRDNKNTVYLQMNSLKPEDTAVYYC AAEAQLAIYYGDSVDYDYWGQGTQVTVSS
8	QVQLVESGGGLVQAGGSLRLSCAASGITFSEYVMGWYRQAPGKEREL VAAISSGGSTYYADSVKGRFTISRDNKNTVYLQMNSLKPEDTAVYYC AKDVYTIYYGGYPYGYDYWGQGTQVTVSS
9 (XNb 4.14)	QVQLVESGGGLVQAGGSLRLSCAASGLIFLEYAMGWYRQAPGKERELV AAISSNGDSTYYADSVKGRFTISRDNKNTVYLQMNSLKPEDTAVYYCA AEDWAPYYGGVADYDYWGQGTQVTVSS
10	QVQLVESGGGLVQAGGSLRLSCAASGRIFYANDMGWYRQAPGKEREF VADIRWSSGGSTYYADSVKGRFTISRDNKNTVYLQMNSLKPEDTAVYY CARRAQAYGGRYDYWGQGTQVTVSS

REFERENCES

1. Millward SW, Agnew HD, Lai B, et al. In situ click chemistry: from small molecule discovery to synthetic antibodies. *Integr Biol (Camb)*. 2013;5(1):87. doi:10.1039/C2IB20110K
2. Alfaleh MA, Alsaab HO, Mahmoud AB, et al. Phage Display Derived Monoclonal Antibodies: From Bench to Bedside. *Front Immunol*. 2020;11:567223. doi:10.3389/FIMMU.2020.01986/BIBTEX
3. Lu RM, Hwang YC, Liu IJ, et al. Development of therapeutic antibodies for the treatment of diseases. *Journal of Biomedical Science 2020 27:1*. 2020;27(1):1-30. doi:10.1186/S12929-019-0592-Z
4. Gklinos P, Papadopoulou M, Stanulovic V, Mitsikostas DD, Papadopoulos D. Monoclonal Antibodies as Neurological Therapeutics. *Pharmaceuticals 2021, Vol 14, Page 92*. 2021;14(2):92. doi:10.3390/PH14020092
5. Alejandra WP, Miriam Irene JP, Fabio Antonio GS, et al. Production of monoclonal antibodies for therapeutic purposes: A review. *Int Immunopharmacol*. 2023;120:110376. doi:10.1016/J.INTIMP.2023.110376
6. Mullard A. FDA approves 100th monoclonal antibody product. *Nat Rev Drug Discov*. 2021;20(7):491-495. doi:10.1038/D41573-021-00079-7
7. Lyu X, Zhao Q, Hui J, et al. The global landscape of approved antibody therapies. *Antib Ther*. 2022;5(4):233. doi:10.1093/ABT/TBAC021
8. Pillay TS, Muyldermans S. Application of Single-Domain Antibodies (“Nanobodies”) to Laboratory Diagnosis. *Ann Lab Med*. 2021;41(6):549-558. doi:10.3343/ALM.2021.41.6.549
9. Steeland S, Vandenbroucke RE, Libert C. Nanobodies as therapeutics: Big opportunities for small antibodies. *Drug Discov Today*. 2016;21(7):1076-1113. doi:10.1016/J.DRUDIS.2016.04.003
10. Cunningham S, Piedra PA, Martinon-Torres F, et al. Nebulised ALX-0171 for respiratory syncytial virus lower respiratory tract infection in hospitalised children: a double-blind, randomised, placebo-controlled, phase 2b trial. *Lancet Respir Med*. 2021;9(1):21-32. doi:10.1016/S2213-2600(20)30320-9
11. Morrison C. Nanobody approval gives domain antibodies a boost. *Nat Rev Drug Discov*. 2019;18(7):485-487. doi:10.1038/D41573-019-00104-W

12. Liu JKH. The history of monoclonal antibody development – Progress, remaining challenges and future innovations. *Annals of Medicine and Surgery*. 2014;3(4):113. doi:10.1016/J.AMSU.2014.09.001
13. Galán A, Comor L, Horvatić A, et al. Library-based display technologies: where do we stand? *Mol Biosyst*. 2016;12(8):2342-2358. doi:10.1039/C6MB00219F
14. Doerner A, Rhiel L, Zielonka S, Kolmar H. Therapeutic antibody engineering by high efficiency cell screening. *FEBS Lett*. 2014;588(2):278-287. doi:10.1016/J.FEBSLET.2013.11.025
15. Wittrup KD. Protein engineering by cell-surface display. *Curr Opin Biotechnol*. 2001;12(4):395-399. doi:10.1016/S0958-1669(00)00233-0
16. Daugherty PS. Protein engineering with bacterial display. *Curr Opin Struct Biol*. 2007;17(4):474-480. doi:10.1016/J.SBI.2007.07.004
17. Gai SA, Wittrup KD. Yeast surface display for protein engineering and characterization. *Curr Opin Struct Biol*. 2007;17(4):467-473. doi:10.1016/J.SBI.2007.08.012
18. Cherf GM, Cochran JR. Applications of yeast surface display for protein engineering. *Methods in Molecular Biology*. 2015;1319:155-175. doi:10.1007/978-1-4939-2748-7_8
19. Kamalinia G, Grindel BJ, Takahashi TT, Millward SW, Roberts RW. Directing evolution of novel ligands by mRNA display. *Chem Soc Rev*. 2021;50(16):9055-9103. doi:10.1039/D1CS00160D
20. Chance R, Kang AS. Eukaryotic ribosome display for antibody discovery: A review. *Hum Antibodies*. 2024;Preprint(Preprint):1-14. doi:10.3233/HAB-240001
21. Boder ET, Wittrup KD. Yeast surface display for screening combinatorial polypeptide libraries. *Nat Biotechnol*. 1997;15(6):553-557. doi:10.1038/NBT0697-553
22. Breijyeh Z, Karaman R, Muñoz-Torrero D, Dembinski R. Comprehensive Review on Alzheimer's Disease: Causes and Treatment. *Molecules* 2020, Vol 25, Page 5789. 2020;25(24):5789. doi:10.3390/MOLECULES25245789
23. 2024 Alzheimer's disease facts and figures. *Alzheimers Dement*. 2024;20(5):3708-3821. doi:10.1002/ALZ.13809
24. Zhang Y, Wu KM, Yang L, Dong Q, Yu JT. Tauopathies: new perspectives and challenges. *Molecular Neurodegeneration* 2022 17:1. 2022;17(1):1-29. doi:10.1186/S13024-022-00533-Z

25. Jadhav S, Avila J, Schöll M, et al. A walk through tau therapeutic strategies. *Acta Neuropathologica Communications* 2019 7:1. 2019;7(1):1-31. doi:10.1186/S40478-019-0664-Z
26. Scheres SH, Zhang W, Falcon B, Goedert M. Cryo-EM structures of tau filaments. *Curr Opin Struct Biol.* 2020;64:17-25. doi:10.1016/j.sbi.2020.05.011
27. Guo Y, Li S, Zeng LH, Tan J. Tau-targeting therapy in Alzheimer's disease: critical advances and future opportunities. *Ageing and Neurodegenerative Diseases.* 2022;2(3):11. doi:10.20517/AND.2022.16
28. Congdon EE, Sigurdsson EM. Tau-targeting therapies for Alzheimer disease. *Nat Rev Neurol.* 2018;14(7):399-415. doi:10.1038/s41582-018-0013-z
29. Mietelska-Porowska A, Wasik U, Goras M, Filipek A, Niewiadomska G. Tau Protein Modifications and Interactions: Their Role in Function and Dysfunction. *Int J Mol Sci.* 2014;15(3):4671. doi:10.3390/IJMS15034671
30. Meraz-Ríos MA, Lira-De León KI, Campos-Peña V, De Anda-Hernández MA, Mena-López R. Tau oligomers and aggregation in Alzheimer's disease. *J Neurochem.* 2010;112(6):1353-1367. doi:10.1111/J.1471-4159.2009.06511.X
31. Ghag G, Bhatt N, Cantu D V., et al. Soluble tau aggregates, not large fibrils, are the toxic species that display seeding and cross-seeding behavior. *Protein Science.* 2018;27(11):1901-1909. doi:10.1002/PRO.3499
32. Song C, Shi J, Zhang P, et al. Immunotherapy for Alzheimer's disease: targeting β -amyloid and beyond. *Transl Neurodegener.* 2022;11(1):1-17. doi:10.1186/S40035-022-00292-3
33. Yiannopoulou KG, Papageorgiou SG. Current and Future Treatments in Alzheimer Disease: An Update. <https://doi.org/10.1177/1179573520907397>. 2020;12:117957352090739. doi:10.1177/1179573520907397
34. Yanamandra K, Kfoury N, Jiang H, et al. Anti-tau antibodies that block tau aggregate seeding invitro markedly decrease pathology and improve cognition in vivo. *Neuron.* 2013;80(2):402-414. doi:10.1016/j.neuron.2013.07.046
35. Yanamandra K, Jiang H, Mahan TE, et al. Anti-tau antibody reduces insoluble tau and decreases brain atrophy. *Ann Clin Transl Neurol.* 2015;2(3):278-288. doi:10.1002/ACN3.176
36. Yanamandra K, Kfoury N, Jiang H, et al. Anti-tau antibodies that block tau aggregate seeding in vitro markedly decrease pathology and improve cognition in vivo. *Neuron.* 2013;80(2):402-414. doi:10.1016/J.NEURON.2013.07.046

37. More Tau Antibodies Bid Adieu; Semorinemab Keeps Foot in Door | ALZFORUM. Accessed November 9, 2022. <https://www.alzforum.org/news/conference-coverage/more-tau-antibodies-bid-adieu-semorinemab-keeps-foot-door>
38. Jicha GA, Bowser R, Kazam IG, Davies P. Alz-50 and MC-1, a New Monoclonal Antibody Raised to Paired Helical Filaments, Recognize Conformational Epitopes on Recombinant Tau. *J Neurosci Res.* 1997;48:128-132. doi:10.1002/(SICI)1097-4547(19970415)48:2<128::AID-JNR5>3.0.CO;2-E
39. Chai X, Wu S, Murray TK, et al. Passive Immunization with Anti-Tau Antibodies in Two Transgenic Models: REDUCTION OF TAU PATHOLOGY AND DELAY OF DISEASE PROGRESSION. *J Biol Chem.* 2011;286(39):34457. doi:10.1074/JBC.M111.229633
40. Fleisher AS, Munsie LM, Perahia DGS, et al. Assessment of Efficacy and Safety of Zagotenemab: Results From PERISCOPE-ALZ, a Phase 2 Study in Early Symptomatic Alzheimer Disease. *Neurology.* 2024;102(5):e208061. doi:10.1212/WNL.0000000000208061
41. Mullard A. Anti-tau antibody failures stack up. *Nat Rev Drug Discov.* 2021;20(12):888. doi:10.1038/D41573-021-00187-4
42. Tai HC, Ma HT, Huang SC, et al. The tau oligomer antibody APNmAb005 detects early-stage pathological tau enriched at synapses and rescues neuronal loss in long-term treatments. doi:10.1101/2022.06.24.497452
43. Chen GF, Xu TH, Yan Y, et al. Amyloid beta: structure, biology and structure-based therapeutic development. *Acta Pharmacologica Sinica 2017* 38:9. 2017;38(9):1205-1235. doi:10.1038/aps.2017.28
44. Zhang Y, Chen H, Li R, Sterling K, Song W. Amyloid β -based therapy for Alzheimer's disease: challenges, successes and future. *Signal Transduction and Targeted Therapy 2023* 8:1. 2023;8(1):1-26. doi:10.1038/s41392-023-01484-7
45. Butcher L. What's Next for Patients Treated With Aducanumab? *Neurology Today.* 2024;24(10):1,22-23. doi:10.1097/01.NT.0001022964.45474.03
46. Jiang S, Hillyer C, Du L. Neutralizing Antibodies against SARS-CoV-2 and Other Human Coronaviruses. *Trends Immunol.* 2020;41(5):355-359. doi:10.1016/J.IT.2020.03.007
47. Vitiello A, Ferrara F, Auti AM, Di Domenico M, Boccellino M. Advances in the Omicron variant development. *J Intern Med.* 2022;292(1):81-90. doi:10.1111/JOIM.13478
48. Pather S, Madhi SA, Cowling BJ, et al. SARS-CoV-2 Omicron variants: burden of disease, impact on vaccine effectiveness and need for variant-adapted vaccines. *Front Immunol.* 2023;14:1130539. doi:10.3389/FIMMU.2023.1130539/BIBTEX

49. Velavan TP, Ntoumi F, Kremsner PG, Lee SS, Meyer CG. Emergence and geographic dominance of Omicron subvariants XBB/XBB.1.5 and BF.7 – the public health challenges. *International Journal of Infectious Diseases*. 2023;128:307-309. doi:10.1016/j.ijid.2023.01.024
50. GenBank Overview. Accessed July 4, 2024. <https://www.ncbi.nlm.nih.gov/genbank/>
51. Cao Y, Jian F, Wang J, et al. Imprinted SARS-CoV-2 humoral immunity induces converging Omicron RBD evolution. *bioRxiv*. Published online September 23, 2022:2022.09.15.507787. doi:10.1101/2022.09.15.507787
52. CDC COVID Data Tracker: Variant Proportions. Accessed June 12, 2024. <https://covid.cdc.gov/covid-data-tracker/#variant-proportions>
53. Dhillon S. Aducanumab: First Approval. *Drugs*. 2021;81(12):1437-1443. doi:10.1007/S40265-021-01569-Z/METRICS
54. Mahase E. Alzheimer's disease: Lecanemab gets full FDA approval and black box safety warning. *BMJ*. 2023;382:p1580. doi:10.1136/BMJ.P1580
55. Karikari TK, Emeršič A, Vrillon A, et al. Head-to-head comparison of clinical performance of CSF phospho-tau T181 and T217 biomarkers for Alzheimer's disease diagnosis. *Alzheimer's and Dementia*. 2021;17(5):755-767. doi:10.1002/ALZ.12236
56. Horie K, Salvadó G, Barthélemy NR, et al. CSF MTBR-tau243 is a specific biomarker of tau tangle pathology in Alzheimer's disease. *Nature Medicine* 2023 29:8. 2023;29(8):1954-1963. doi:10.1038/s41591-023-02443-z
57. Iqbal K, Fei AE, Ae L, Gong CX, Alejandra AE, Alonso DC. Mechanisms of tau-induced neurodegeneration. doi:10.1007/s00401-009-0486-3
58. Arriagada P V., Growdon JH, Hedley-Whyte ET, Hyman BT. Neurofibrillary tangles but not senile plaques parallel duration and severity of Alzheimer's disease. *Neurology*. 1992;42(3):631-631. doi:10.1212/WNL.42.3.631
59. Gaikwad S, Senapati S, Haque MA, Kayed R. Senescence, brain inflammation, and oligomeric tau drive cognitive decline in Alzheimer's disease: Evidence from clinical and preclinical studies. Published online 2023. doi:10.1002/alz.13490
60. Ghoshal N, García-Sierra F, Wu J, et al. Tau conformational changes correspond to impairments of episodic memory in mild cognitive impairment and Alzheimer's disease. *Exp Neurol*. 2002;177(2):475-493. doi:10.1006/exnr.2002.8014
61. Rosseels J, Van Den Brande J, Violet M, et al. Tau Monoclonal Antibody Generation Based on Humanized Yeast Models: IMPACT ON TAU

OLIGOMERIZATION AND DIAGNOSTICS. *Journal of Biological Chemistry*. 2015;290(7):4059-4074. doi:10.1074/JBC.M114.627919

62. Combs B, Hamel C, Kanaan NM. Pathological conformations involving the amino terminus of tau occur early in Alzheimer's disease and are differentially detected by monoclonal antibodies. *Neurobiol Dis*. 2016;94:18-31. doi:10.1016/J.NBD.2016.05.016
63. Porzig R, Singer D, Hoffmann R. Epitope mapping of mAbs AT8 and Tau5 directed against hyperphosphorylated regions of the human tau protein. *Biochem Biophys Res Commun*. 2007;358(2):644-649. doi:10.1016/J.BBRC.2007.04.187
64. Ercan E, Eid S, Weber C, et al. A validated antibody panel for the characterization of tau post-translational modifications. *Mol Neurodegener*. 2017;12(1). doi:10.1186/S13024-017-0229-1
65. Castillo-Carranza DL, Gerson JE, Sengupta U, Guerrero-Muñoz MJ, Lasagna-Reeves CA, Kaye R. Specific targeting of tau oligomers in Htau mice prevents cognitive impairment and tau toxicity following injection with brain-derived tau oligomeric seeds. *J Alzheimers Dis*. 2014;40 Suppl 1(S1). doi:10.3233/JAD-132477
66. Zupancic JM, Smith MD, Trzeciakiewicz H, et al. Quantitative flow cytometric selection of tau conformational nanobodies specific for pathological aggregates. *Front Immunol*. 2023;14:1164080. doi:10.3389/FIMMU.2023.1164080
67. Desai AA, Zupancic JM, Trzeciakiewicz H, et al. Flow cytometric isolation of drug-like conformational antibodies specific for amyloid fibrils. *bioRxiv*. Published online July 4, 2023:2023.07.04.547698. doi:10.1101/2023.07.04.547698
68. Abskharon R, Seidler PM, Sawaya MR, et al. Crystal structure of a conformational antibody that binds tau oligomers and inhibits pathological seeding by extracts from donors with Alzheimer's disease. *J Biol Chem*. 2020;295(31):10662. doi:10.1074/JBC.RA120.013638
69. Lasagna-Reeves CA, Castillo-Carranza DL, Sengupta U, et al. Identification of oligomers at early stages of tau aggregation in Alzheimer's disease. *The FASEB Journal*. 2012;26(5):1946-1959. doi:10.1096/fj.11-199851
70. Dupré E, Clément D†, Danis C, et al. Single Domain Antibody Fragments as New Tools for the Detection of Neuronal Tau Protein in Cells and in Mice Studies. Published online 2019. doi:10.1021/acschemneuro.9b00217
71. Danis C, Dupré E, Zejneli O, et al. Inhibition of Tau seeding by targeting Tau nucleation core within neurons with a single domain antibody fragment. Published online 2022. doi:10.1016/j.ymthe.2022.01.009

72. Desai AA, Zupancic JM, Smith MD, Tessier PM. Isolating Anti-amyloid Antibodies from Yeast-Displayed Libraries. *Methods Mol Biol.* 2022;2491:471-490. doi:10.1007/978-1-0716-2285-8_22
73. Jovčevska I, Muyldermans S. The Therapeutic Potential of Nanobodies. *BioDrugs.* 123AD;34. doi:10.1007/s40259-019-00392-z
74. Muyldermans S. Annual Review of Animal Biosciences Applications of Nanobodies. Published online 2020. doi:10.1146/annurev-animal-021419
75. Li T, Vandesquille M, Koukouli F, et al. Camelid single-domain antibodies: A versatile tool for in vivo imaging of extracellular and intracellular brain targets. *J Control Release.* 2016;243:1-10. doi:10.1016/J.JCONREL.2016.09.019
76. Congdon EE, Pan R, Jiang Y, et al. Single domain antibodies targeting pathological tau protein: Influence of four IgG subclasses on efficacy and toxicity. Published online 2022. doi:10.1016/j
77. Abskharon R, Pan H, Sawaya MR, et al. Structure-based design of nanobodies that inhibit seeding of Alzheimer's patient-extracted tau fibrils. *Proc Natl Acad Sci U S A.* 2023;120(41). doi:10.1073/pnas.2300258120
78. Jiang Y, Lin Y, Krishnaswamy S, et al. Single-domain antibody-based noninvasive in vivo imaging of α -synuclein or tau pathology. *Sci Adv.* 2023;9(19). doi:10.1126/SCIADV.ADF3775
79. McArthur N, Kang B, Rivera Moctezuma FG, et al. Development of a pan-tau multivalent nanobody that binds tau aggregation motifs and recognizes pathological tau aggregates. *Biotechnol Prog.* Published online 2024:e3463. doi:10.1002/BTPR.3463
80. McMahon C, Baier AS, Pascolutti R, et al. Yeast surface display platform for rapid discovery of conformationally selective nanobodies. *Nat Struct Mol Biol.* 2018;25(3):289-296. doi:10.1038/s41594-018-0028-6
81. Gera N, Hussain M, Rao BM. Protein selection using yeast surface display. *Methods.* 2013;60(1):15-26. doi:10.1016/j.ymeth.2012.03.014
82. Crespo R, Koudstaal W, Apetri A. In Vitro Assay for Studying the Aggregation of Tau Protein and Drug Screening. *Journal of Visualized Experiments.* 2018;(November):1-10. doi:10.3791/58570
83. Fitzpatrick AWP, Falcon B, He S, et al. Cryo-EM structures of tau filaments from Alzheimer's disease. *Nature.* 2017;547(7662):185-190. doi:10.1038/nature23002
84. Cisek K, Cooper GL, Huseby CJ, Kuret J. Structure and mechanism of action of tau aggregation inhibitors. *Curr Alzheimer Res.* 2014;11(10):918. doi:10.2174/1567205011666141107150331

85. Seidler PM, Boyer DR, Rodriguez JA, et al. Structure-based inhibitors of tau aggregation. *Nat Chem.* 2018;10(2):170. doi:10.1038/NCHEM.2889
86. Chao G, Lau WL, Hackel BJ, Sazinsky SL, Lippow SM, Wittrup KD. Isolating and engineering human antibodies using yeast surface display. *Nature Protocols* 2006 1:2. 2006;1(2):755-768. doi:10.1038/nprot.2006.94
87. Mehta N, Maddineni S, Kelly RL, et al. An engineered antibody binds a distinct epitope and is a potent inhibitor of murine and human VISTA. *Scientific Reports* 2020 10:1. 2020;10(1):1-15. doi:10.1038/s41598-020-71519-4
88. SantaCruz K, Lewis J, Spires T, et al. Tau Suppression in a Neurodegenerative Mouse Model Improves Memory Function. *Science (1979).* 2005;309(5733):476-481. doi:10.1126/science.1113694
89. Schroeder S, Joly-Amado A, Soliman A, et al. Oligomeric tau-targeted immunotherapy in Tg4510 mice. *Alzheimers Res Ther.* 2017;9(1). doi:10.1186/s13195-017-0274-6
90. Ramsden M, Kotilinek L, Forster C, et al. Age-dependent neurofibrillary tangle formation, neuron loss, and memory impairment in a mouse model of human tauopathy (P301L). *Journal of Neuroscience.* 2005;25(46):10637-10647. doi:10.1523/JNEUROSCI.3279-05.2005
91. Desai AA, Smith MD, Zhang Y, et al. Rational affinity maturation of anti-amyloid antibodies with high conformational and sequence specificity. *Journal of Biological Chemistry.* 2021;296:100508. doi:10.1016/J.JBC.2021.100508
92. Julian MC, Rabia LA, Desai AA, et al. Nature-inspired design and evolution of anti-amyloid antibodies. *Journal of Biological Chemistry.* 2019;294(21):8438-8451. doi:10.1074/jbc.RA118.004731
93. Warne T, Edwards PC, Dorfe AS, Leslie AGW, Tate CG. Molecular basis for high affinity agonist binding in GPCRs. *Science.* 2019;364(6442):775. doi:10.1126/SCIENCE.AAU5595
94. Rasmussen SGF, Choi HJ, Fung JJ, et al. Structure of a nanobody-stabilized active state of the β 2 adrenoceptor. *Nature.* 2011;469(7329):175. doi:10.1038/NATURE09648
95. Ring AM, Manglik A, Kruse AC, et al. Adrenaline-activated structure of the β 2-adrenoceptor stabilized by an engineered nanobody. *Nature.* 2013;502(7472):575. doi:10.1038/NATURE12572
96. Che T, Majumdar S, Zaidi SA, et al. Structure of a nanobody-stabilized active state of the kappa opioid receptor. *Cell.* 2018;172(1-2):55. doi:10.1016/J.CELL.2017.12.011

97. Kruse AC, Ring AM, Manglik A, et al. Activation and allosteric modulation of a muscarinic acetylcholine receptor. *Nature*. 2013;504(7478):101. doi:10.1038/NATURE12735
98. Burg JS, Ingram JR, Venkatakrishnan AJ, et al. Structural basis for chemokine recognition and activation of a viral G protein–coupled receptor. *Science*. 2015;347(6226):1113. doi:10.1126/SCIENCE.AAA5026
99. Koehl A, Hu H, Feng D, et al. Structural Insights into Metabotropic Glutamate Receptor Activation. *Nature*. 2019;566(7742):79. doi:10.1038/S41586-019-0881-4
100. Masureel M, Zou Y, Picard LP, et al. Structural insights into binding specificity, efficacy and bias of a β 2AR partial agonist. *Nat Chem Biol*. 2018;14(11):1059. doi:10.1038/S41589-018-0145-X
101. Haffke M, Fehlmann D, Rummel G, et al. Structural basis of species-selective antagonist binding to the succinate receptor. *Nature*. 2019;574(7779):581-585. doi:10.1038/S41586-019-1663-8
102. Staus DP, Strachan RT, Manglik A, et al. Allosteric Nanobodies Reveal the Dynamic Range and Diverse Mechanisms of GPCR Activation. *Nature*. 2016;535(7612):448. doi:10.1038/NATURE18636
103. Hassaine G, Deluz C, Grasso L, et al. X-ray structure of the mouse serotonin 5-HT₃ receptor. *Nature*. 2014;512(7514):276-281. doi:10.1038/NATURE13552
104. Hénault CM, Govaerts C, Spurny R, et al. A lipid site shapes the agonist response of a pentameric ligand-gated ion channel. *Nat Chem Biol*. 2019;15(12):1156. doi:10.1038/S41589-019-0369-4
105. Laverty D, Desai R, Uchański T, et al. Cryo-EM structure of the human α 1 β 3 γ 2 GABAA receptor in a lipid bilayer. *Nature*. 2019;565(7740):516-520. doi:10.1038/S41586-018-0833-4
106. Ehrnstorfer IA, Geertsma ER, Pardon E, Steyaert J, Dutzler R. Crystal structure of a SLC11 (NRAMP) transporter reveals the basis for transition-metal ion transport. *Nat Struct Mol Biol*. 2014;21(11):990-996. doi:10.1038/NSMB.2904
107. Oyen D, Srinivasan V, Steyaert J, Barlow JN. Constraining enzyme conformational change by an antibody leads to hyperbolic inhibition. *J Mol Biol*. 2011;407(1):138-148. doi:10.1016/J.JMB.2011.01.017
108. Chaikuad A, Keates T, Vincke C, et al. Structure of cyclin G-associated kinase (GAK) trapped in different conformations using nanobodies. *Biochemical Journal*. 2014;459(Pt 1):59. doi:10.1042/BJ20131399

109. Hou YN, Cai Y, Li WH, et al. A conformation-specific nanobody targeting the nicotinamide mononucleotide-activated state of SARM1. *Nat Commun.* 2022;13(1). doi:10.1038/S41467-022-35581-Y
110. Butler YR, Liu Y, Kumbhar R, et al. α -Synuclein fibril-specific nanobody reduces prion-like α -synuclein spreading in mice. *Nature Communications* 2022 13:1. 2022;13(1):1-13. doi:10.1038/s41467-022-31787-2
111. Habicht G, Haupt C, Friedrich RP, et al. Directed selection of a conformational antibody domain that prevents mature amyloid fibril formation by stabilizing A β protofibrils. *Proc Natl Acad Sci U S A.* 2007;104(49):19232-19237. doi:10.1073/PNAS.0703793104
112. Lafaye P, Achour I, England P, Duyckaerts C, Rougeon F. Single-domain antibodies recognize selectively small oligomeric forms of amyloid β , prevent A β -induced neurotoxicity and inhibit fibril formation. *Mol Immunol.* 2009;46(4):695-704. doi:10.1016/J.MOLIMM.2008.09.008
113. 2019 Alzheimer's disease facts and figures. *Alzheimer's & Dementia.* 2019;15(3):321-387. doi:10.1016/J.JALZ.2019.01.010
114. Kalia L V., Lang AE. Parkinson's disease. *Lancet.* 2015;386(9996):896-912. doi:10.1016/S0140-6736(14)61393-3
115. De Genst EJ, Guilliams T, Wellens J, et al. Structure and properties of a complex of α -synuclein and a single-domain camelid antibody. *J Mol Biol.* 2010;402(2):326-343. doi:10.1016/J.JMB.2010.07.001
116. Guilliams T, El-Turk F, Buell AK, et al. Nanobodies raised against monomeric α -synuclein distinguish between fibrils at different maturation stages. *J Mol Biol.* 2013;425(14):2397-2411. doi:10.1016/J.JMB.2013.01.040
117. Morgado I, Wieligmann K, Bereza M, et al. Molecular basis of β -amyloid oligomer recognition with a conformational antibody fragment. *Proc Natl Acad Sci U S A.* 2012;109(31):12503-12508. doi:10.1073/PNAS.1206433109
118. Terstappen GC, Meyer AH, Bell RD, Zhang W. Strategies for delivering therapeutics across the blood-brain barrier. *Nature Reviews Drug Discovery* 2021 20:5. 2021;20(5):362-383. doi:10.1038/s41573-021-00139-y
119. Gao Y, Zhu J, Lu H. Single domain antibody-based vectors in the delivery of biologics across the blood-brain barrier: a review. *Drug Deliv Transl Res.* 2021;11(5):1818-1828. doi:10.1007/S13346-020-00873-7
120. Cheng Y, Zak O, Aisen P, Harrison SC, Walz T. Structure of the Human Transferrin Receptor-Transferrin Complex. *Cell.* 2004;116(4):565-576. doi:10.1016/S0092-8674(04)00130-8

121. Wouters Y, Jaspers T, De Strooper B, Dewilde M. Identification and in vivo characterization of a brain-penetrating nanobody. *Fluids Barriers CNS*. 2020;17(1):1-10. doi:10.1186/S12987-020-00226-Z
122. Niewoehner J, Bohrmann B, Collin L, et al. Increased Brain Penetration and Potency of a Therapeutic Antibody Using a Monovalent Molecular Shuttle. *Neuron*. 2014;81(1):49-60. doi:10.1016/J.NEURON.2013.10.061
123. Feldhaus MJ, Siegel RW, Opresko LK, et al. Flow-cytometric isolation of human antibodies from a nonimmune *Saccharomyces cerevisiae* surface display library. *Nat Biotechnol*. 2003;21(2):163-170. doi:10.1038/NBT785
124. Hasler J, Rutkowski JL, Wicher KB. TfR SELECTIVE BINDING COMPOUNDS AND RELATED METHODS. Published online December 7, 2017. Accessed July 20, 2022. <https://patents.google.com/patent/US20170348416A1/en>
125. Cohen R, David M, Khrestchatsky M. TRANSFERRIN RECEPTOR-BINDING MOLECULES , CONJUGATES THEREOF. Published online March 24, 2022.
126. Guo X, Yan L, Zhang D, Zhao Y. Passive immunotherapy for Alzheimer's disease. *Ageing Res Rev*. 2024;94:102192. doi:10.1016/J.ARR.2024.102192
127. Castillo-Carranza DL, Sengupta U, Guerrero-Muñoz MJ, et al. Passive Immunization with Tau Oligomer Monoclonal Antibody Reverses Tauopathy Phenotypes without Affecting Hyperphosphorylated Neurofibrillary Tangles. *The Journal of Neuroscience*. 2014;34(12):4260. doi:10.1523/JNEUROSCI.3192-13.2014
128. He P, Schulz P, Sierks MR. A conformation-specific antibody against oligomeric β -amyloid restores neuronal integrity in a mouse model of Alzheimer's disease. *Journal of Biological Chemistry*. 2021;296:100241. doi:10.1074/jbc.RA120.015327
129. Henderson MX, Covell DJ, Chung CHY, et al. Characterization of novel conformation-selective α -synuclein antibodies as potential immunotherapeutic agents for Parkinson's disease. *Neurobiol Dis*. 2020;136:104712. doi:10.1016/J.NBD.2019.104712
130. Congdon EE, Ji C, Tetlow AM, Jiang Y, Sigurdsson EM. Tau-targeting therapies for Alzheimer disease: current status and future directions. *Nature Reviews Neurology* 2023 19:12. 2023;19(12):715-736. doi:10.1038/s41582-023-00883-2
131. Niewiadomska G, Niewiadomski W, Steczkowska M, Gasiorowska A. Tau Oligomers Neurotoxicity. *Life (Basel)*. 2021;11(1):1-28. doi:10.3390/LIFE11010028

132. Cárdenas-Aguayo MDC, Gómez-Virgilio L, DeRosa S, Meraz-Ríos MA. The role of tau Oligomers in the onset of Alzheimer's disease neuropathology. *ACS Chem Neurosci*. 2014;5(12):1178-1191. doi:10.1021/cn500148z
133. Shafiei SS, Guerrero-Muñoz MJ, Castillo-Carranza DL. Tau Oligomers: Cytotoxicity, Propagation, and Mitochondrial Damage. *Front Aging Neurosci*. 2017;9(APR). doi:10.3389/FNAGI.2017.00083
134. Gerson JE, Castillo-Carranza DL, Kaye R. Advances in therapeutics for neurodegenerative tauopathies: Moving toward the specific targeting of the most toxic tau species. *ACS Chem Neurosci*. 2014;5(9):752-769. doi:10.1021/CN500143N
135. Kaye R, Canto I, Breydo L, et al. Conformation dependent monoclonal antibodies distinguish different replicating strains or conformers of prefibrillar A β oligomers. *Molecular Neurodegeneration* 2010 5:1. 2010;5(1):1-10. doi:10.1186/1750-1326-5-57
136. Patterson KR, Remmers C, Fu Y, et al. Characterization of prefibrillar tau oligomers in vitro and in Alzheimer disease. *Journal of Biological Chemistry*. 2011;286(26):23063-23076. doi:10.1074/jbc.M111.237974
137. Bao G, Tang M, Zhao J, Zhu X. Nanobody: a promising toolkit for molecular imaging and disease therapy. *EJNMMI Res*. 2021;11(1):1-13. doi:10.1186/S13550-021-00750-5/
138. De Leiris N, Perret P, Lombardi C, et al. A single-domain antibody for the detection of pathological Tau protein in the early stages of oligomerization. *J Transl Med*. 2024;22(1):1-14. doi:10.1186/S12967-024-04987-1
139. Bigi A, Napolitano L, Vadukul DM, et al. A single-domain antibody detects and neutralises toxic A β 42 oligomers in the Alzheimer's disease CSF. *Alzheimers Res Ther*. 2024;16(1):1-19. doi:10.1186/S13195-023-01361-Z
140. Kasturirangan S, Li L, Emadi S, Boddapati S, Schulz P, Sierks MR. Nanobody specific for oligomeric beta-amyloid stabilizes nontoxic form. *Neurobiol Aging*. 2012;33(7):1320-1328. doi:10.1016/J.NEUROBIOLAGING.2010.09.020
141. Moore BD, Rangachari V, Tay WM, Milkovic NM, Rosenberry TL. Biophysical analyses of synthetic amyloid- β (1-42) aggregates before and after covalent cross-linking. Implications for deducing the structure of endogenous amyloid- β oligomers. *Biochemistry*. 2009;48(49):11796-11806. doi:10.1021/BI901571T
142. Sun P, Ju H, Liu Z, et al. Bioinformatics resources and tools for conformational B-cell epitope prediction. *Comput Math Methods Med*. 2013;2013. doi:10.1155/2013/943636

143. Kolarova M, Sengupta U, Bartos A, Ricny J, Kayed R. Tau Oligomers in Sera of Patients with Alzheimer's Disease and Aged Controls. *Journal of Alzheimer's Disease*. 2017;58(2):471-478. doi:10.3233/JAD-170048
144. Maeda S, Sahara N, Saito Y, Murayama S, Ikai A, Takashima A. Increased levels of granular tau oligomers: An early sign of brain aging and Alzheimer's disease. *Neurosci Res*. 2006;54(3):197-201. doi:10.1016/J.NEURES.2005.11.009
145. Tian D, Sun Y, Xu H, Ye Q. The emergence and epidemic characteristics of the highly mutated SARS-CoV-2 Omicron variant. *J Med Virol*. 2022;94(6):2376-2383. doi:10.1002/JMV.27643
146. Chakraborty C, Bhattacharya M, Sharma AR, Mallik B. Omicron (B.1.1.529) - A new heavily mutated variant: Mapped location and probable properties of its mutations with an emphasis on S-glycoprotein. *Int J Biol Macromol*. 2022;219:980-997. doi:10.1016/J.IJBIOMAC.2022.07.254
147. Yang J, Petitjean SJL, Koehler M, et al. Molecular interaction and inhibition of SARS-CoV-2 binding to the ACE2 receptor. *Nature Communications* 2020 11:1. 2020;11(1):1-10. doi:10.1038/s41467-020-18319-6
148. Dejnirattisai W, Zhou D, Ginn HM, et al. The antigenic anatomy of SARS-CoV-2 receptor binding domain. *Cell*. 2021;184(8):2183-2200.e22. doi:10.1016/j.cell.2021.02.032
149. McCallum M, Czudnochowski N, Rosen LE, et al. Structural basis of SARS-CoV-2 Omicron immune evasion and receptor engagement. *Science (1979)*. 2022;375(6583):894-898. doi:10.1126/SCIENCE.ABN8652
150. Planas D, Staropoli I, Michel V, et al. Distinct evolution of SARS-CoV-2 Omicron XBB and BA.2.86/JN.1 lineages combining increased fitness and antibody evasion. *Nature Communications* 2024 15:1. 2024;15(1):1-17. doi:10.1038/s41467-024-46490-7
151. Dougan M, investigators B 1, Azizad M, et al. A Randomized, Placebo-Controlled Clinical Trial of Bamlanivimab and Etesevimab Together in High-Risk Ambulatory Patients With COVID-19 and Validation of the Prognostic Value of Persistently High Viral Load. *Clinical Infectious Diseases*. 2022;75(1):e440-e449. doi:10.1093/CID/CIAB912
152. Weinreich DM, Sivapalasingam S, Norton T, et al. REGEN-COV Antibody Combination and Outcomes in Outpatients with Covid-19. *New England Journal of Medicine*. 2021;385(23). doi:10.1056/NEJM0A2108163
153. Emergency Use Authorization | FDA. Accessed June 30, 2024. <https://www.fda.gov/emergency-preparedness-and-response/mcm-legal-regulatory-and-policy-framework/emergency-use-authorization>

154. Cao Y, Wang J, Jian F, et al. Omicron escapes the majority of existing SARS-CoV-2 neutralizing antibodies. *Nature* 2021 602:7898. 2021;602(7898):657-663. doi:10.1038/s41586-021-04385-3
155. VanBlargan LA, Errico JM, Halfmann PJ, et al. An infectious SARS-CoV-2 B.1.1.529 Omicron virus escapes neutralization by therapeutic monoclonal antibodies. *Nature Medicine* 2022 28:3. 2022;28(3):490-495. doi:10.1038/s41591-021-01678-y
156. Ao D, He X, Hong W, Wei X. The rapid rise of SARS-CoV-2 Omicron subvariants with immune evasion properties: XBB.1.5 and BQ.1.1 subvariants. *MedComm (Beijing)*. 2023;4(2):e239. doi:10.1002/MCO2.239
157. Harris E. Monoclonal Antibody Authorized to Protect At-Risk People From COVID-19. *JAMA*. 2024;331(23):1982-1982. doi:10.1001/JAMA.2024.8628
158. Rothenberger S, Hurdiss DL, Walser M, et al. The trisppecific DARPin ensovibep inhibits diverse SARS-CoV-2 variants. *Nature Biotechnology* 2022 40:12. 2022;40(12):1845-1854. doi:10.1038/s41587-022-01382-3
159. Chonira V, Kwon YD, Gorman J, et al. A potent and broad neutralization of SARS-CoV-2 variants of concern by DARPins. *Nature Chemical Biology* 2022 19:3. 2022;19(3):284-291. doi:10.1038/s41589-022-01193-2
160. Kondo T, Iwatani Y, Matsuoka K, et al. Antibody-like proteins that capture and neutralize SARS-CoV-2. *Sci Adv*. 2020;6(42):3916-3930. doi:10.1126/SCIADV.ABD3916
161. Kondo T, Matsuoka K, Umemoto S, et al. Monobodies with potent neutralizing activity against SARS-CoV-2 Delta and other variants of concern. *Life Sci Alliance*. 2022;5(6). doi:10.26508/LSA.202101322
162. Miller CJ, McGinnis JE, Martinez MJ, et al. FN3-based monobodies selective for the receptor binding domain of the SARS-CoV-2 spike protein. *N Biotechnol*. 2021;62:79-85. doi:10.1016/J.NBT.2021.01.010
163. Khramtsov Y V., Ulasov A V., Lupanova TN, Georgiev GP, Sobolev AS. Delivery of Antibody-Like Molecules, Monobodies, Capable of Binding with SARS-CoV-2 Virus Nucleocapsid Protein, into Target Cells. *Dokl Biochem Biophys*. 2022;506(1):220-222. doi:10.1134/S1607672922050088
164. Khramtsov Y V., Ulasov A V., Lupanova TN, Georgiev GP, Sobolev AS. Among Antibody-Like Molecules, Monobodies, Able to Interact with Nucleocapsid Protein of SARS-CoV Virus, There Are Monobodies with High Affinity to Nucleocapsid Protein of SARS-CoV-2 Virus. *Dokl Biochem Biophys*. 2022;503(1):90-92. doi:10.1134/S1607672922020077

165. Y D, T Z, X M, et al. Development of high affinity monobodies recognizing SARS-CoV-2 antigen. Published online April 28, 2020. doi:10.21203/RS.3.RS-25828/V1
166. Tripathi NM, Bandyopadhyay A. Virtual screening of knottin and defensin peptides perceives hits against the SARS CoV-2 RBD domain and hACE2 interaction. Published online January 18, 2023. doi:10.26434/CHEMRXIV-2023-5P74J
167. Du W, Jiang P, Li Q, et al. Novel Affibody Molecules Specifically Bind to SARS-CoV-2 Spike Protein and Efficiently Neutralize Delta and Omicron Variants. *Microbiol Spectr.* 2023;11(1). doi:10.1128/SPECTRUM.03562-22
168. Mijit A, Wang X, Li Y, Xu H, Chen Y, Xue W. Mapping synthetic binding proteins epitopes on diverse protein targets by protein structure prediction and protein-protein docking. *Comput Biol Med.* 2023;163:107183. doi:10.1016/J.COMPBIOMED.2023.107183
169. David TI, Pestov NB, Korneenko T V., Barlev NA. Non-Immunoglobulin Synthetic Binding Proteins for Oncology. *Biochemistry (Moscow)* 2023 88:9. 2023;88(9):1232-1247. doi:10.1134/S0006297923090043
170. Kingsley J, Kumarasamy N, Abrishamian L, et al. The Designed Ankyrin Repeat Protein Antiviral Ensovibep for Nonhospitalized Patients With Coronavirus Disease 2019: Results From EMPATHY, a Randomized, Placebo-Controlled Phase 2 Study. *Open Forum Infect Dis.* 2024;11(6). doi:10.1093/OFID/OFAE233
171. Lim SP. Targeting SARS-CoV-2 and host cell receptor interactions. *Antiviral Res.* 2023;210:105514. doi:10.1016/J.ANTIVIRAL.2022.105514
172. Hamers-Casterman C, Atarhouch T, Muyldermans S, et al. Naturally occurring antibodies devoid of light chains. *Nature* 1993 363:6428. 1993;363(6428):446-448. doi:10.1038/363446a0
173. Jin BK, Odongo S, Radwanska M, Magez S. NANOBODIES®: A Review of Diagnostic and Therapeutic Applications. *International Journal of Molecular Sciences* 2023, Vol 24, Page 5994. 2023;24(6):5994. doi:10.3390/IJMS24065994
174. Kunz P, Zinner K, Mücke N, Bartoschik T, Muyldermans S, Hoheisel JD. The structural basis of nanobody unfolding reversibility and thermoresistance. *Scientific Reports* 2018 8:1. 2018;8(1):1-10. doi:10.1038/s41598-018-26338-z
175. Modhiran N, Lauer SM, Amarilla AA, et al. A nanobody recognizes a unique conserved epitope and potently neutralizes SARS-CoV-2 omicron variants. *iScience.* 2023;26(7):107085. doi:10.1016/j.isci.2023.107085
176. Yao H, Wang H, Zhang Z, et al. A potent and broad-spectrum neutralizing nanobody for SARS-CoV-2 viruses, including all major Omicron strains. *MedComm (Beijing).* 2023;4(6):e397. doi:10.1002/MCO2.397

177. Ma H, Zhang X, Zeng W, et al. A bispecific nanobody dimer broadly neutralizes SARS-CoV-1 & 2 variants of concern and offers substantial protection against Omicron via low-dose intranasal administration. *Cell Discovery* 2022 8:1. 2022;8(1):1-14. doi:10.1038/s41421-022-00497-w
178. Solodkov PP, Najakshin AM, Chikaev NA, et al. Serial Llama Immunization with Various SARS-CoV-2 RBD Variants Induces Broad Spectrum Virus-Neutralizing Nanobodies. *Vaccines (Basel)*. 2024;12(2):129. doi:10.3390/VACCINES12020129/S1
179. Yang J, Lin S, Chen Z, et al. Development of a bispecific nanobody conjugate broadly neutralizes diverse SARS-CoV-2 variants and structural basis for its broad neutralization. *PLoS Pathog.* 2023;19(11):e1011804. doi:10.1371/JOURNAL.PPAT.1011804
180. Liu H, Wu L, Liu B, et al. Two pan-SARS-CoV-2 nanobodies and their multivalent derivatives effectively prevent Omicron infections in mice. *Cell Rep Med.* 2023;4(2):100918. doi:10.1016/J.XCRM.2023.100918
181. Yang Y, Zhang J, Zhang S, et al. A novel nanobody broadly neutralizes SARS-CoV-2 via induction of spike trimer dimers conformation. *Exploration*. 2024;4(3). doi:10.1002/EXP.20230086
182. Ye G, Pan R, Bu F, et al. Discovery of Nanosota-2, -3, and -4 as super potent and broad-spectrum therapeutic nanobody candidates against COVID-19. *J Virol.* 2023;97(11). doi:10.1128/JVI.01448-23
183. Nagata K, Utsumi D, Asaka MN, et al. Intratracheal trimerized nanobody cocktail administration suppresses weight loss and prolongs survival of SARS-CoV-2 infected mice. *Communications Medicine* 2022 2:1. 2022;2(1):1-6. doi:10.1038/s43856-022-00213-5
184. Favorskaya IA, Shcheblyakov D V., Esmagambetov IB, et al. Single-Domain Antibodies Efficiently Neutralize SARS-CoV-2 Variants of Concern. *Front Immunol.* 2022;13:822159. doi:10.3389/FIMMU.2022.822159/BIBTEX
185. Li T, Zhou B, Li Y, et al. Isolation, characterization, and structure-based engineering of a neutralizing nanobody against SARS-CoV-2. *Int J Biol Macromol.* 2022;209(Pt A):1379-1388. doi:10.1016/J.IJBIOMAC.2022.04.096
186. Yuan M, Wu NC, Zhu X, et al. A highly conserved cryptic epitope in the receptor binding domains of SARS-CoV-2 and SARS-CoV. *Science (1979)*. 2020;368(6491):630-633. doi:10.1126/SCIENCE.ABB7269
187. Pinto D, Park YJ, Beltramello M, et al. Cross-neutralization of SARS-CoV-2 by a human monoclonal SARS-CoV antibody. *Nature*. 2020;583(7815):290-295. doi:10.1038/S41586-020-2349-Y

188. Uraki R, Kiso M, Iwatsuki-Horimoto K, et al. Characterization of a SARS-CoV-2 EG.5.1 clinical isolate in vitro and in vivo. *Cell Rep.* 2023;42(12):113580. doi:10.1016/j.celrep.2023.113580